6 *Annexes*

Annexe 1 : les corrélations éventuelles entre paramètres présentées par un « scatter plot » sous forme matricielle

Matrice des Paramètres Intrinseque; l'échantillon:D1.5F8_L5

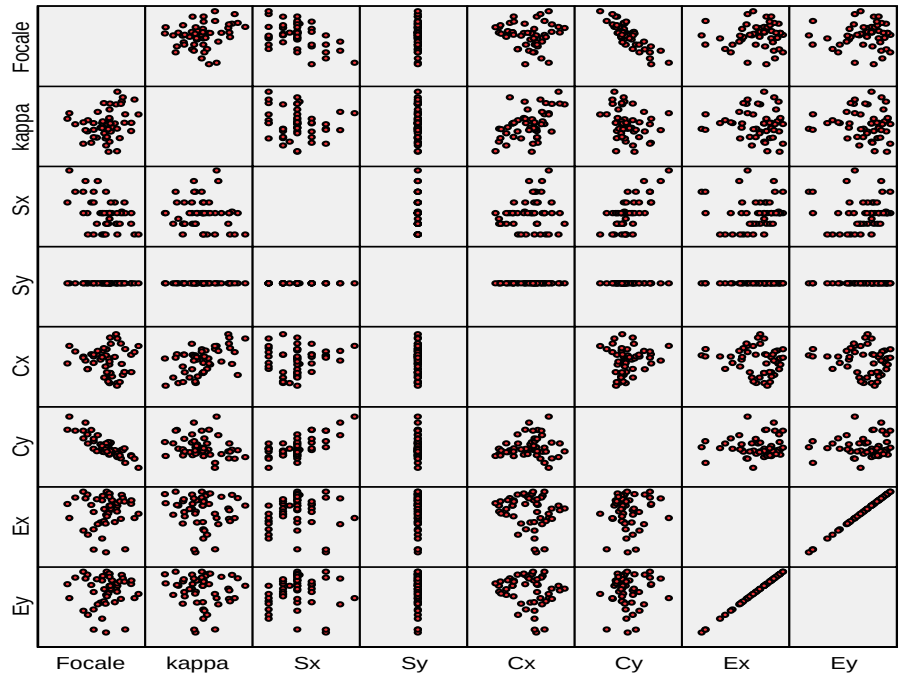

Matrice des Paramètres Intrinseque; l'échantillon:D1.5F16_L5

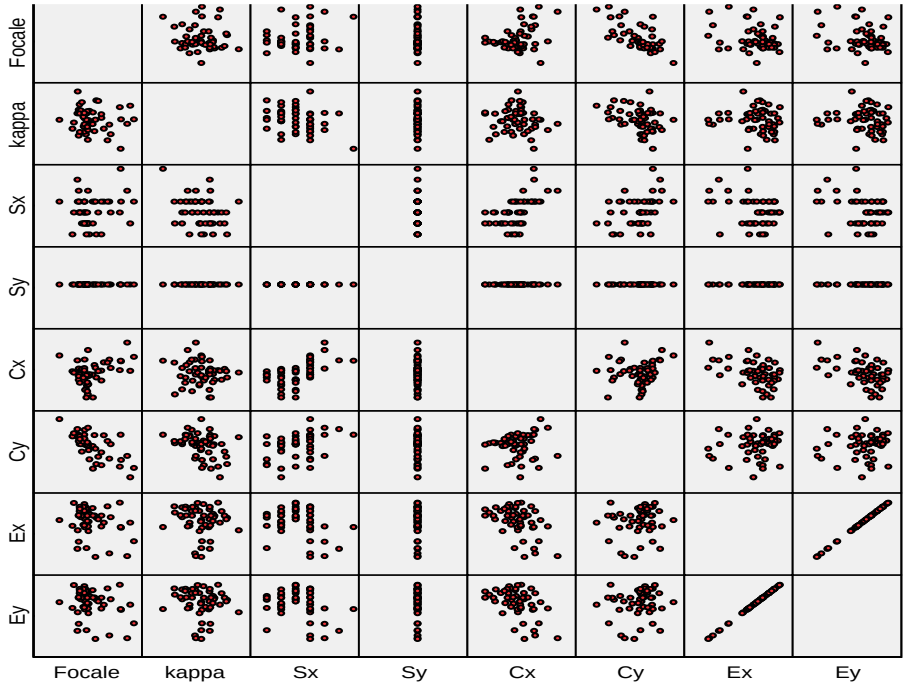

Matrice des Paramètres Intrinseque; l'échantillon:D15F4_L20

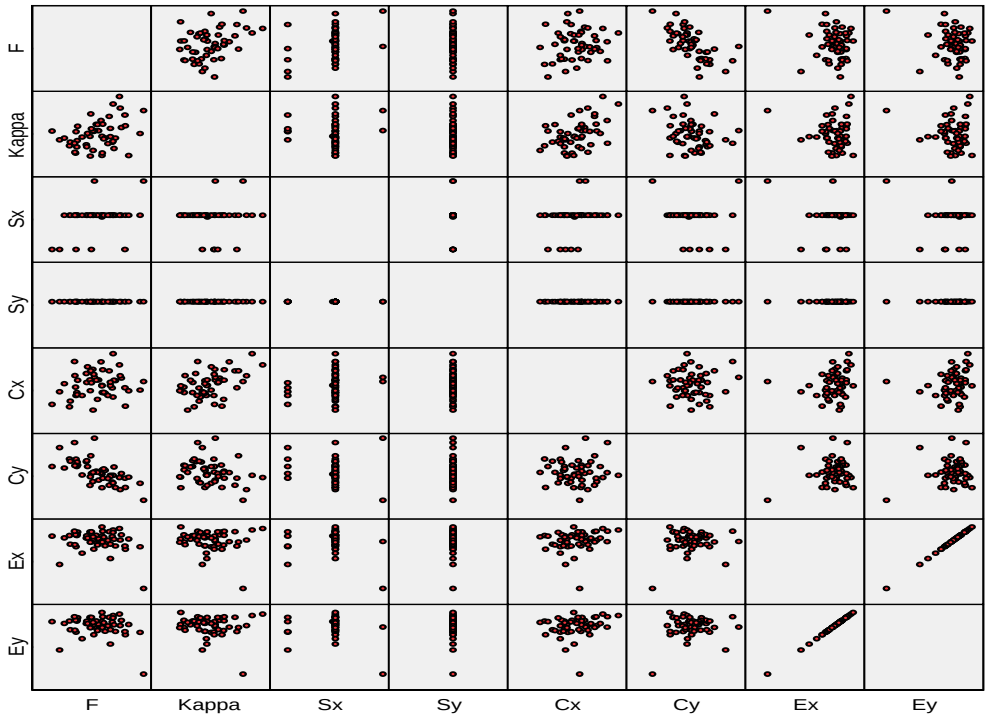

Matrice des Paramètres Intrinseque; l'échantillon:D45F4_L20

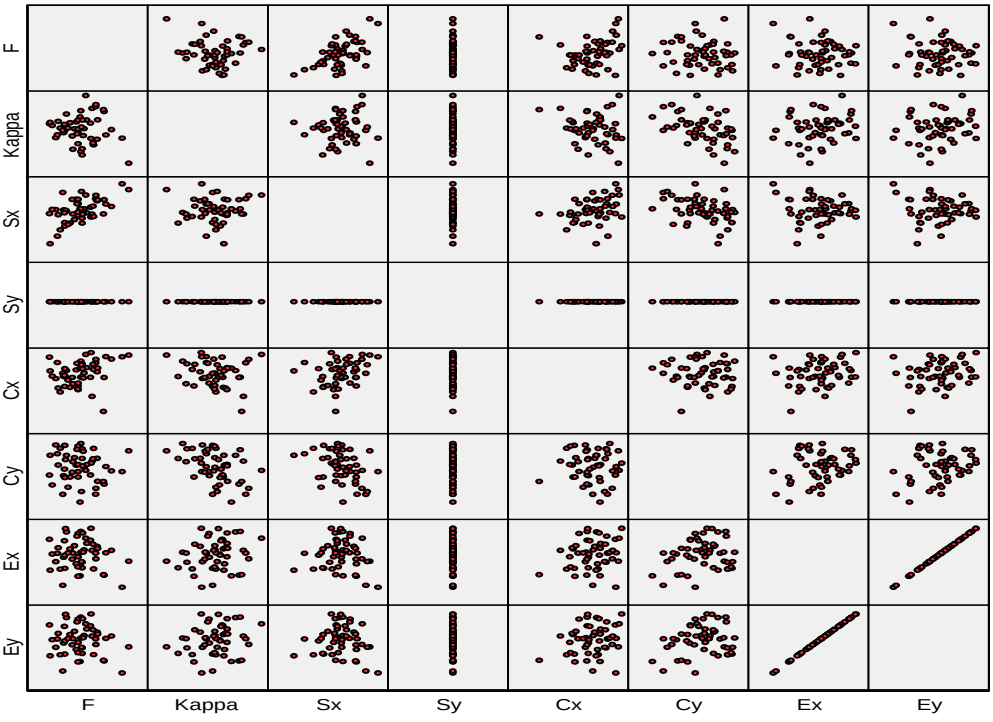

Annexe 2 : Variabilité de l'estimation des différents paramètres et analyse de sensibilité.

1. Les Erreurs :

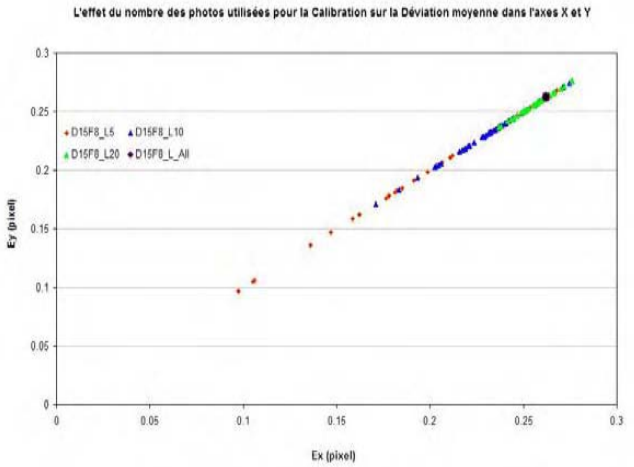

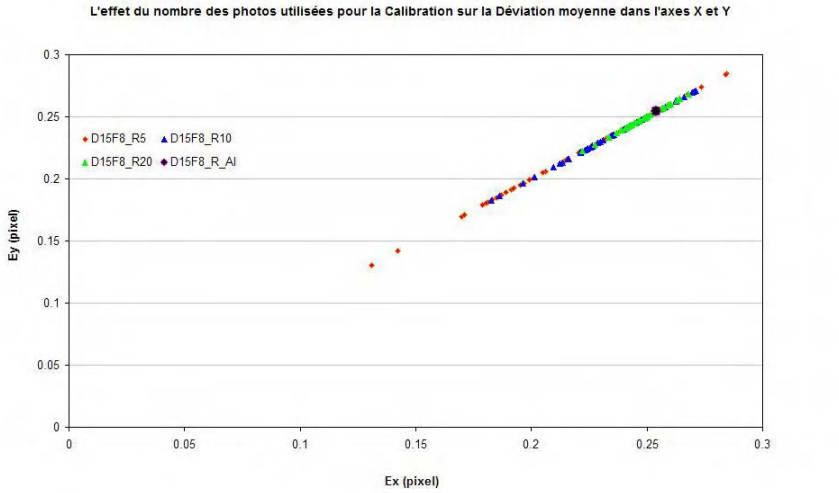

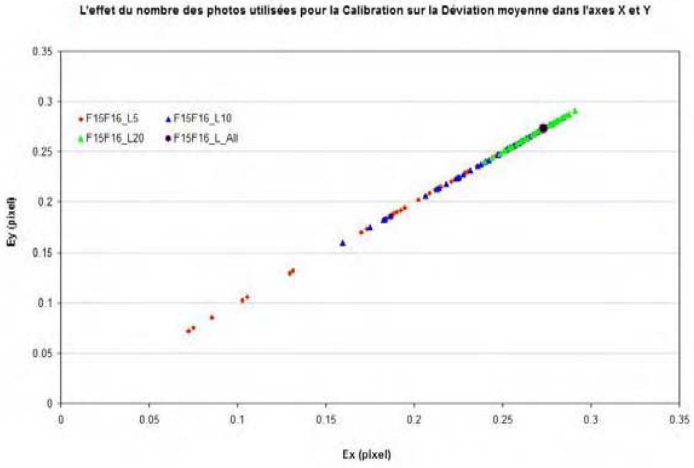

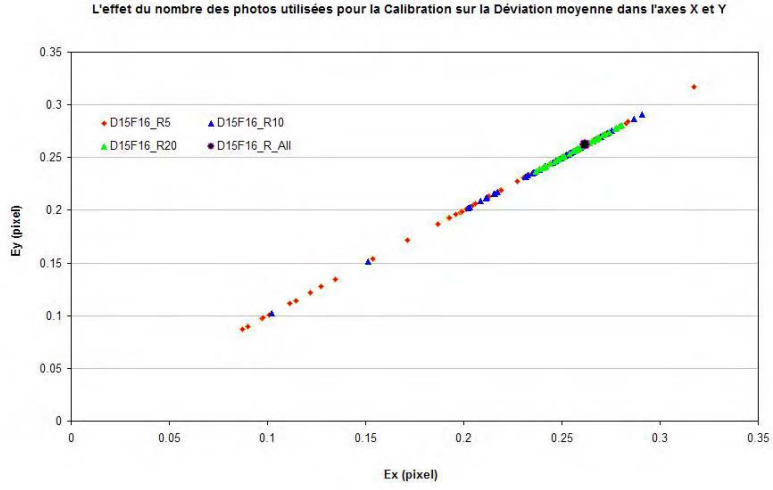

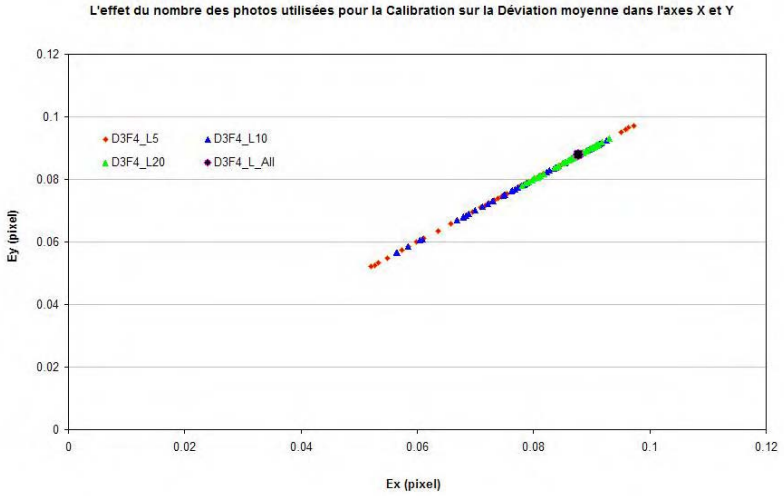
L'effet du nombre des photos utilisées pour la Calibration sur la Déviation moyenne dans l'axes X et Y
D3F4_L5
D3F4_L10
D3F4_L20
D3F4_L_All
Ey (pixel)
Ex (pixel)
0.12
0.1
0.08
0.06
0.04
0.02
0
0.02
0.04
0.06
0.08
0.1
0.12

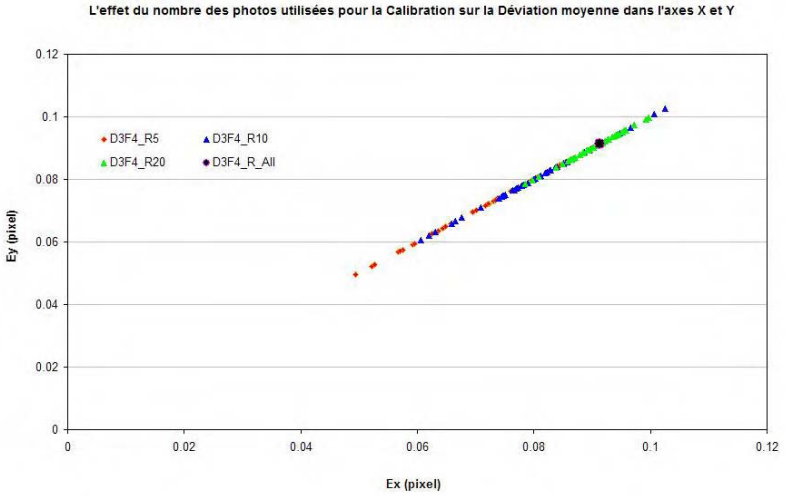
L'effet du nombre des photos utilisées pour la Calibration sur la Déviation moyenne dans l'axes X et Y
D3F4_R5
D3F4_R10
D3F4_R20
D3F4_R_All
Ey (pixel)
Ex (pixel)
0.12
0.1
0.08
0.06
0.04
0.02
0
0.02
0.04
0.06
0.08
0.1
0.12

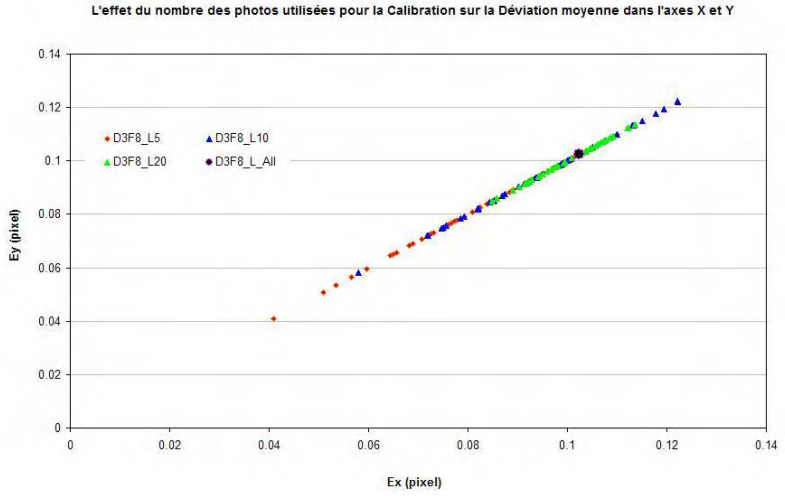
L'effet du nombre des photos utilisées pour la Calibration sur la Déviation moyenne dans l'axes X et Y
D3F8_L5
D3F8_L10
D3F8_L20
D3F8_L_All
Ey (pixel)
Ex (pixel)
0.14
0.12
0.1
0.08
0.06
0.04
0.02
0
0.02
0.04
0.06
0.08
0.1
0.12
0.14

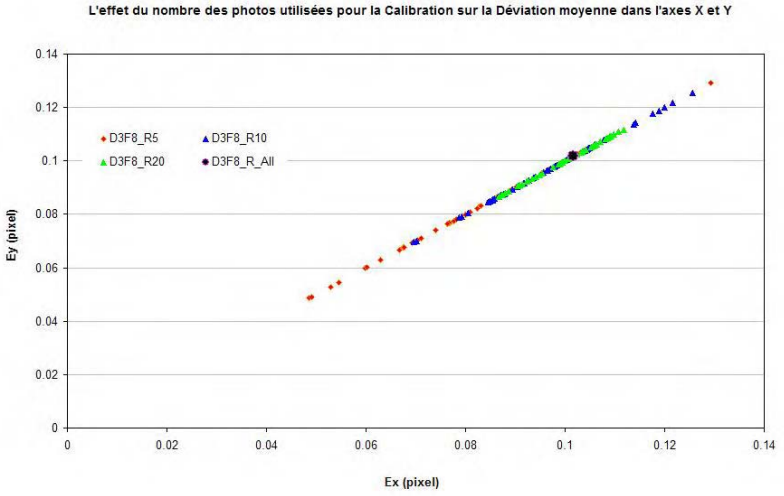
L'effet du nombre des photos utilisées pour la Calibration sur la Déviation moyenne dans l'axes X et Y
D3F8_R5
D3F8_R10
D3F8_R20
D3F8_R_All
Ey (pixel)
Ex (pixel)
0.14
0.12
0.1
0.08
0.06
0.04
0.02
0
0.02
0.04
0.06
0.08
0.1
0.12
0.14

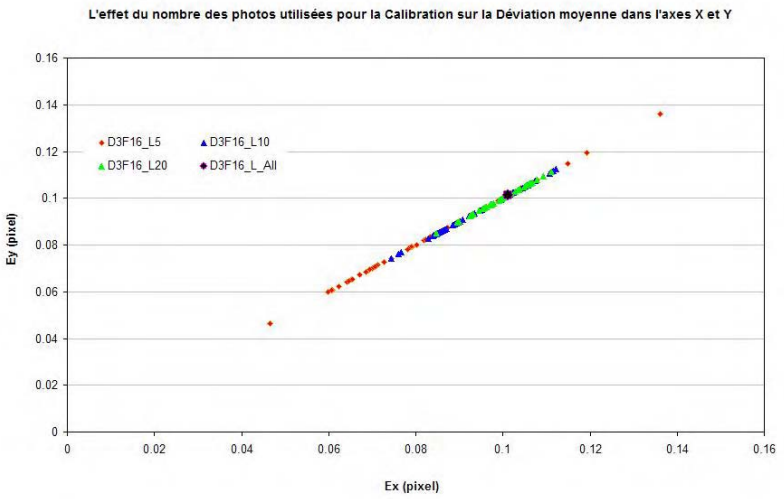
L'effet du nombre des photos utilisées pour la Calibration sur la Déviation moyenne dans l'axes X et Y
D3F16_L5
D3F16_L10
D3F16_L20
D3F16_L_All
Ey (pixel)
Ex (pixel)

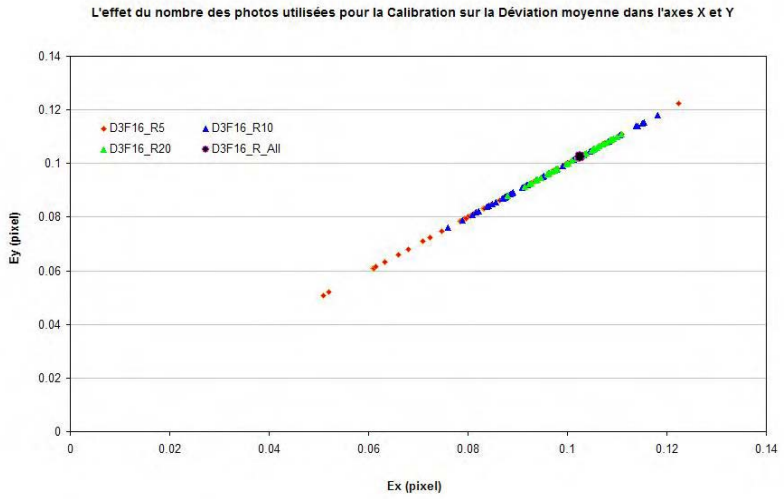
L'effet du nombre des photos utilisées pour la Calibration sur la Déviation moyenne dans l'axes X et Y
D3F16_R5
D3F16_R10
D3F16_R20
D3F16_R_All
Ey (pixel)
Ex (pixel)

D45

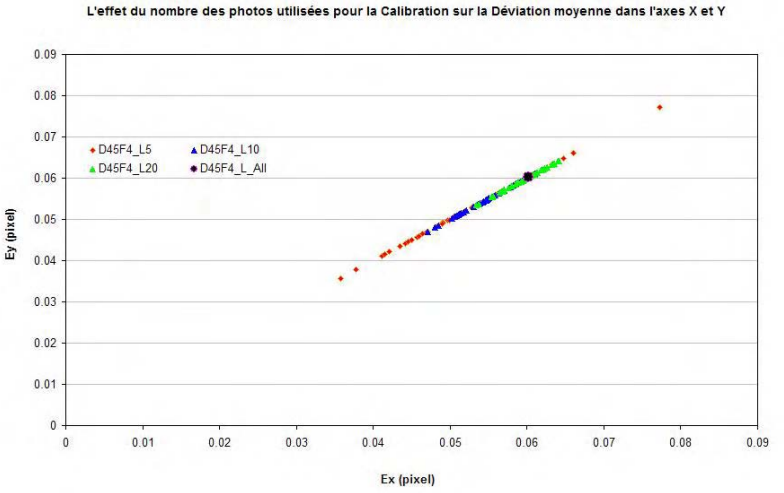
L'effet du nombre des photos utilisées pour la Calibration sur la Déviation moyenne dans l'axes X et Y
D45F4_L5
D45F4_L10
D45F4_L20
D45F4_L_All
Ey (pixel)
Ex (pixel)

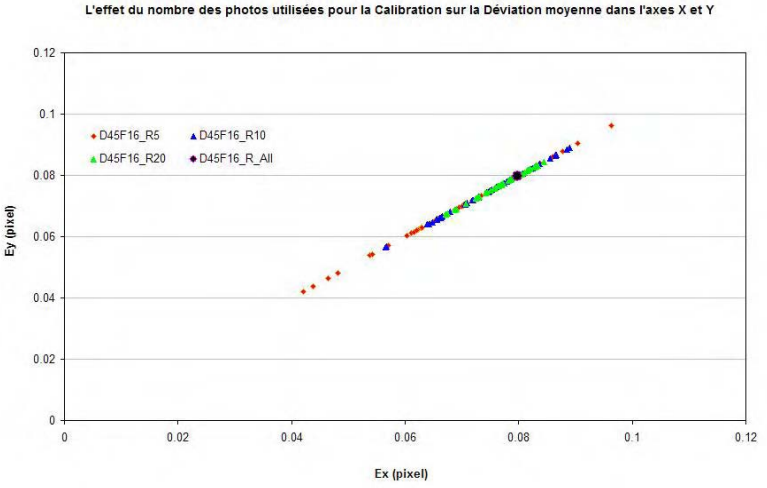
L'effet du nombre des photos utilisées pour la Calibration sur la Déviation moyenne dans l'axes X et Y
D45F16_R5
D45F16_R10
D45F16_R20
D45F16_R_All
Ey (pixel)
Ex (pixel)

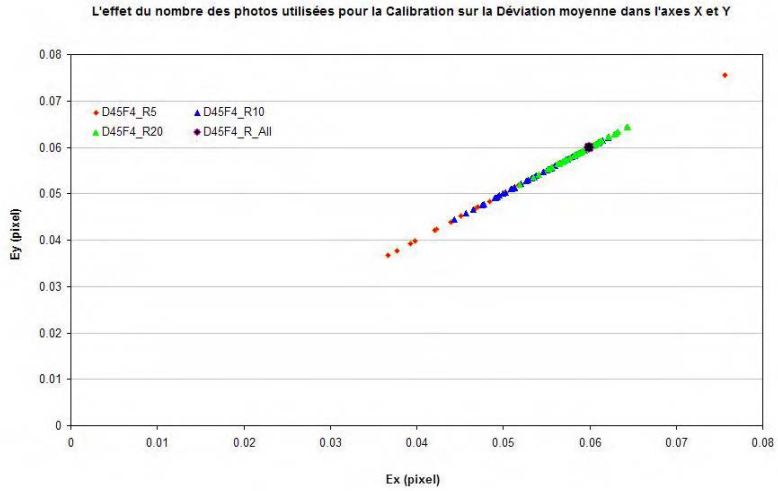
L'effet du nombre des photos utilisées pour la Calibration sur la Déviation moyenne dans l'axes X et Y
D45F4_R5
D45F4_R10
D45F4_R20
D45F4_R_All
Ey (pixel)
Ex (pixel)

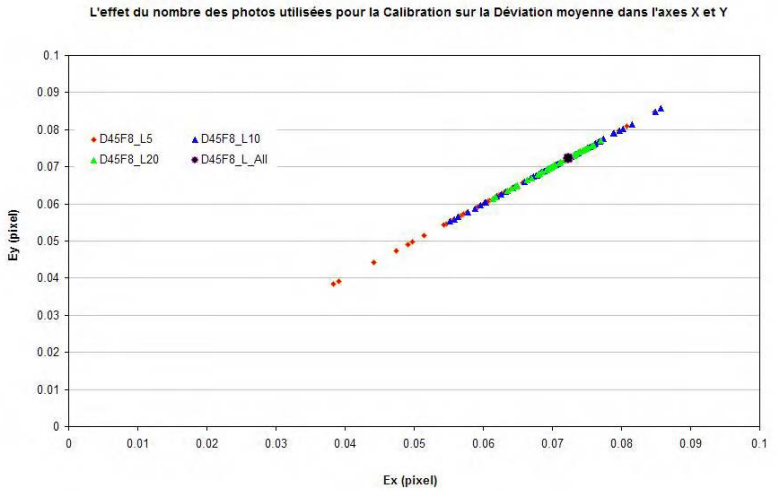
L'effet du nombre des photos utilisées pour la Calibration sur la Déviation moyenne dans l'axes X et Y
D45F8_L5
D45F8_L10
D45F8_L20
D45F8_L_All
Ey (pixel)
Ex (pixel)

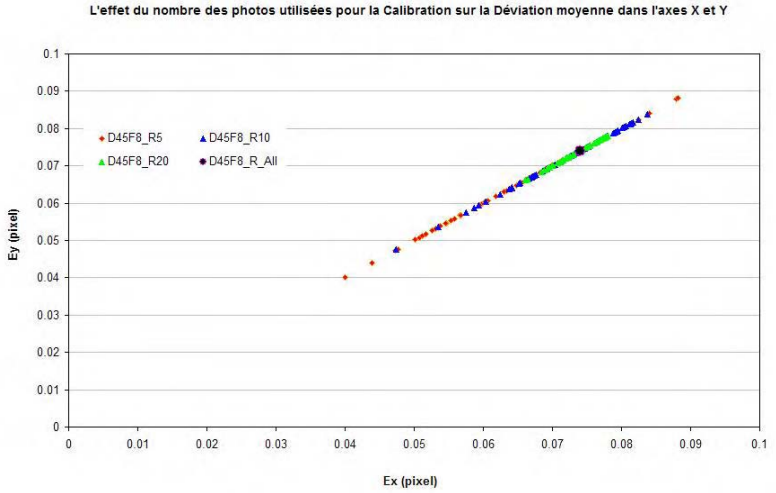
L'effet du nombre des photos utilisées pour la Calibration sur la Déviation moyenne dans l'axes X et Y
D45F8_R5
D45F8_R10
D45F8_R20
D45F8_R_All
Ey (pixel)
Ex (pixel)

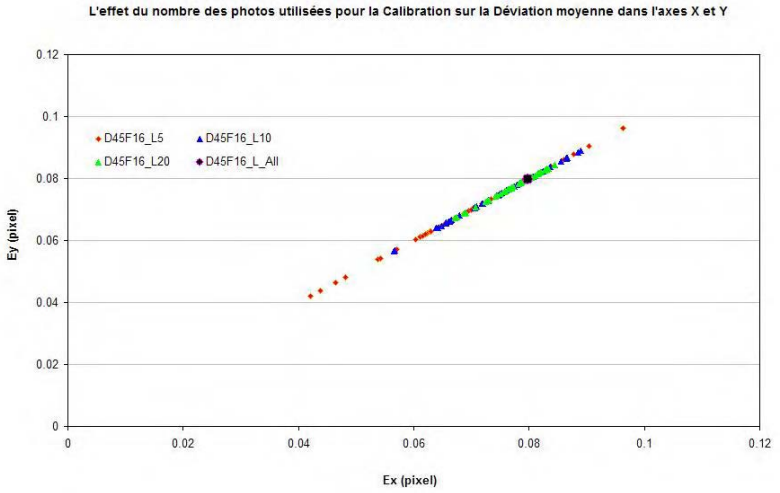
L'effet du nombre des photos utilisées pour la Calibration sur la Déviation moyenne dans l'axes X et Y
D45F16_L5
D45F16_L10
D45F16_L20
D45F16_L_All
Ey (pixel)
Ex (pixel)

Centre d’image

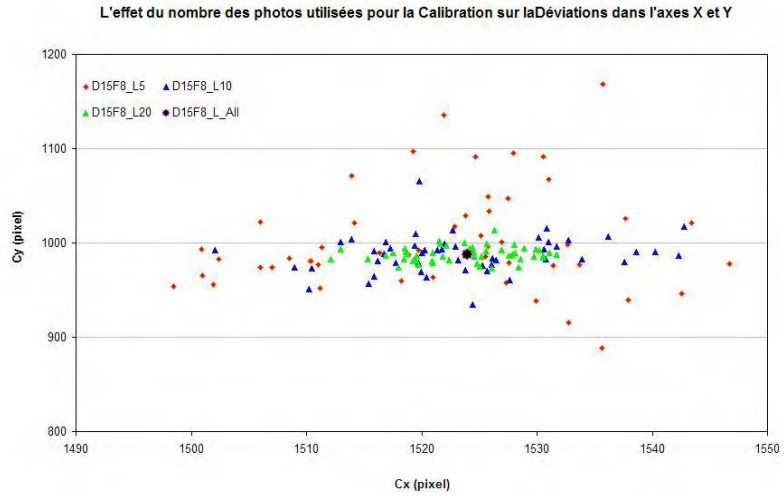

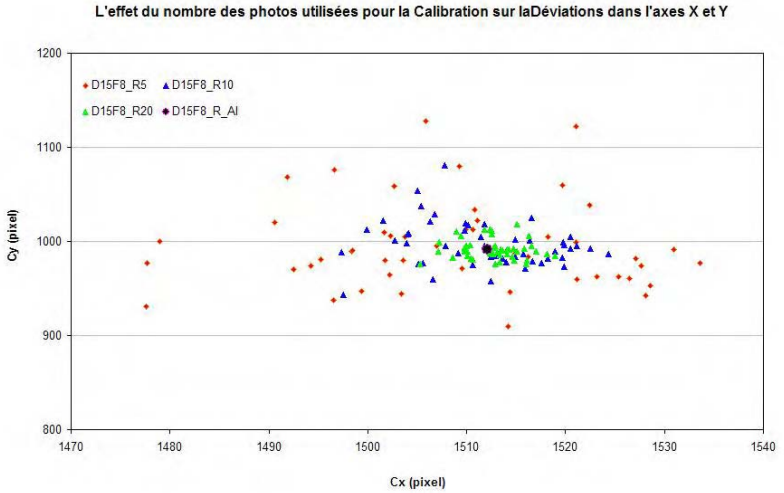

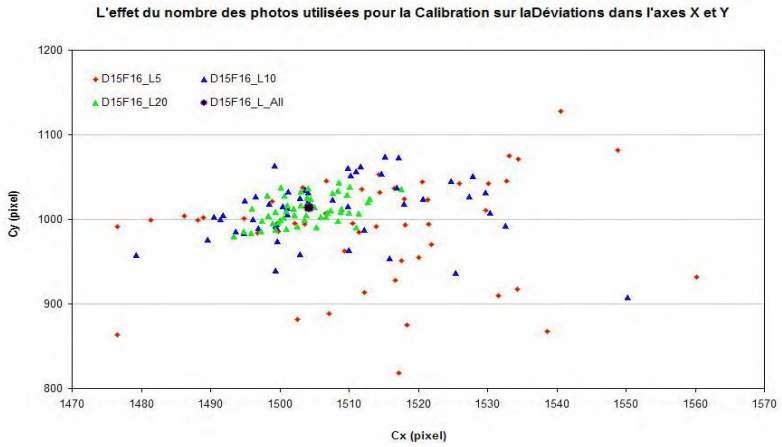

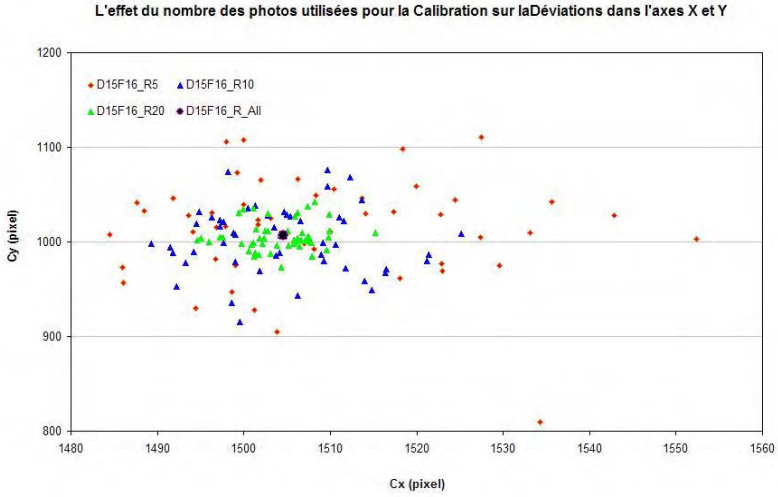

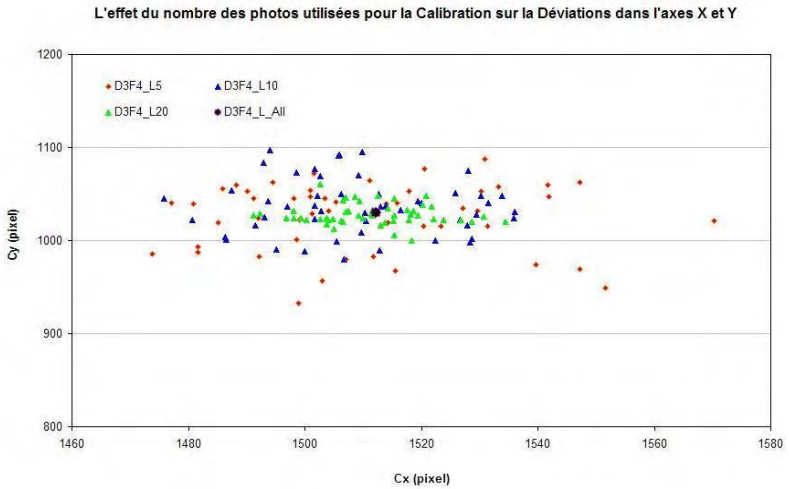
L'effet du nombre des photos utilisées pour la Calibration sur la Déviations dans l'axes X et Y
D3F4_L5
D3F4_L10
D3F4_L20
D3F4_L_All
Cy (pixel)
Cx (pixel)
1200
1100
1000
900
800
1460
1480
1500
1520
1540
1560
1580

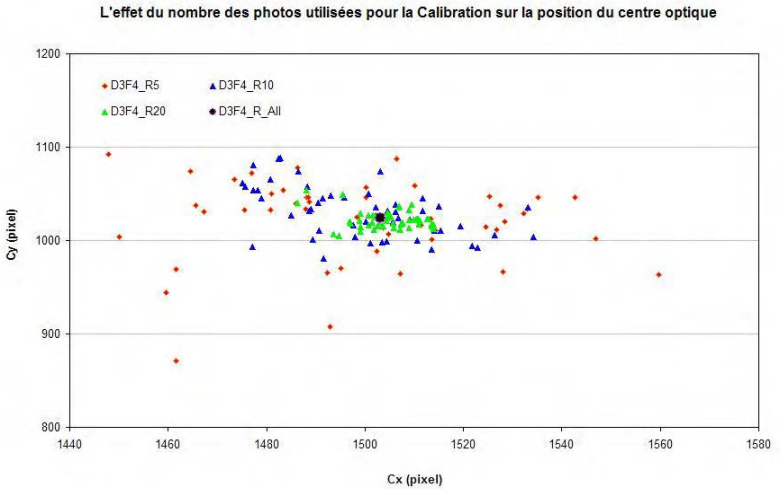
L'effet du nombre des photos utilisées pour la Calibration sur la position du centre optique
D3F4_R5
D3F4_R10
D3F4_R20
D3F4_R_All
Cy (pixel)
Cx (pixel)
1200
1100
1000
900
800
1440
1460
1480
1500
1520
1540
1560
1580

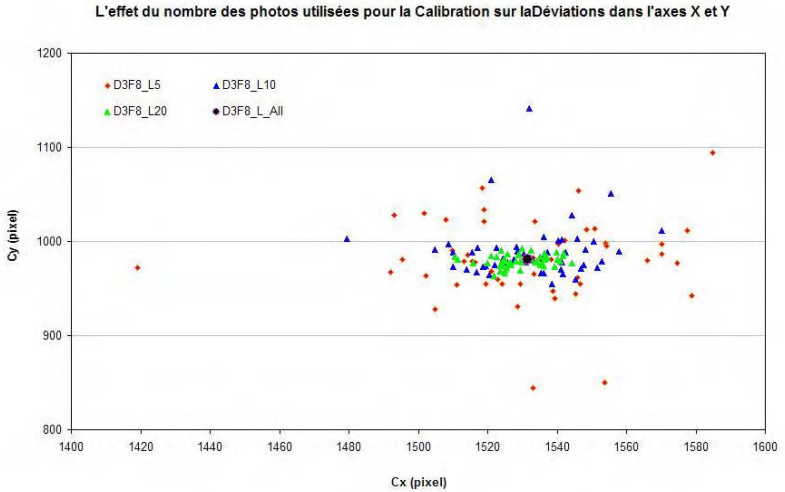
L'effet du nombre des photos utilisées pour la Calibration sur laDéviations dans l'axes X et Y
D3F8_L5
D3F8_L10
D3F8_L20
D3F8_L_All
Cy (pixel)
Cx (pixel)
1200
1100
1000
900
800
1400
1420
1440
1460
1480
1500
1520
1540
1560
1580
1600

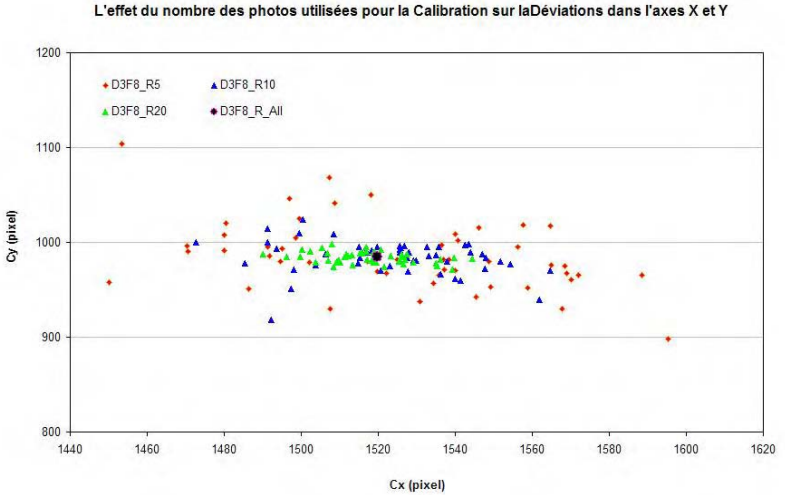
L'effet du nombre des photos utilisées pour la Calibration sur laDéviations dans l'axes X et Y
D3F8_R5
D3F8_R10
D3F8_R20
D3F8_R_All
Cy (pixel)
Cx (pixel)
1200
1100
1000
900
800
1440
1460
1480
1500
1520
1540
1560
1580
1600
1620

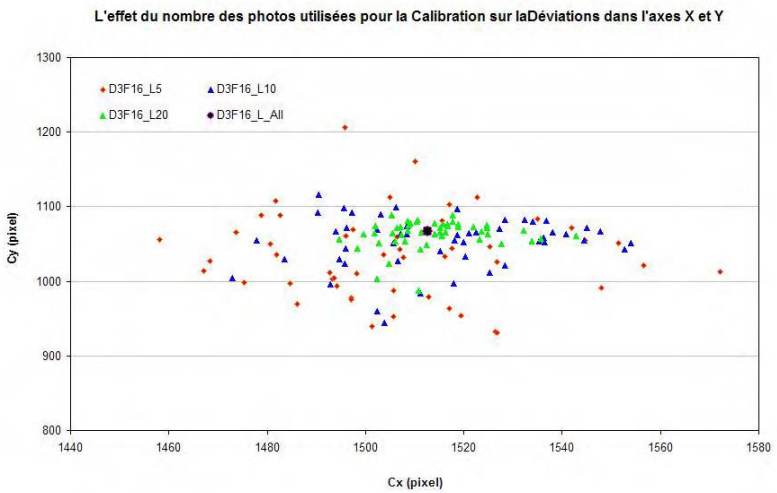
L'effet du nombre des photos utilisées pour la Calibration sur laDéviations dans l'axes X et Y
D3F16_L5
D3F16_L10
D3F16_L20
D3F16_L_All
Cy (pixel)
Cx (pixel)
1300
1200
1100
1000
900
800
1440
1460
1480
1500
1520
1540
1560
1580

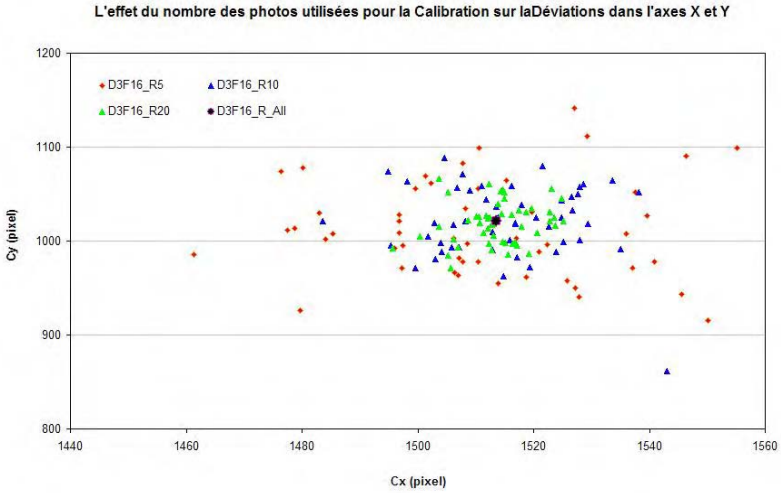
L'effet du nombre des photos utilisées pour la Calibration sur laDéviations dans l'axes X et Y
D3F16_R5
D3F16_R10
D3F16_R20
D3F16_R_All
Cy (pixel)
Cx (pixel)
1200
1100
1000
900
800
1440
1460
1480
1500
1520
1540
1560

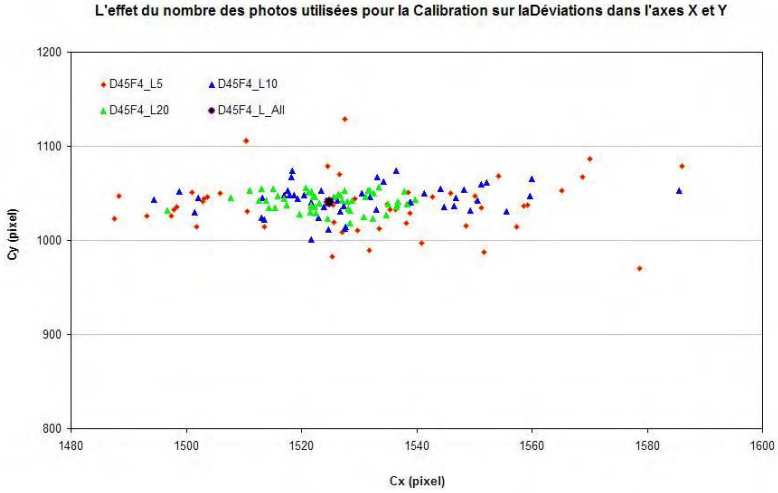
L'effet du nombre des photos utilisées pour la Calibration sur laDéviations dans l'axes X et Y
D45F4_L5
D45F4_L10
D45F4_L20
D45F4_L_All
Cy (pixel)
Cx (pixel)
1200
1100
1000
900
800
1480
1500
1520
1540
1560
1580
1600

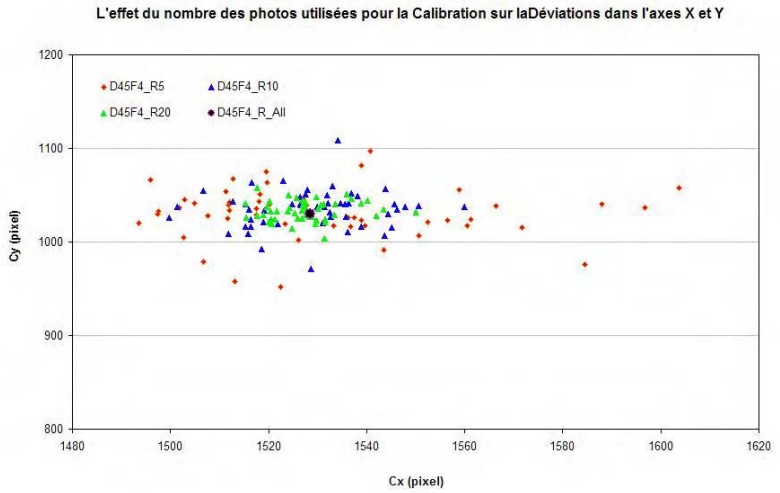
L'effet du nombre des photos utilisées pour la Calibration sur laDéviations dans l'axes X et Y
D45F4_R5
D45F4_R10
D45F4_R20
D45F4_R_All
Cy (pixel)
Cx (pixel)
1200
1100
1000
900
800
1480
1500
1520
1540
1560
1580
1600
1620

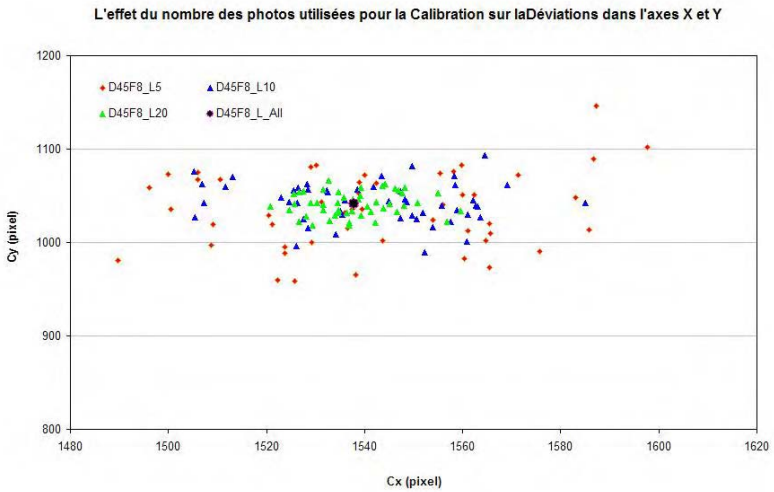
L'effet du nombre des photos utilisées pour la Calibration sur laDéviations dans l'axes X et Y
D45F8_L5
D45F8_L10
D45F8_L20
D45F8_L_All
Cy (pixel)
Cx (pixel)
1200
1100
1000
900
800
1480
1500
1520
1540
1560
1580
1600
1620

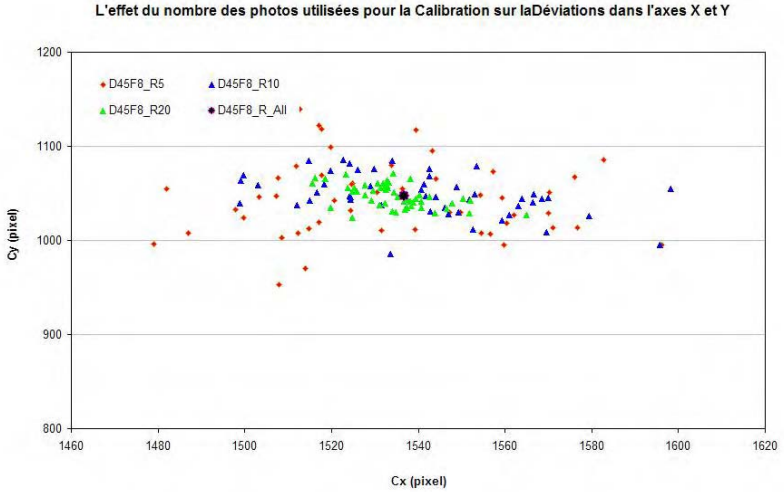
L'effet du nombre des photos utilisées pour la Calibration sur laDéviations dans l'axes X et Y
D45F8_R5
D45F8_R10
D45F8_R20
D45F8_R_All
Cy (pixel)
Cx (pixel)
1200
1100
1000
900
800
1460
1480
1500
1520
1540
1560
1580
1600
1620

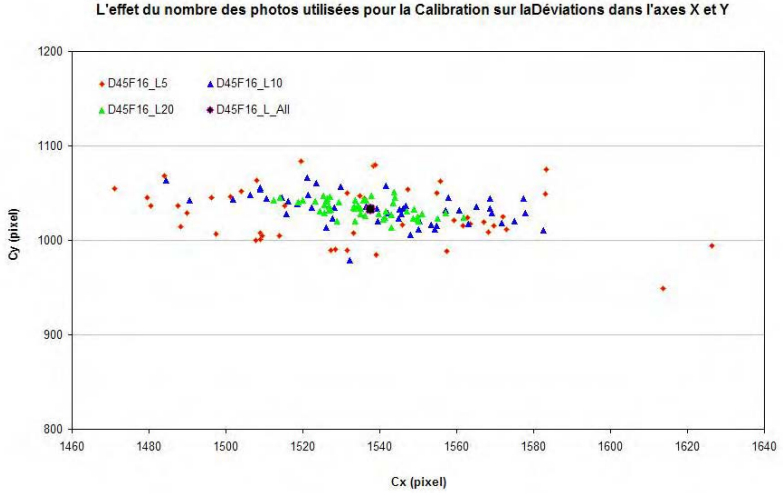
L'effet du nombre des photos utilisées pour la Calibration sur laDéviations dans l'axes X et Y
D45F16_L5
D45F16_L10
D45F16_L20
D45F16_L_All
Cy (pixel)
Cx (pixel)
1200
1100
1000
900
800
1460
1480
1500
1520
1540
1560
1580
1600
1620
1640

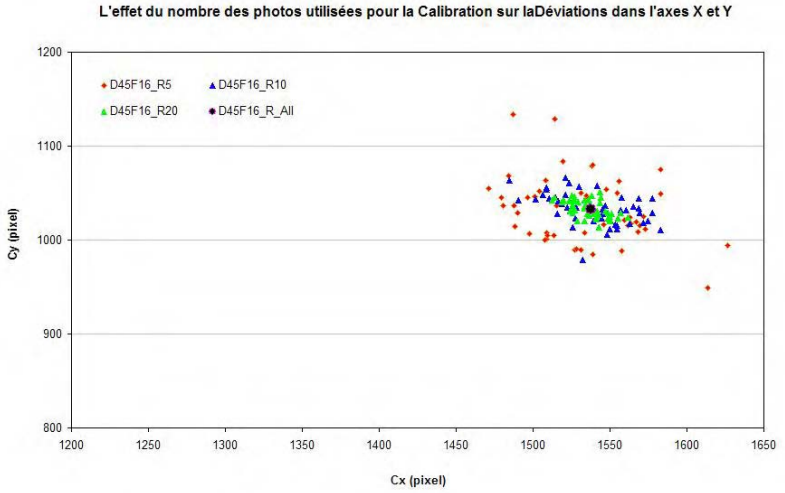
L'effet du nombre des photos utilisées pour la Calibration sur laDéviations dans l'axes X et Y
D45F16_R5
D45F16_R10
D45F16_R20
D45F16_R_All
Cy (pixel)
Cx (pixel)
1200
1100
1000
900
800
1200
1250
1300
1350
1400
1450
1500
1550
1600
1650

3. Relation entre focale et C_x, C_y

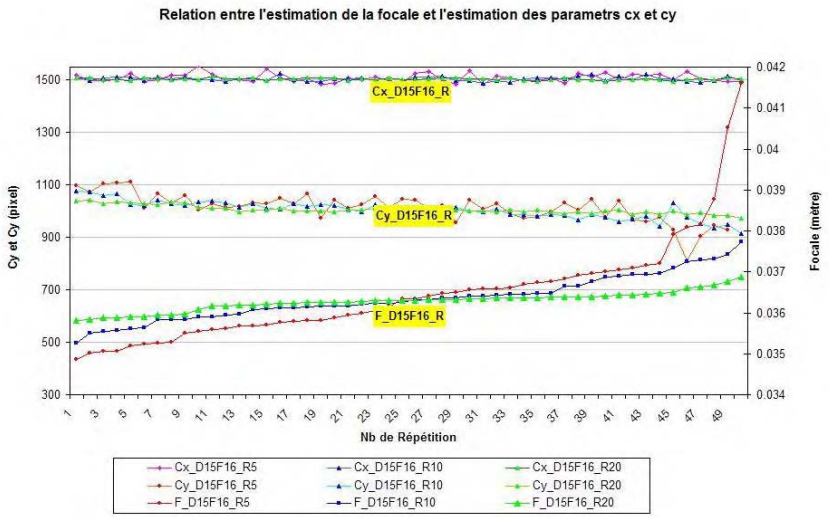

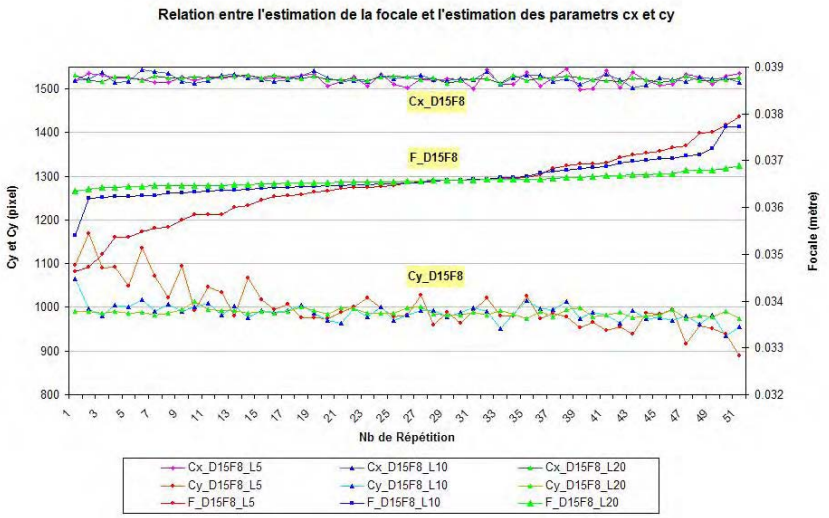

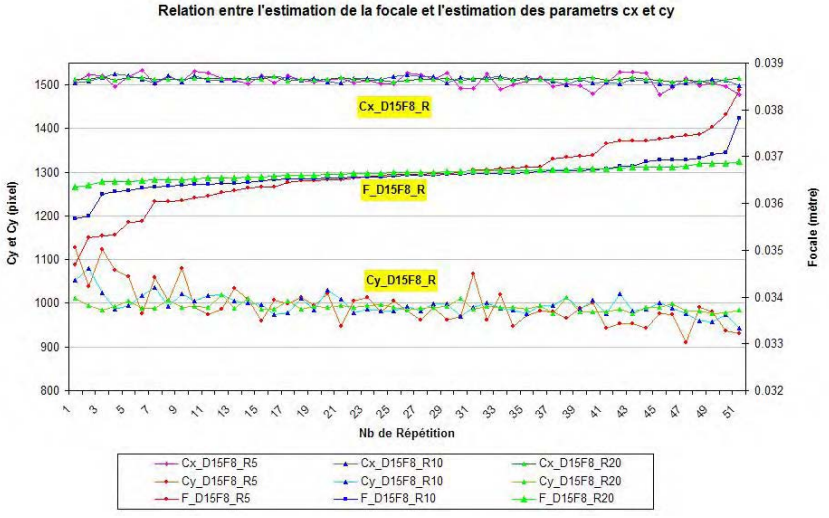

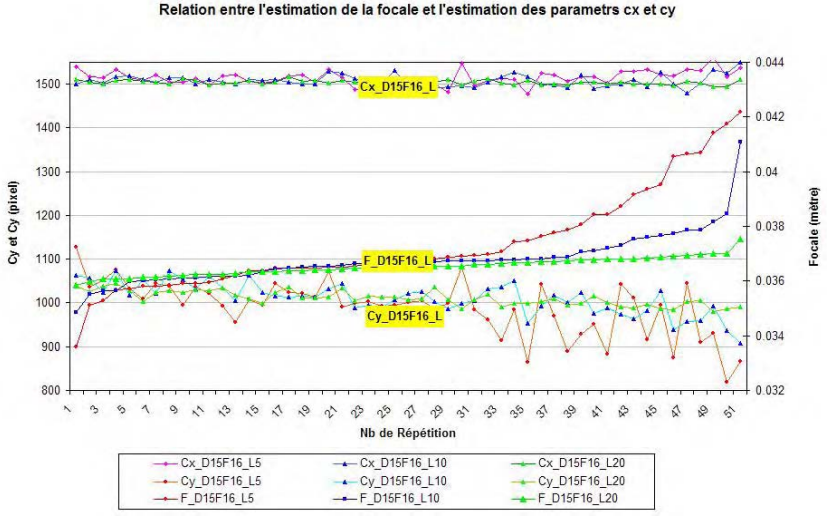

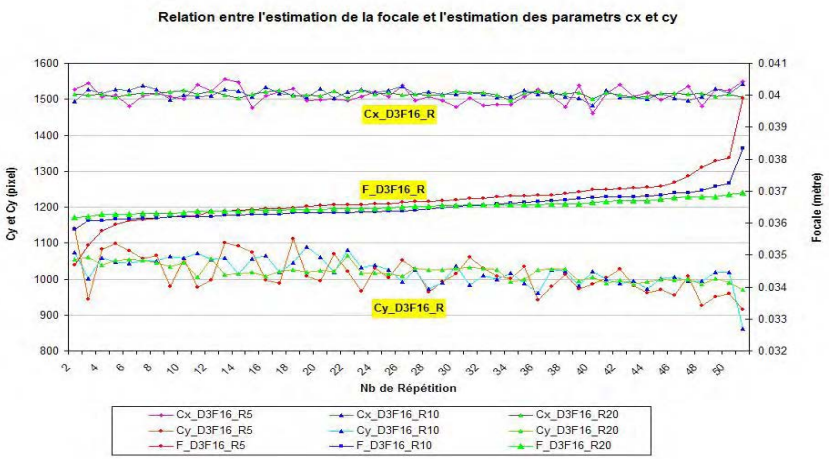
Relation entre l'estimation de la focale et l'estimation des parametrs cx et cy
Cx_D3F16_R
F_D3F16_R
Cy_D3F16_R
Cy et Cy (pixel)
Focale (mètre)
Nb de Répétition
Cx_D3F16_R5
Cx_D3F16_R10
Cx_D3F16_R20
Cy_D3F16_R5
Cy_D3F16_R10
Cy_D3F16_R20
F_D3F16_R5
F_D3F16_R10
F_D3F16_R20

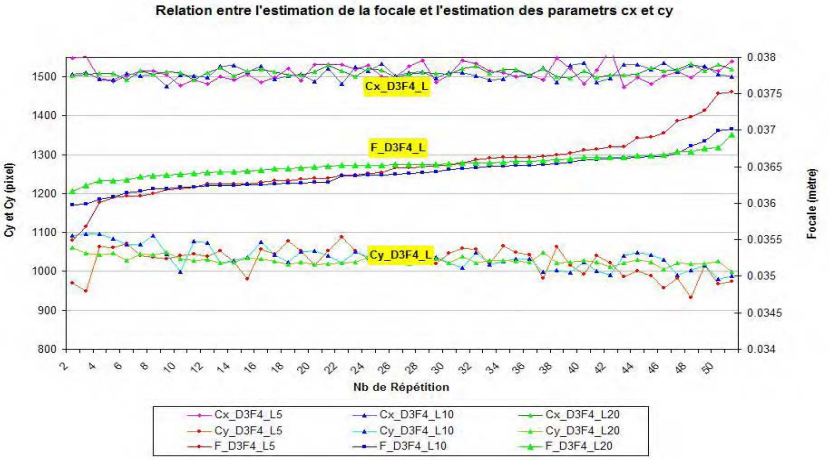
Relation entre l'estimation de la focale et l'estimation des parametrs cx et cy
Cx_D3F4_L
F_D3F4_L
Cy_D3F4_L
Cy et Cy (pixel)
Focale (mètre)
Nb de Répétition
Cx_D3F4_L5
Cx_D3F4_L10
Cx_D3F4_L20
Cy_D3F4_L5
Cy_D3F4_L10
Cy_D3F4_L20
F_D3F4_L5
F_D3F4_L10
F_D3F4_L20

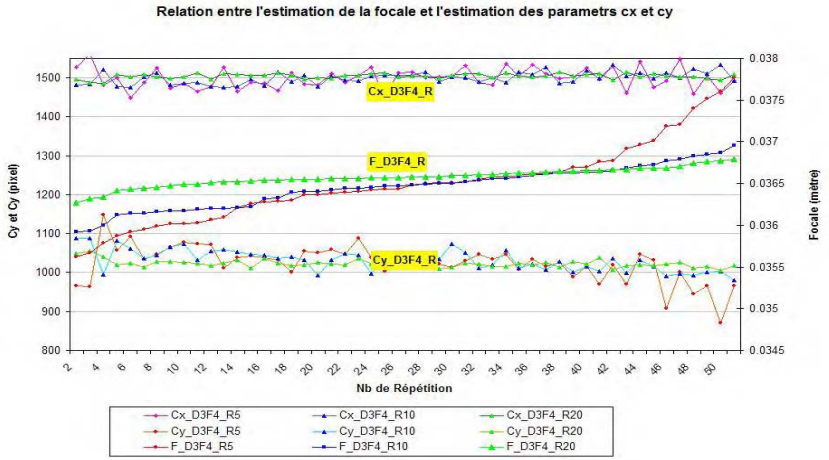
Relation entre l'estimation de la focale et l'estimation des parametrs cx et cy
Cx_D3F4_R
F_D3F4_R
Cy_D3F4_R
Cy et Cy (pixel)
Focale (mètre)
Nb de Répétition
Cx_D3F4_R5
Cx_D3F4_R10
Cx_D3F4_R20
Cy_D3F4_R5
Cy_D3F4_R10
Cy_D3F4_R20
F_D3F4_R5
F_D3F4_R10
F_D3F4_R20

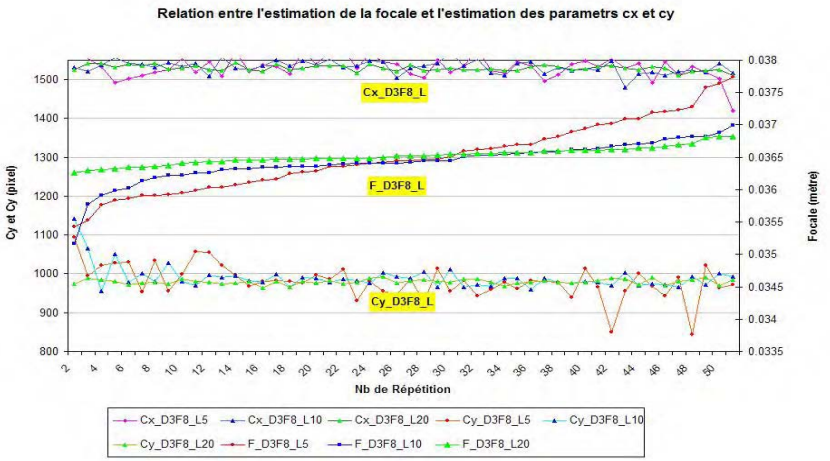
Relation entre l'estimation de la focale et l'estimation des parametrs cx et cy
Cx_D3F8_L
F_D3F8_L
Cy_D3F8_L
Cy et Cy (pixel)
Focale (mètre)
Nb de Répétition
Cx_D3F8_L5
Cx_D3F8_L10
Cx_D3F8_L20
Cy_D3F8_L5
Cy_D3F8_L10
Cy_D3F8_L20
F_D3F8_L5
F_D3F8_L10
F_D3F8_L20

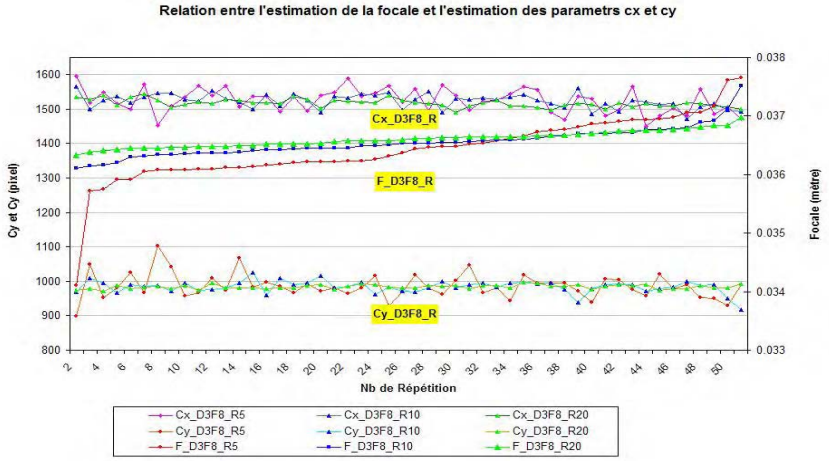
Relation entre l'estimation de la focale et l'estimation des parametrs cx et cy
Cx_D3F8_R
F_D3F8_R
Cy_D3F8_R
Cy et Cy (pixel)
Focale (mètre)
Nb de Répétition
Cx_D3F8_R5
Cx_D3F8_R10
Cx_D3F8_R20
Cy_D3F8_R5
Cy_D3F8_R10
Cy_D3F8_R20
F_D3F8_R5
F_D3F8_R10
F_D3F8_R20

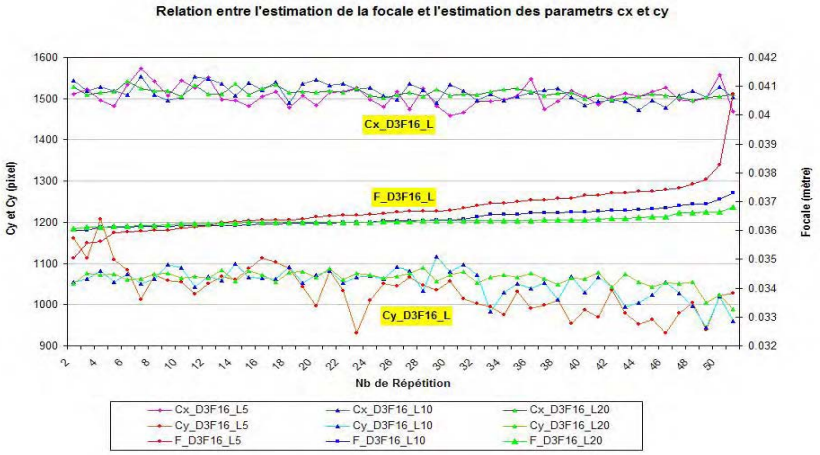
Relation entre l'estimation de la focale et l'estimation des parametrs cx et cy
Cx_D3F16_L
F_D3F16_L
Cy_D3F16_L
Cy et Cy (pixel)
Focale (mètre)
Nb de Répétition
Cx_D3F16_L5
Cx_D3F16_L10
Cx_D3F16_L20
Cy_D3F16_L5
Cy_D3F16_L10
Cy_D3F16_L20
F_D3F16_L5
F_D3F16_L10
F_D3F16_L20

D45

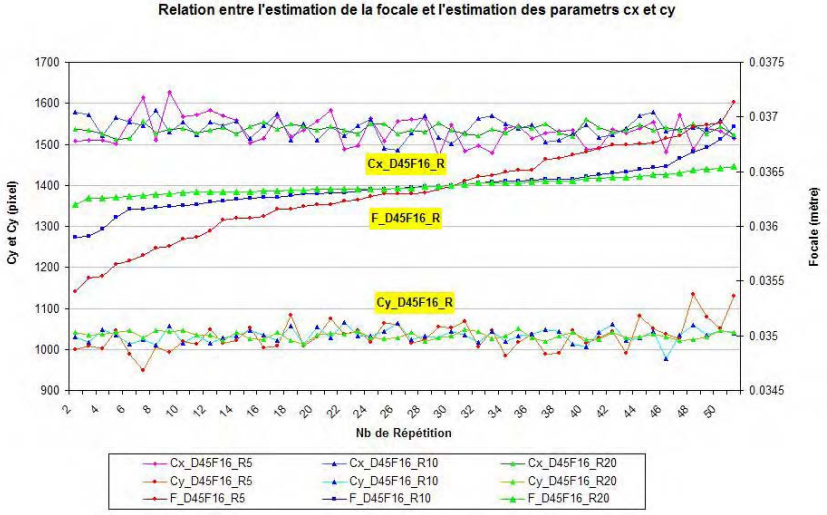
Relation entre l'estimation de la focale et l'estimation des parametrs cx et cy
Cx_D45F16_R
F_D45F16_R
Cy_D45F16_R
Cy et Cy (pixel)
Focale (mètre)
Nb de Répétition
Cx_D45F16_R5
Cx_D45F16_R10
Cx_D45F16_R20
Cy_D45F16_R5
Cy_D45F16_R10
Cy_D45F16_R20
F_D45F16_R5
F_D45F16_R10
F_D45F16_R20

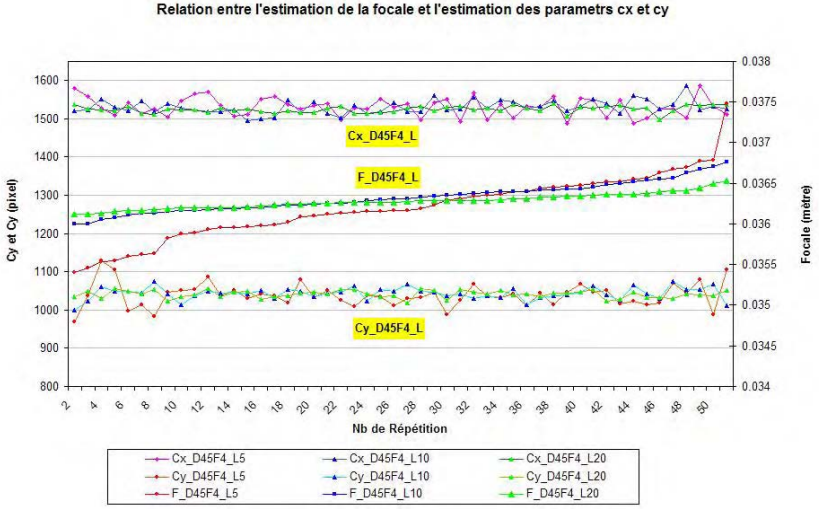
Relation entre l'estimation de la focale et l'estimation des parametrs cx et cy
Cx_D45F4_L
F_D45F4_L
Cy_D45F4_L
Cy et Cy (pixel)
Focale (mètre)
Nb de Répétition
Cx_D45F4_L5
Cx_D45F4_L10
Cx_D45F4_L20
Cy_D45F4_L5
Cy_D45F4_L10
Cy_D45F4_L20
F_D45F4_L5
F_D45F4_L10
F_D45F4_L20

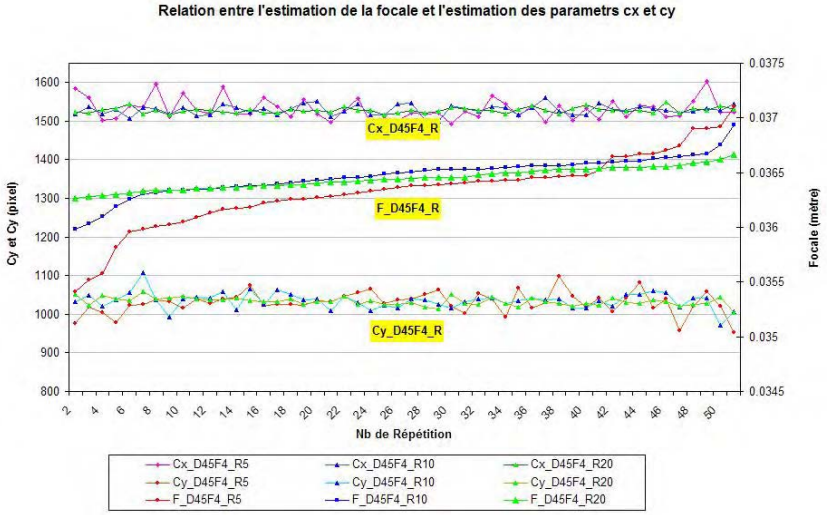
Relation entre l'estimation de la focale et l'estimation des parametrs cx et cy
Cx_D45F4_R
F_D45F4_R
Cy_D45F4_R
Cy et Cy (pixel)
Focale (mètre)
Nb de Répétition
Cx_D45F4_R5
Cx_D45F4_R10
Cx_D45F4_R20
Cy_D45F4_R5
Cy_D45F4_R10
Cy_D45F4_R20
F_D45F4_R5
F_D45F4_R10
F_D45F4_R20

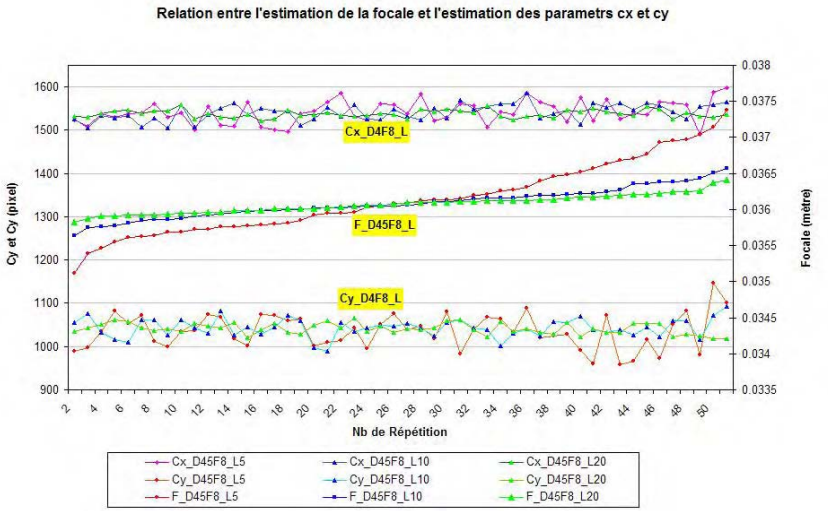
Relation entre l'estimation de la focale et l'estimation des parametrs cx et cy
Cx_D4F8_L
F_D45F8_L
Cy_D4F8_L
Cy et Cy (pixel)
Focale (mètre)
Nb de Répétition
Cx_D45F8_L5
Cx_D45F8_L10
Cx_D45F8_L20
Cy_D45F8_L5
Cy_D45F8_L10
Cy_D45F8_L20
F_D45F8_L5
F_D45F8_L10
F_D45F8_L20

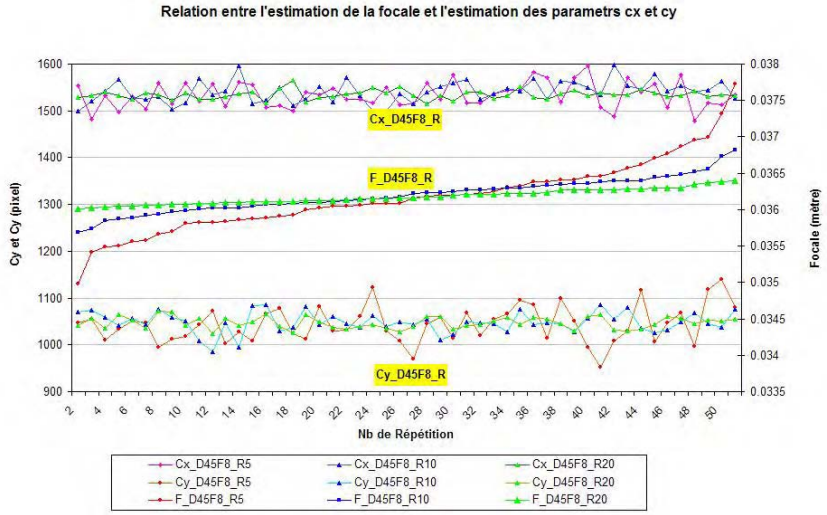
Relation entre l'estimation de la focale et l'estimation des parametrs cx et cy
Cx_D45F8_R
F_D45F8_R
Cy_D45F8_R
Cy et Cy (pixel)
Focale (mètre)
Nb de Répétition
Cx_D45F8_R5
Cx_D45F8_R10
Cx_D45F8_R20
Cy_D45F8_R5
Cy_D45F8_R10
Cy_D45F8_R20
F_D45F8_R5
F_D45F8_R10
F_D45F8_R20

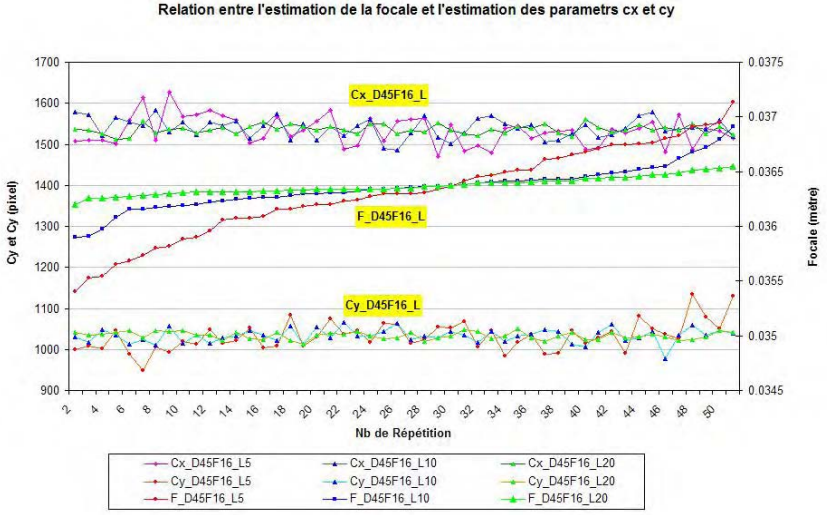
Relation entre l'estimation de la focale et l'estimation des parametrs cx et cy
Cx_D45F16_L
F_D45F16_L
Cy_D45F16_L
Cy et Cy (pixel)
Focale (mètre)
Nb de Répétition
Cx_D45F16_L5
Cx_D45F16_L10
Cx_D45F16_L20
Cy_D45F16_L5
Cy_D45F16_L10
Cy_D45F16_L20
F_D45F16_L5
F_D45F16_L10
F_D45F16_L20

Annexe 3 : Soil microtopography studies using photogrammetry and Laser-Scanning methods : Article accepte (en perse, résumé anglais)

Title: Soil microtopography studies using photogrammetry and Laser-Scanning methods.

M.R. Mirzaei[1], S. Ruy[2], Gh. Ghazavi[3], Cristina Boaner[4]

[1]Avignon University and INRA-Avignon, France, Sol Section,

Email : mmirzaei@inra.avignon.fr

[2]INRA- Avignon, France

[3]Ecole Nationale supérieure Agronomique, Rennes, France

[4] Bayrauth University (Germany) and Avignon University (France)

Abstract

At the present, soil surface characteristics (SSC) are recognised as key parameters controlling infiltration rates, runoff generation and erosion. Microtopography of surface among SSC is the main one. The work presented in this paper is based on a set of digital elevation models (DEMs) supplied by two different methods: Laser roughness-meter and photogrammetry method. We used two maquettes. The considered maquettes correspond to various roughness surfaces (rough and soft). These methods were compared using different statistical parameters of SSC such as heights and slopes histograms. In addition we studied estimation of Random Roughness (RR) coefficient and Maximum Depression Storage (MDS). RR is considered as an indicator of microtopography and it is one of the main parameters influence erosion and runoff-infiltration processes. Obtained RR by photogrammetry method showed en average 10 percent difference from laser method for soft maquette and 5 percent for the rough maquette. The range of this difference for the MDS varies from 2 to 34 percent i.e. maximum 0.17 millimetres. In this study, photogrammetric method gives the DEMs with a lower slop for the rough maquette (en average 40.5 versus 46 for the laser method) and higher slop for the soft maquette (about 23.5 versus 20.7 for the laser method). The presented work showed the DEMs provided from photogrammetric is enable to do accurate estimation for RR and give good estimation for the MDS, so it be can be useful in erosion and hydraulic studies.

Keywords:

Photogrammetry, Laser Roughness-Meter, Random Roughness, Digital Elevation Model, Maximum Depression Storage.

بسمعه تعالی
برگه مشخصات مقاله
عنوان
بررسی دو روش فتوگرامتری و زبری سنج لیزری به منظور اندازه گیری میکروتوپوگرافی خاک

محمد رضا میرزایی[1،2]، استفان قوی[2]، غلامرضا قضاوي[3]، کریستینا بونر[4]

[1] دانشگاه یاسوج، ایران

[2] دانشگاه اوینیون- انستیتو ملی تحقیقات کشاورزی مرکز اوینیون، آزمایشگاه مکانیك خاك

Email: mmirzaei@inra.avignon.fr

Adresse : **INRA - Unite Climat, Sol et Environnement**

Domaine St Paul – Agroparc 84 914

Avignon Cedex 9 FRANCE

Tel: +33 (0)4 32 72 22 16 Fax: +33 (0)4 32 72 22 12

[3] دانشگاه شیراز، ایران

[4] دانشگاه اوینیون (فر انسه)– دانشگاه بایروت (آلمان)

بررسی دو روش فتوگرامتری و زبری سنج لیزری به منظور اندازه گیری میکروتوپوگرافی خاک

چکیده

اساس کار ارائه شده بر مبنای تهیه یک مدل رقومی زمین (DEM) در دو ماکت با ابعاد 50×50 سانتی متر و با شرایط زبری متفاوت (زبری تند و زبری ملایم) می باشد. برای تهیه DEM از دو روش زبری سنج لیزری و فتوگرامتری استفاده شد. تصاویر فتوگرامتری در دو تکرار و در تاریخ‌های متفاوت بدست آمد. روش لیزری با داشتن صحت و دقت بسیار بالا به عنوان روش شاهد به منظور ارزیابی روش فتوگرامتری در نظر گرفته شد و سپس این دو روش با استفاده از پارامترهای مختلف آماری و خصوصیات خاک نظیر هیستوگرام‌های شیب و ارتفاع مورد مقایسه قرار گرفتند. در نهایت با استفاده از مدل‌های رقومی زمین دو روش میزان ضریب زبری تصادفی (RR) و حداکثر نگهداشت سطحی خاک تعیین شد. RR عنوان نماینده میکروتوپوگرافی سطح خاک و یکی از عوامل کلیدی در بسیاری از فرآیندهای هیدرولیکی و فرسایش مورد مطالعه قرار گرفت. میزان خطای RR محاسبه شده بوسیله روش فتوگرامتری در مقایسه با لیزری بطور متوسط 10 درصد در ماکت با زبری پایین و 5 درصد در ماکت با زبری بالا می‌باشد. این میزان خطا در محاسبه حداکثر نگهداشت سطحی (MDS) بین 2 تا 34 درصد یعنی حداکثر حدود 0/17 میلی‌متر تغییر می‌کند. در این تحقیق روش، فتوگرامتری مدل رقومی با شیب ملایم‌تری برای ماکت با زبری بالا در مقابل لیزری (یعنی بطور متوسط حدود 40/5 در برابر 46 درجه برای لیزری) و شیب تندتری برای ماکت با زبری پایین (متوسط23/5 در مقابل 20/7 برای لیزری) ارائه داده است. نتایج این تحقیق نشان می‌دهد که روش فتوگرامتری روشی مناسب برای تخمینی با دقت کافی از میزان RR و تخمین مناسبی از میزان MDS می‌باشد.

واژه های کلیدی

فتوگرامتری، زبری سنج لیزری، زبری تصادفی، مدل رقومی زمین

مقدمه

اثرات مخرب رواناب و فرسایش خاک حاصل از آن یکی از تهدیدات محیط زیستی در دنیا و در ایران به شمار می روند و به منظور کاهش اثرات منفی آنها شناخت فرآیند ایجاد رواناب و نحوه پراکنش آن مهم می‌باشد. زمانی که مکانیسم اصلی ایجاد رواناب از نوع هورتونی (رواناب ایجاد شده به وسیله آب مازاد بر نفوذپذیری) باشد، کنترل و هدایت رواناب سطحی به طور مستقیم به وسیله میکروتوپوگرافی سطح خاک صورت می‌گیرد.

زبری سطح خاک همان میکروتوپوگرافی و توزیع مکانی بلندی‌های سطح خاک در مقیاس سانتی‌متر تا دسی‌متر می‌باشد، البته در این مقاله دو کلمه معادل هم استفاده شده است. به طورکلی می‌توان دو نوع زبری عمده را تشخیص داد: 1- زبری جهتدار[1] که بر اثر شیب زمین یا نوع کاربری و یا تیماری که به وسیله وسایل کشاورزی صورت می‌گیرد، ایجاد می‌شود و 2- زبری تصادفی[2] که بر اثر توزیع ذرات و ریزدانه‌های خاک بر روی یک سطح صاف می‌باشد (1 و 7).

به نظر می‌رسد این فاکتور از دو جنبه مورد بررسی قرار گرفته است: 1- اثر توپوگرافی (اصطکاک) بر روی سرعت جریان آب که عموما با ضرایبی چون مانینگ و یا شزی تفسیر می‌شود. 2- اثر آن بر روی نحوه ایجاد رواناب که در این بخش عموما زبری نماینده میزان ظرفیت نگهداشت سطحی در خاک می‌باشد و بنابراین در بعضی از مدل‌های رواناب و فرسایش مورد استفاده قرار گرفته است. معمولا در این مدلها از یکسری روابط تجربی برای تعیین ظرفیت نگهداشت سطحی استفاده می شود.

در واقع میزان زبری سطح خاک به طور همزمان بر روی میزان ذخیره چالابی و میزان نفوذپذیری تاثیر می‌گذارد به طوری که جریان کلی نفوذپذیری بستگی به ارتفاع آب در سطح خاک دارد و در نتیجه قابلیت نفوذپذیری خاک بستگی به میزان آب ذخیره شده در داخل چاله‌ها دارد(4). بنابراین با تعیین پر و خالی شدن چاله‌ها موجود در سطح خاک و ارتباط بین آنها؛ زمان پیدایش رواناب قابل پیش‌بینی خواهد بود ولی رسیدن به این هدف نیازمند توسعه و بهینه‌سازی وسایل اندازه‌گیری (مانند لیزرسنجها و یا تجهیزات مورد استفاده در روش فتوگرامتری) موجود می‌باشد.

روشهای اندازه‌گیری زبری خاک با استفاده از زبری‌سنجها را می‌توان در دو کلاس بزرگ دسته‌بندی کرد: 1- روشهای تماسی[3] که در آنها وسایل مکانیکی (مانند میله‌های که بر روی یک قالب با فواصل مساوی و معین نصب شده است) به طور مستقیم با خاک تماس برقرار می‌کنند. یکی از نارساییهای اصلی این وسایل تغییر سطح خاک بر اثر تماس دستگاه، زمان مورد نیاز برای جمع آوری داده‌ها و دقت کار می‌باشد. از این گروه می‌توان پروفیل متر سوزنی (15) و یا روش استفاده از زنجیر ارائه شده توسط صالح (22) را نام برد. 2- روشهای

[1] Oriented roughness
[2] Random Roughness
[3] Contact methods

غیرتماسی[4] که وسایل اندازه‌گیری از سطح خاک فاصله داشته و با سطح خاک تماسی ندارند. اساس این روش‌ها بر دریافت امواج منعکس شده و امواج برگشتی می‌باشد. این علائم می‌تواند یک منبع اشعه مادون قرمز(21)، یک منبع ماورای صوت (20) و یا یک دسته اشعه لیزر (23، 24، و 3) باشد. این نوع از زبری‌سنجها بر عکس زبری‌سنجهای تماسی، بایستی واسنجی شوند. معمولا برای تعیین مدل رقومی زمین از سطح یک خاک، باید ارتفاع نقاط را در ترانسکت‌های نزدیک به هم برداشت کرد.

به علت این‌که میزان نفوذپذیري قابل کنترل نمی‌باشد، هنوز هیچ روشی برای اندازه‌گیری مستقیم میزان واقعی نگهداشت سطحی (آب داخل چاله‌ها) وجود ندارد. با توجه به روش‌های موجود، تنها متغیر قابل دسترسی، میزان ظرفیت نگهداشت سطحی می‌باشد. گروهی از محققان با ارائه روابط آماری و با استفاده از شاخص‌های متفاوتی و در بعضی موارد، یک‌سری پارامترهای خارجی مانند شیب زمین سعی در برآورد ظرفیت نگهداشت سطحی داشته‌اند(2،18،14 و 23). این روش‌ها علی‌رغم تعیین نتایج نسبتا مناسب،در دامنه‌ای خارج از داده‌های مورد استفاده برای تعیین رابطه اولیه، دارای دقت کافی نیستند(14). معمولا استفاده از الگوریتم‌های پرکردن (چاله‌های موجود در سطح خاک به صورت تدریجی پر می‌شوند و سپس چاله‌های پر شده سطح زمین با هم ادغام شده و به ترتیب چاله‌های بزرگتر پر می‌گردند) و یا الگوریتم‌های خالی کردن مدل رقومی زمین (در این روش تمامی مدل رقومی زمین تا بالاترین ارتفاع یا قله موجود، از آب پر می‌شود و سپس با خالی کردن تدریجی آب نهایتا مدل رقومی بدون چاله تعیین می‌گردد) به عنوان نماینده میکروتوپوگرافی زمین روشی مناسب جهت برآورد ظرفیت نگهداشت سطحی می‌باشد (3،8 ،17 و24).

از طرف دیگر میزان ظرفیت نگهداشت سطحی یک متغیر ثابت می‌باشد که برای تخمین میزان رواناب در مقیاس کوچک ناکافی است. در واقع حداکثر نگهداشت سطحی است که معمولا در مدل‌های هیدرولوژیکی بکار گرفته می‌شوند(12)، که این متغیر با مدل‌های محلی[5] (در مقیاس کوچک) پیدایش رواناب سازگار نمی‌باشد، زیرا در این مقیاس ممکن است رواناب قبل از رسیدن به حداکثر نگهداشت سطحی، شروع شود(10، 14 و 16).

تکنیک‌های تصویربرداری مانند فتوگرامتری روش‌های کاملا جدیدی می‌باشند. مقالات اندکی نیز در این مورد انتشار یافته است و در این اواخر توجه زیادی را به خود جلب کرده است (5، 11 و 23). زریبي (26) در یکی از حوزه‌های آبخیز پاریس، استفاده از دوربین‌های انعکاسی رقومی را برای بررسی کردن تغییرات میکروتوپوگرافی یک خاک لسی آزمایش کرده است. این کار تحت شرایط چند بارندگی صورت گرفته است. الگوریتم اجرایی به صورت اتوماتیک می باشد اما نقاط متناظر مربوط به واسنجی هنوز هم باید با دست وارد شود. فتوگرامتری همچنین به صورت یک وسیله استخراج اطلاعات مربوط به ژئومورفولوژی بکار رفته است. گاسکوئل _اودو و برونو (6) یک کارتوگرافی از چاله‌های کوچک[6] بین ردیف‌های یک کشت ذرت انجام داده‌اند و نقش آنها را در هدایت رواناب سطحی مشخص شده است.

---

[4] Noncontact methods
[5] Local model
[6] microdepression

اصولا در مورد تمرکز رواناب و فرسایش باید آنها را در مقیاسهای بزرگی مانند کرتهای کشاورزی و یا در مقیاس حوزه آبخیز انجام داد. اما در مورد مطالعه نحوه ایجاد رواناب این کار باید در مقیاس کوچک (چند متر مربع) صورت بپذیرد. در حقیقت در این مقیاس است که فرآیندهای اساسی و اولیه پیدایش رواناب شکل می‌گیرد.

به منظور توسعه یک مدل سه بعدی نفوذپذیری-رواناب، نیاز به توسعه یک متدولوژی برای تعیین میزان نگهداشت سطحی و نحوه تغییرات زمانی میکروتوپوگرافی می‌باشد و برای این هدف نیاز به تهیه مدل رقومی زمین می‌باشد. از بین روشهای موجود جهت تهیه مدل رقومی زمین، روش لیزری روش مرسومی است که نیاز به تنظیم بسیار دقیق داشته و به همین دلیل استفاده از آنها بر روی سایت مطالعاتی در خارج از آزمایشگاه بسیار محدود است. روشی که به تازگی برای مطالعه فرآیند نفوذپذیری و رواناب استفاده می‌شود، روش فتوگرامتری یا فتوگرامتری می‌باشد، و هدف از انجام این تحقیق بررسی دقت و کارائی این روش می‌باشد.

مواد و روشها

شکل 1: ماکت‌های استفاده شده در تحقیق ، ماکت سمت راست با زبري بالا، و سمت چپ بازبري پايين

شکل 2: لیزر سنج بکار گرفته شده در تهیه داده های لیزری (13)

در این تحقیق از دو ماکت (شکل 1) استفاده شد که دارای دو بافت زبری متفاوت (زبری بالا و ملایم) می‌باشند. نحوه ساخت این ماکتها توسط کامفورست و دوال (13) شرح داده شده است. ابتدا با استفاده از روش‌های زبری سنج لیزری و فتوگرامتری مدل رقومی زمین بدست آمد. سپس از روش لیزری به عنوان روش مرجع، برای سنجش دقت مدل رقومی زمین بدست آمده از روش فتوگرامتری استفاده شد. به این منظور از فاکتورهای متفاوتی همچون مقایسه مستقیم بر روی ترانسکت‌ها، هیستوگرام‌های ارتفاع و شیب استفاده شد.

در نهایت با استفاده از دو روش، شاخص‌های زبری تصادفی (RR) و حداکثر نگهداشت سطحی (به عنوان نماینده خصوصیات سطحی خاک) تعیین شدند. سپس با مقایسه نتایج دو روش، کیفیت روش فتوگرامتری در تعیین این خصوصیات مورد بررسی قرار گرفت.

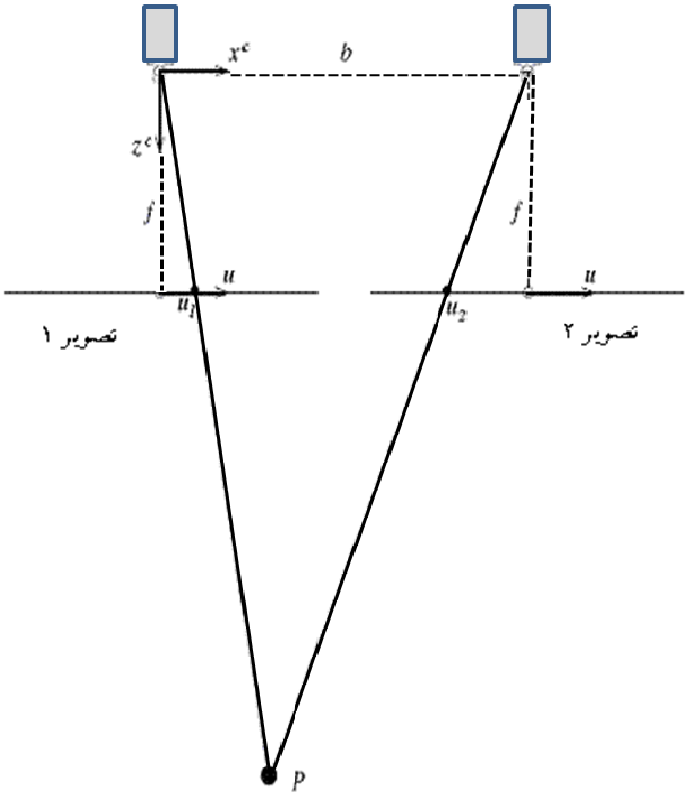

3

2

3

$$d = (u_1 - u_2) = \frac{f.b}{z^c}$$

که در آن d: اختلاف مکان قرار گرفتن دو نقطه متناظر در دو تصویر[7] ؛ Zc: ارتفاع نقاط؛ f: فاصله کانونی دوربین؛و b: فاصله بین دو دوربین از هم می‌باشد. بنابراین برای بدست آوردن ارتفاعات باید قادر به تعیین میزان d برای هر پیکسل بوده که خود وابسته به پارامترهای داخلی وخارجی دوربین می‌باشد و برای این هدف باید واسنجی دوربین صورت گیرد.

به طور خلاصه فتوگرامتری در چهار مرحله اصلی صورت گرفت: 1- مرحله واسنجی دوربین‌های مورد استفاده در استرئوگرافی (دید سه بعدی) و تعیین پارامترهای دوربین. در این مرحله تعدادی عکس (شکل 4) از صفحه واسنجی گرفته شد. این صفحه با دقت بسیار بالایی تهیه و مختصات نقاط آن کاملا تهیه شد. 2- عکس‌ها از شئ مورد نظر بدست آمد. تصاویر استرئو به وسیله یک جفت دوربین واسنجی شده بدست می‌آید. 3- بعد از بدست آوردن تصاویراسترئو، تصاویر اصلاح شدند؛ به صورتی‌که نقاط متناظر در دو تصویر اصلاح شده، بر روی همان ردیف همسان قرار گیرند.4- مرحله آخر بدست آوردن اطلاعات سه بعدی می‌باشد. برای هر نقطه موجود در تصویر اول نقطه متناظر آن در تصویر دوم بدست آمد که با بدست آوردن جابجایی نقاط[1] می‌توان میزان فاصله شئ را از دستگاه مختصات دوربین‌ها بدست آورد.

نکته قابل ذکر این است که در مرحله (1) و (2) که عکسبرداری صورت می‌پذیرد، رعایت بعضی نکات ضروری می‌باشد مانند این‌که هیچ گونه تغییری نباید در خصوصیات دوربین مانند سرعت شاتر و دیافراگم و فاصله کانونی بوجود آید.

با توجه به موارد ذکر شده در بالا، بدست آوردن تصاویر مناسب (دارای وضوح و نوردهی مطلوب) دارای اهمیت بسیاری می‌باشد که برای بررسی این موضوع تحقیق دیگری (25) بر روی نحوه عکسبرداری و استفاده از پارامترهای مناسب داخلی صورت گرفت. برای تهیه تصاویر دوربین‌ها برروی یک نگهدارنده نصب شد.

ساخت نگهدارنده دوربین:

به منظور نصب دوربین‌ها به‌صورت ثابت و عمودی، یک تکیه‌گاه در انستیتو ملی تحقیقات کشاورزی فرانسه (INRA) در شهر اوینیون ساخته شد که تصویر آن در شکل (شکل 4) آمده است. در طراحی و ساخت تکیه‌گاه دوربین‌ها، موارد متعددی (مانند تنظیم فاصله بین دوربین‌ها، دقت در ساخت محل نصب دوربین‌ها جهت عمودی قرار گرفتن محور اپتیکی دوربین، و قرار دادن تنظیم کننده‌های زاویه برای دوربین‌ها، حداکثر همپوشانی 1/8× 1/8 متر، استحکام تکیه‌گاه) در نظر گرفته شد.

خصوصیات دوربین:

تصاویر با استفاده از دوربین‌های دیجیتالی D100 مارک Nikon با فاصله کانونی 35 میلی‌متر تهیه شد. دوربین‌ها نیز در فاصله نسبی 40 سانتی‌متری و

[7] Disparity

ارتفاع حدود 3/4 متری سطح زمین قرار گرفتند.

تهیه مدل رقومی با استفاده از فتوگرامتری:

به طور کلی دو عکسبرداری در دو تاریخ متفاوت از دو ماکت صورت گرفت. در یک قسمت برای بررسی اینکه آیا روش فتوگرامتری را میتوان تحت شرایط بارندگی نیز استفاده کرد، با دست مقادیر مشخصی آب به ماکت اضافه گردید. این عمل

شکل 4: تکیه گاه و وسایل مورد استفاده در این روش

جدول 1: میزان خطای متوسط مجموع خطا (به میلی متر) در جهت x، y، z در عملیات انتقال سیستم مختصات مدل رقومی بدست آمده از روش فتوگرامتری به روش لیزری

عکسبرداری اول		عکسبرداری دوم	
زبري بالا	زبري پايين	زبري بالا	زبري پايين
1/34	1/62	1/24	1/114

برای بررسی عملکرد روش فتوگرامتری در صورت وجود آب در داخل چاله‌ها صورت گرفت. برای تهیه مدل رقومی زمین از نرم افزار پردازش تصویر Halcon تحت لیسانس اینرای اوینیون استفاده شد. با انجام برنامه نویسی در این نرم‌افزار برای مراحل (3) و (4) فتوگرامتری (رجوع شود به قسمت فتوگرامتری) ارتفاع نقاط برای هر پیکسل بدست آمد. در فایل خروجی مختصات نقاط در فواصل منظم نمی‌باشد؛ که علت آن اصلاحات انجام شده بر روی تصویر[8] در اثر اعوجاج[9] تصویر در مرحله (3) و انتخاب دفتی کمتر از اندازه پیکسل[10] می‌باشد. داده‌های ارتفاعی بدست آمده، به طور مستقیم و بدون هیچگونه پردازش، حذف و یا اصلاح برای مقایسه با روش لیزری استفاده شدند.

نتایج:

آماده سازی داده‌ها:

برای مقایسه مدل‌های رقومی بدست آمده در اولین قدم باید هر دو برداشت دارای دیمانسیون، دستگاه مختصات یکسان و اندازه پیکسل یکسان باشند. به این منظور، تمامی داده‌های مختصاتی به مقیاس میلی‌متر در آمدند و سیستم مختصات مدل رقومی روش فتوگرامتری به روش لیزری انتقال یافت. برنامه‌ای برای اینکار به زبان R نوشته شد. چهار گوشه داخلی ماکتها به عنوان نقاط مشخص در نظر گرفته شد. سپس با حداقل کردن متوسط خطاها، میزان پارامترهای انتقال و چرخش محورهای مختصات برای هر مدل رقومی بدست آمده از روش فتوگرامتری محاسبه گردید(جدول 1). با توجه به RMSE بدست آمده حداکثر خطا 1/4 و حداقل آن 1/1 میلی‌متر می‌باشد. با توجه به اینکه این خطا مجموع قدرمطلق در سه جهت x، y و z می‌باشد خطای قابل قبولی به حساب می‌آید. با استفاده از میانیابی اندازه پیکسل داده‌های ارتفاعی محاسبه شده با روش فتوگرامتری به لیزری یعنی 2 میلی‌متر تغییر یافت.

در مرحله آخر آماده سازی داده‌ها، کادر اطراف مربوط به ماکتها برداشته شد. تمامی مراحل و تصویرها به وسیله برنامه نویسی در R بدست آمده است. به منظور جلوگیری از خطای بوجود آمده بوسیله سایه کادرها بر روی منطقه و زاویه دید، منطقه اصلی برای مطالعه منطقه میانی ماکتها بین 5 تا 500 سانتی متر در نظر گرفته شد.

مقایسه مدل‌های رقومی بدست آمده:

با رسم مدل کلی سطح (شکل 5) مشاهده می‌شود که روش فتوگرامتری توانسته است شکل عمومی زمین، ریزدانه‌ها و کلوخه‌ها بخصوص برجستگی‌های اصلی را مشخص کند، اما در تعیین شکل کامل، ریزدانه‌های کوچک و مخصوصا در حاشیه‌ها، دارای بی‌نظمی‌هایی می‌باشد. از دلایل این امر می‌توان به نیافتن نقاط متناظر در حین روش فتوگرامتری و یا انجام میانیابی و حتی انتقال محورها باشد. از طرفی به همین علت به نظر میرسد که فتوگرامتری دارای سطح ملایمتری نسبت به

[8] Image Rectifying
[9] Distortion
[10] Sub-pixel precision

11

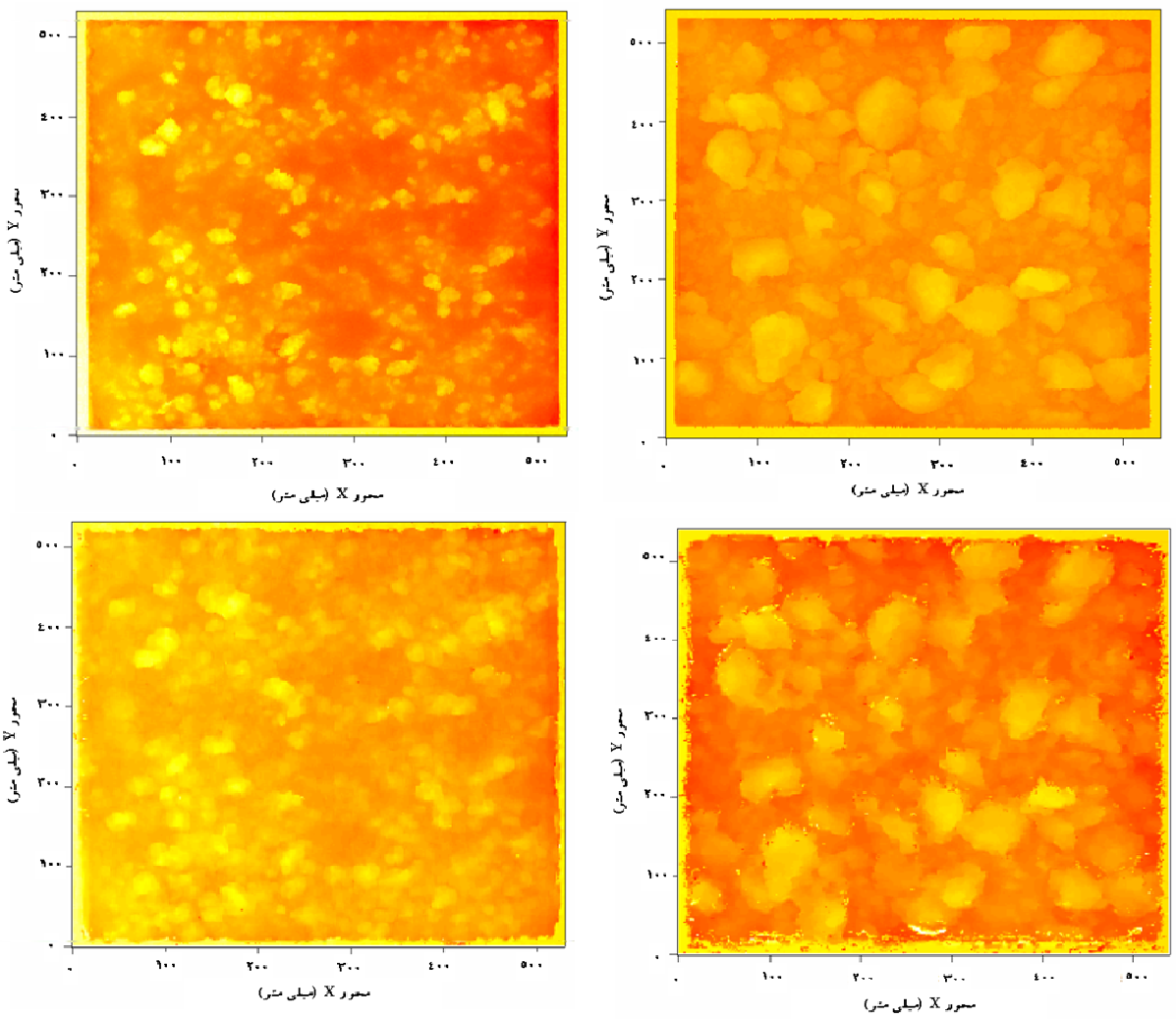

5

2

	/ / - / - / /
	/ - / - / - / / -

[11] Ponded Area

/ / - / - / / / - / - / - / / / -	
/ / - / - / / / - / - / - / / / -	

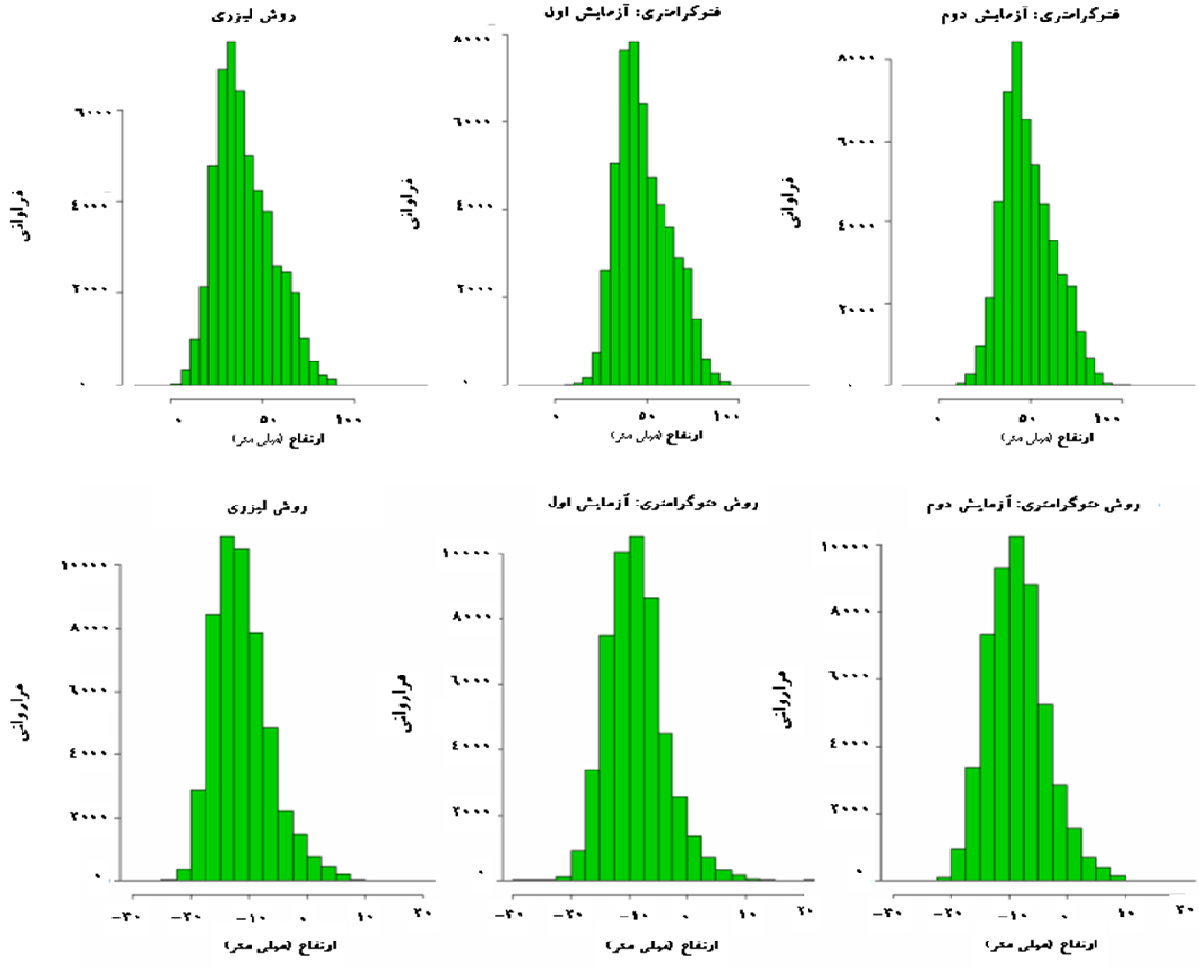
فتوگرامتری: آزمایش دوم
فتوگرامتری: آزمایش اول
روش لیزری
روش فتوگرامتری: آزمایش دوم
روش فتوگرامتری: آزمایش اول
روش لیزری
فراوانی
ارتفاع (میلی متر)

6

(

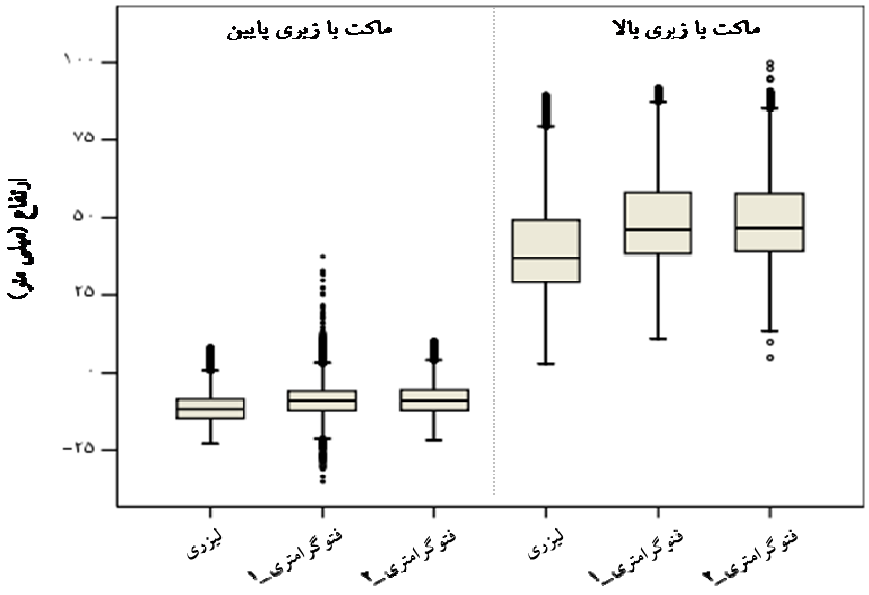
ماکت با زیری پایین
ماکت با زیری بالا
ارتفاع (میلی متر)
۱۰۰
۷۵
۵۰
۲۵
۰
-۲۵
لیزری
فتوگرامتری_۱
فتوگرامتری_۲
لیزری
فتوگرامتری_۱
فتوگرامتری_۲

7

R

6

7

3

			-	-	-		
	-	-	-	-	-		
			-	-	-		

(جدول 3) مشاهده می‌شود چولگی دارای مقدار عددی بالاتری در روش لیزری می‌باشد. در هر صورت این این اعداد نسبتا به یکدیگر نزدیک می‌باشند. روش فتوگرامتری دارای دامنه اعداد بالاتر (حدود 15- تا 130 میلی‌متر در مقابل 3/4- تا 90 میلی‌متر برای لیزری) و انحراف معیار پایین‌تری (حدود 14/3 در مقابل 15/3 برای لیزری) می‌باشد. جستر و کلیك (11) با مقایسه دو روش نشان داده‌اند که انحراف معیار در روش فتوگرامتری افزایش یافته است. در هر سه مورد(روش لیزری و دو تکرار فتوگرامتری) میزان میانگین با میانه آن تفاوت معنی‌داری نشان نداد. اما از طرف دیگر میزان میانگین به ترتیب برای روش لیزری و دو تکرار فتوگرامتری 39/7، 48/55 و 48/68 میلی‌متر می‌باشد که نشان می‌دهد در حدود یک سانتی‌متر تفاوت بین روش فتوگرامتری و روش لیزری فاصله وجود دارد. بین دو تکرار تفاوتی دیده نشد.

در مورد ماکت با زبری ملایم نیز توزیع مناسب ارتفاعات در گروه‌های متفاوت به دست آمد. انحراف معیار حاصل از دو روش نزدیک بوده و در روش فتوگرامتری مقدار کمی بالاتر (حدود 5 در برابر 4/87) است. میانه و میانگین نسبتا برابر بوده ولی در اینجا نیز میزان میانگین در روش فتوگرامتری حدود 3 میلی‌متر بیشتر تخمین زده شده است. به طورکلی با توجه به توزیع داده‌ها در کلاسهای مختلف می‌توان گفت که در این ماکت میزان همخوانی ارتفاعات بیشتر می‌باشد. در هر دو نوع ماکت مورد نیز اندازه پلات باکسها تقریبا در یک حدود می‌باشد. نکته جالب توانایی روش فتوگرامتری در تشخیص این دو نوع زبری از هم می‌باشد (شکل 7).

بررسی هیستوگرام‌های شیب:

همانطور که در هیستوگرام‌های شیب (شکل 8) و پلات باکسهای (شکل 9) مربوطه دیده می‌شود، مقایسه شیب می‌تواند اختلاف دو روش را بهتر از مقایسه ارتفاعها نشان دهد.

جدول 4 آمار توصیفی مربوط به دو روش را نشان میدهد. در مورد ماکت‌هایی با زبری بالا میزان انحراف معیار دو تکنیک بسیار نزدیک به هم بوده (حدود 19/7) اختلافی در حد چند صدم نشان داد. با مقایسه میانگینها و میانه ها در دو تکنیك ليزري (ميانگين 46 و ميانه 46/7) و فتوگرامتراي (ميانگين حدود 41 و ميانه حدود 40)، مشاهده مي‌شود كه در تكنيك ليزري ميانگين شيبي كوچكتر از ميانه است كه نشان دهنده مقداري چولگی به سمت راست (تمايل به شيبهاي بالاتر از 46 و مقدار چولگی 0/14-) مي‌باشد. بالعكس آن، در روش فتوگرامتری ديده مي‌شود كه چولگی افزايش يافته كمي به سمت چپ (تكرار اول 0/13 و دوم 0/14) يعنی شيب‌های پايين دارد. از طرف ديگر ميانگين شيب ليزري در حدود 6 درجه بالاتر مي‌باشد كه به خوبی در پلات باكسها (شكل 9) مشخص است. با مقايسه بالا اين نتيجه عايد مي‌شود كه شيب فتوگرامتري حالت ملايمتری دارد. يعني از فراوانی شيبهاي تند كم شده به فراوانی شيبهاي پايين‌تر افزوده شده است. اختلاف در هيستوگرامها هم بيشتر به شيبهاي بالا مربوط مي‌شود، در هيستوگرام، روش ليزري شيب تندي را در قسمت سمت راست نشان می‌دهد در حاليكه در روش فتوگرامتري اين شيب تعديل شده است.

در مورد ماكتها با زبری پايين (شكل 8 قسمت پايين)، به طور كلي روش ليزري داراي ميانگيني كمتر (20/7) نسبت به فتوگرامتری (تكرار اول 26 و دوم

-

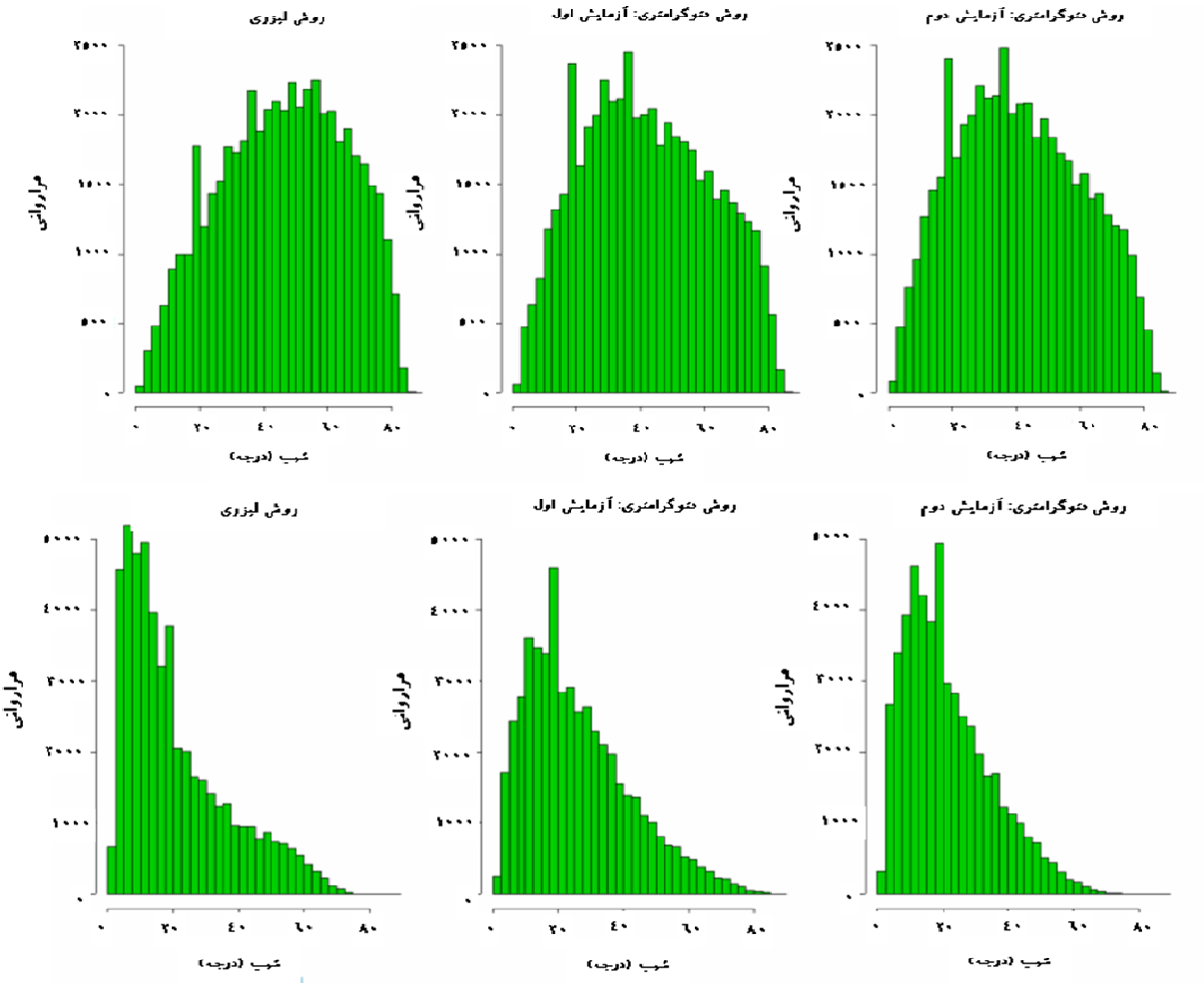
روش لبزوی
روش دئوگرامتری: آزمایش اول
روش دئوگرامتری: آزمایش دوم
فراوانی
شب (درجه)

8

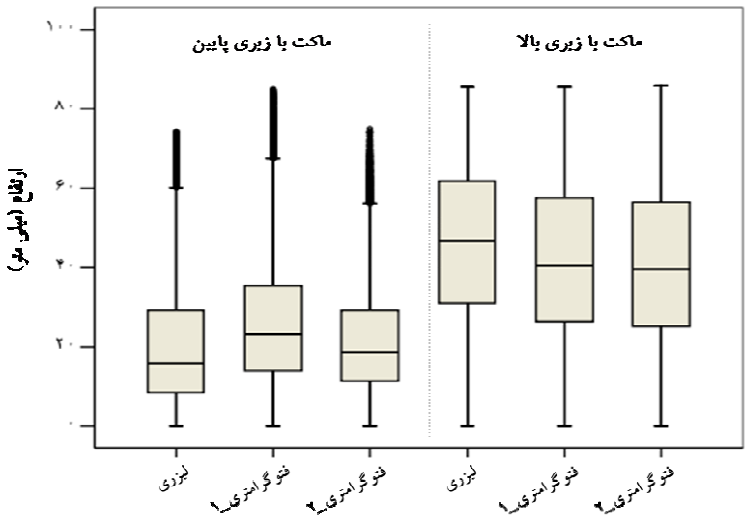
ماکت با زیری پایین
ماکت با زیری بالا
ارتفاع (میلی متر)
۱۰۰
۸۰
۶۰
۴۰
۲۰
۰
لیزری
فتوگرامتری_۱
فتوگرامتری_۲
لیزری
فتوگرامتری_۱
فتوگرامتری_۲

9

4

-		

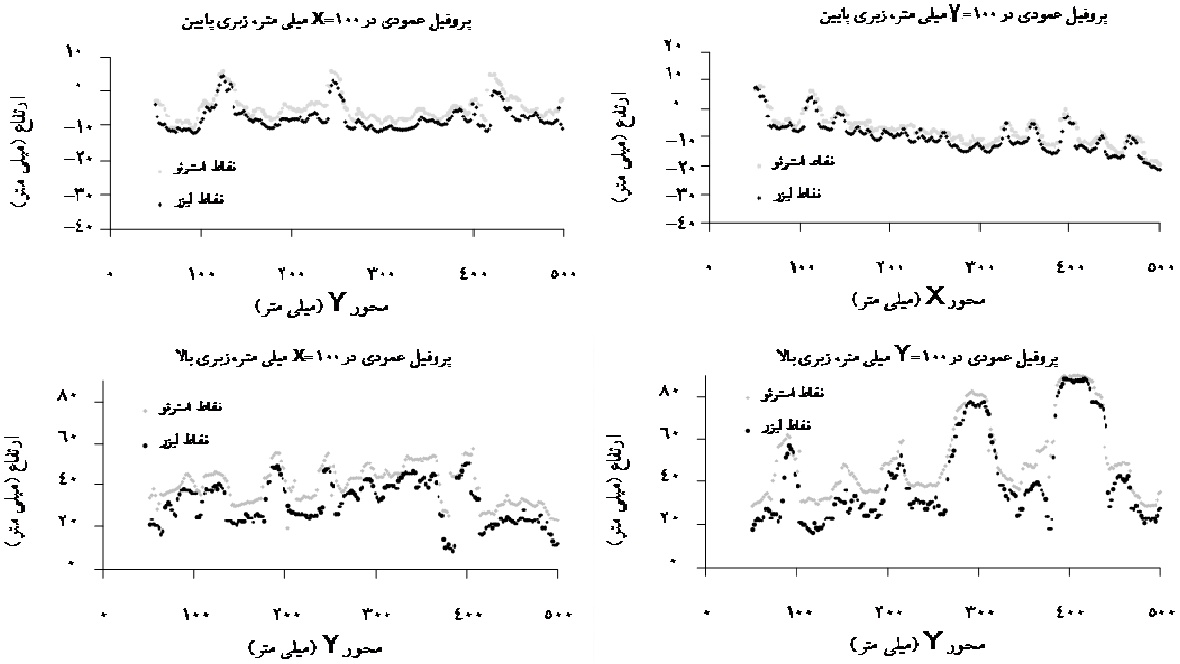

y x **10**

7

2

10

10

11

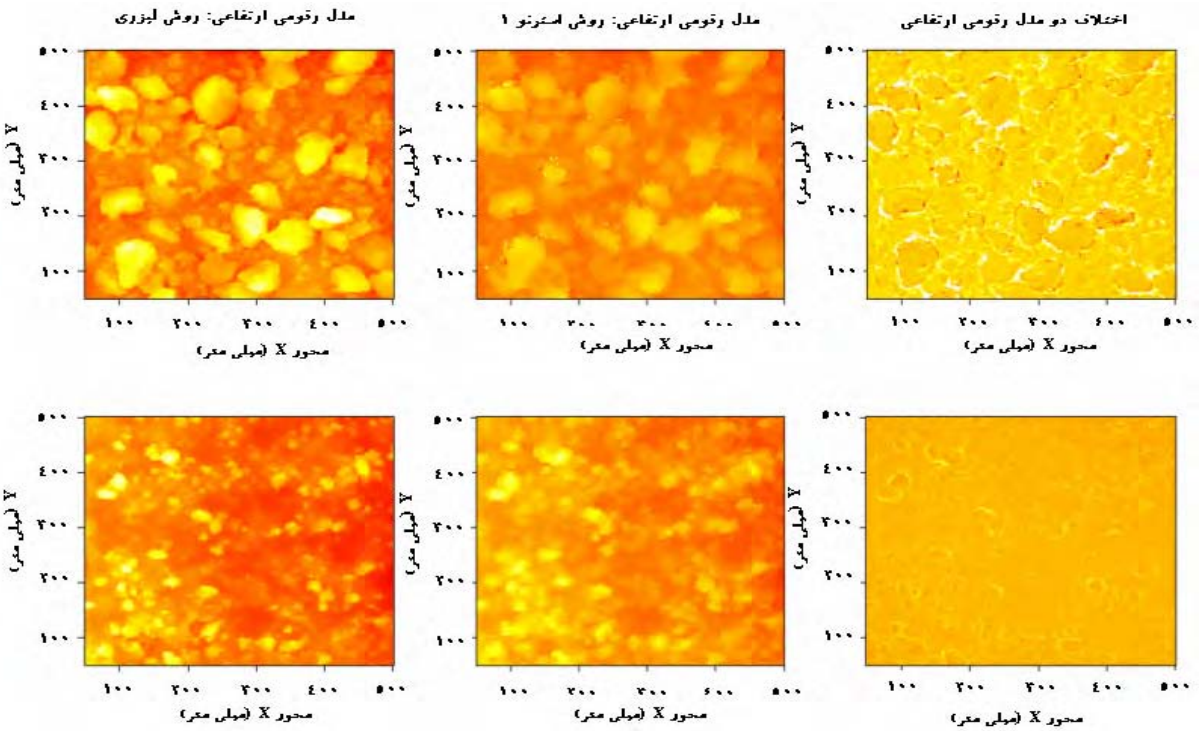

شکل 11: نمایش منطقه کار در هر دو ماکت و تفاضل مدل رقومی زمین دو روش فتوگرامتری و روش لیزری در دو ماکت با زبری بالا (تصویر بالا) و زبری پایین (تصویر پایین)

وجود این خطای سیستماتیک، خطا در انتقال سیستم مختصات را می‌توان نام برد که به علت تعداد پایین نقاط متناظر و همچنین قرار داشتن آنها در ارتفاع نسبتا برابر می‌باشد. با دقت در تصویر تفاضل دو روش فتوگرامتری و لیزری مشاهده می‌شود که اختلاف دو روش در حاشیه کلوخه‌ها و پستی و بلندیها بیشتر از سایر قسمتها می‌باشد و هر چه زبری شدیدتر باشد این اختلافات مشخص‌تر خواهد بود. این عمل بر روی تصاویر تکرار اول نیز انجام شد که در عمل همین نتیجه گرفته شد.

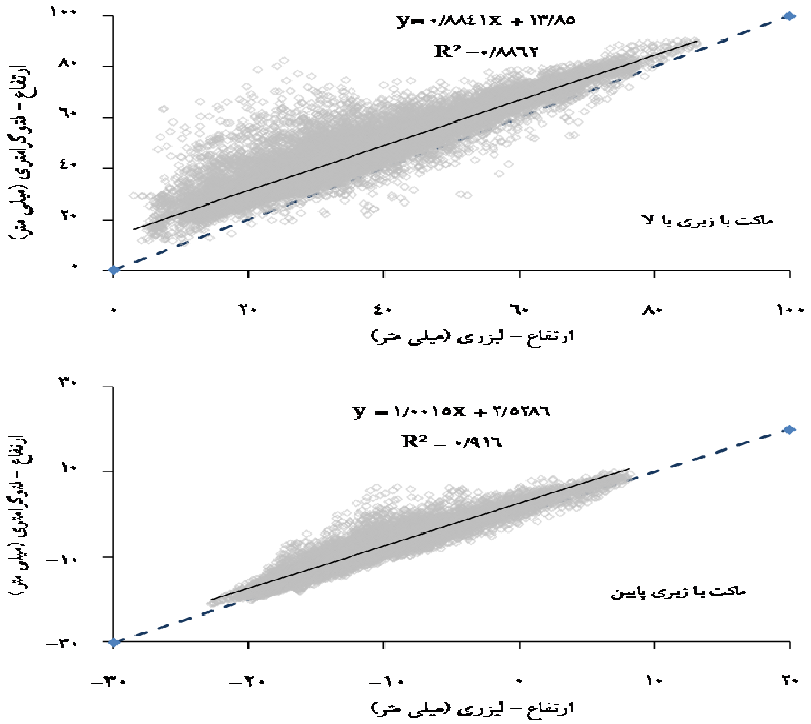

12 -

5

y= a+bx 6

	b	a		
		-		
		-		
		-		
		-		

12

با توجه به نتایج آنالیز انجام شده (جدول 5) با نرم افزار SPSS، مقدار سطح معنی‌دار بدست آمده بسیار کوچک می‌باشد که نشان دهنده همبستگی معنی‌دار در سطح 0/01 می‌باشد. همچنین میزان خطای استاندارد برای ضرایب معادله در مقایسه با خود ضرایب (جدول 6) مقادیر کمی را نشان می‌دهد که برای این ضرایب نیز سطح معنی‌داری کمتر از 0/01 می‌باشد. در شکل فوق می‌توان گفت که در مورد ماکت با زبری پایین‌تر همبستگی بیشتری وجود دارد. در هر صورت با توجه به ضرایب تعیین و آنالیز انجام شده می‌توان گفت این دو همبستگی بسیار مناسبی را به هم نشان می‌دهند. در صورت همبستگی 100 درصد و دقت و کامل تمام داده‌ها، باید بر روی خط 1 : 1 قرار گیرند. اما خط برازش یافته در هر دو مورد پایین‌تر از خط نقطه چین و تقریبا موازی (در جدول جدول 7 مقادیر شیب خطها بسیار نزدیک به 1 یعنی شیب خط 1:1 هستند) با آن قرار گرفته است. که می‌تواند تایید دوباره‌ای بر خطای سیتماتیک باشد.

با مقایسه‌ایی که انجام شد کیفیت روش فتوگرامتری در مقابل روش لیزری مشخص شد. در این مرحله برای پاسخ به این سوال که آیا با این روش می توان خصوصیات سطحی خاک را بدست آورد، ضریب زبری خاک به عنوان یکی از خصوصیات کلیدی خاک در فرآیند ایجاد رواناب و فرسایش آبی - بادی انتخاب شد. محققان زبری خاک را مترادف با میکروتوپوگرافی سطح خاک می‌دانند. برای تعیین ضریب زبری خاک از شاخص‌های متعددی استفاده می‌شود که در اینجا شاخص زبری تصادفی مورد مطالعه قرار گرفت.

مطالعه ضرایب زبری

شاخص زبری تصادفی را با RR نمایش می‌دهند واز این ضریب زبری به علت سادگی به طور گسترده استفاده می‌شود. تاکونت و سیارلتي (23) در تحقیق خود نقش کلیدی این فاکتور بر روی کنترل بسیاری از فرآیندهای هیدرولیکی و فرسایش در مقیاس مزرعه را مورد تاکید قرار داده‌اند.

نحوه تعیین این شاخص بر روی یک پروفیل ارتفاعی خاک به صورت زیر است(1) که در واقع همان انحراف معیار داده‌های ارتفاعی بر روی یک ترانسکت می‌باشد.

$$RR = \left[\frac{1}{n} \sum_{i=1}^{n} (z_i - \bar{z})^2 \right]^{1/2} \qquad (2)$$

که در آن zi: مقدار ارتفاع در هر نقطه و z، میانگین می‌باشد. این شاخص تنها زبری حاصل از نحوه قرار گرفتن تصادفی ریزدانه های خاک در کنار هم را نشان می‌دهد. به همین منظور ترانسکت‌های بسیاری در جهات مختلف X و Y تهیه شد. در جدول (جدول 7) میانگین بدست آمده در هر جهت ارایه شده است.

همانطور که مشاهده می‌شود در هر دو تکرار، و در هر دو ماکت جوابها بسیار به هم نزدیک می‌باشند که نشان دهنده این است که برای تعیین ضریب زبری می‌توان از این روش استفاده کرد. عدد 14/2 برای ماکت با زبری بالا در روش لیزری بوده که میزان محاسبه شده آن به روش فتوگرامتری به ترتیب 12/9 و 13/4 می‌باشد. به نظر می رسد مقدار برآورد شده از روش فتوگرامتری اندکی کمتر از مقدار برآورد شده از روش لیزری در ماکت بازبری بالا باشد. به طور کلی می‌توان گفت که در تمامی موارد در جهت y زبری بالاتری نسبت به x مشاهده می‌شود.

جدول 7: مقایسه ضرایب زبری بدست آمده با دو روش لیزری و فتوگرامتری در جهات مختلف

روش	ماکت با زبری بالا		ماکت با زبری پایین	
	محور افقي	محور عمودي	محور افقي	محور عمودي
لیزری	14/2	15	3/6	4/5
استرئو 1	12/9	14/6	4/2	5/5
استرئو 2	13/4	13/9	3/5	4/7

محاسبه حداکثر نگهداشت سطحی خاک (MDS):

دقیق‌ترین روش محاسبه حداکثر نگهداشت سطحی[12] خاک با استفاده از مدل رقومی دقیق از زمین می‌باشد. این‌کار با استفاده از الگوریتم های پر شدن چاله ها (13) و یا خالی کردن چاله ها (19) انجام مي پذيرد. در نرم افزارهای GIS معمولا از الگوریتم پرکردن و حذف چاله ها استفاده می‌کنند. در این تحقیق با استفاده از یک نرم افزار GIS برای هر مدل رقومی زمین، مدل رقومی بدون چاله آن نیز به دست آمد. در نهایت از تفریق این دو میزان مساحت منطقه آب گرفته شده و حداکثر نگهداشت سطحی تعیین شد. میزان MDS بدست آمده در روش لیزری به ترتیب برای ماکت با زبری بالا و پایین 0/78 و 0/23 بدست آمد. نتایج حاصل در جدول 8 آمده است.

محاسبه شده برای دو روش برای هر ماکت بر حسب میلی‌مترMDS: میزان 8جدول

روش / ماکت	لیزری	استرئو تکرار اول	استرئو تکرار دوم
زبری بالا	0/78	0/76	0/61
زبری پایین	0/23	0/31	0/25

با توجه به جدول 8 در ماکت با زبری بالا، میزان تغییرات چندان زیاد نمی‌باشد. در تکرار اول میزان MDS محاسبه شده دقیقا با روش لیزری یکسان بوده و در تکرار دوم حدود 20 درصد کمتر از میزان محاسبه با روش لیزری می‌باشد. در ماکت با زبری پایین نیز این میزان در ماکت دوم با روش لیزری یکسان بوده در حالیکه در تکرار اول در حدود 25 درصد بالاتر از میزان واقعی محاسبه شده است.

با توجه به نتایج می‌توان گفت که این روش توانسته است تا حدود زیادی میزان حداکثر نگهداشت سطحی را نزدیک به مقدار واقعی آن تعیین کند. برای درک علت این تغییرات میزان مساحت سهیم در ایجاد MDS با توجه به ارتفاع آنها مورد بررسی قرار گرفت که نمودارهای آن در شکل 12 ارائه شده‌اند. همانطور که در نمودار شکل 12 مشاهده می‌شود؛ در ماکت با زبری بالا و پایین به

[12] Maximum Depressional Storage

ترتیب 79 و 74 درصد از زمین فاقد چاله بوده و در تشکیل نگهداشت سطحی سهمی ندارند.

در ماکت با زبری بالا در تکرار دوم تعداد چاله‌هایی با ارتفاع پایین بالاتر و بالعکس فاقد چاله‌هایی با ارتفاع بالای 18 میلی‌متر می‌باشد که همین امر باعث تخمین کمتر از واقعیت گردیده است. در ماکت با زبری پایین نیز در تکرار اول به علت وجود چاله هایی با ارتفاع زیاد میزان MDS بیشتر ازمیزان واقعی تخمین زده شده است.

شکل 14 تفاوت بین عملکرد دو روش را روشن‌تر نشان می‌دهد. میزان حجم آب تجمع یافته در هر شش مورد در چاله‌هایی با ارتفاع پایین همپوشانی بسیار خوبی دارند. تفاوت در چاله هایی با ارتفاع بالاتر می‌باشد. در نمودار سمت چپ ماکت با زبری بالا در تکرار دوم (فقدان چاله هایی با ارتفاع بالا) و در نمودار سمت راست ماکت با زبری پایین تکرار اول (وجود چاله هایی با ارتفاع بالا) هر دو در قسمت انتهایی بیشتر ین اختلاف را با بقیه موارد دارند. چیزی که نیاز به مطالعه در موارد با زبریهای شدیدتر را نشان می دهد.

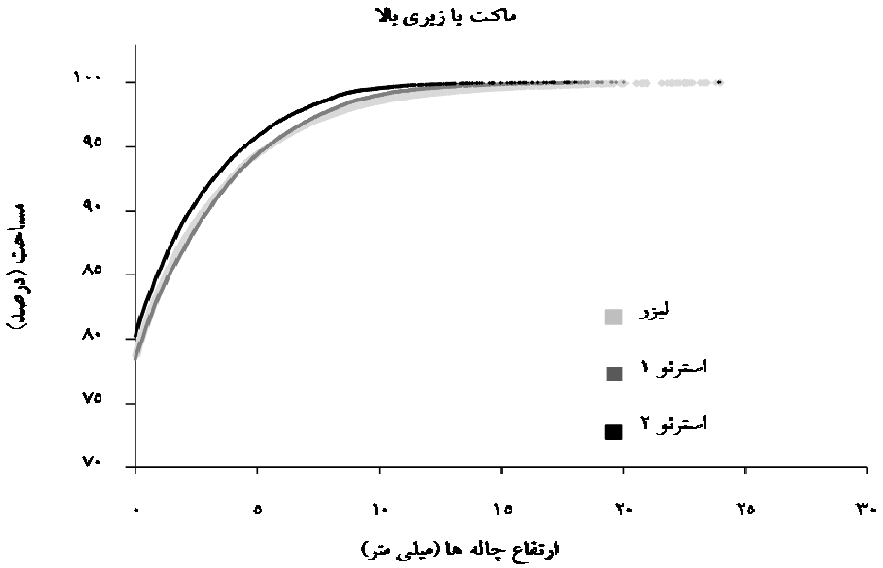
ماکت با زیری بالا
مساحت (درصد)
۱۰۰
۹۵
۹۰
۸۵
۸۰
۷۵
۷۰
۰
۵
۱۰
۱۵
۲۰
۲۵
۳۰
لیزر
استرئو ۱
استرئو ۲
ارتفاع چاله ها (میلی متر)

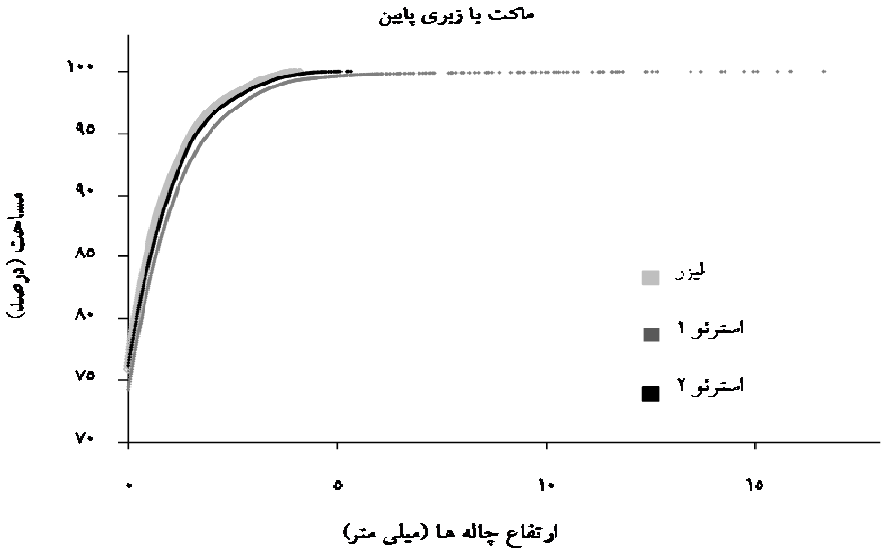
ماکت با زیری پایین
مساحت (درصد)
۱۰۰
۹۵
۹۰
۸۵
۸۰
۷۵
۷۰
۰
۵
۱۰
۱۵
لیزر
استرئو ۱
استرئو ۲
ارتفاع چاله ها (میلی متر)

13

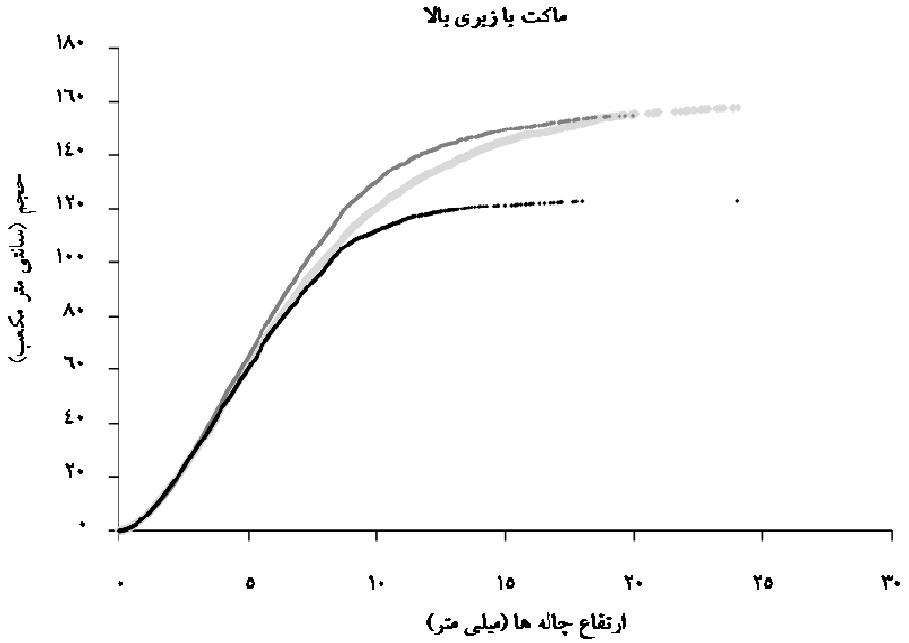
ماکت با زیری بالا
حجم (سانتی متر مکعب)
۱۸۰
۱۶۰
۱۴۰
۱۲۰
۱۰۰
۸۰
۶۰
۴۰
۲۰
۰
۰
۵
۱۰
۱۵
۲۰
۲۵
۳۰
ارتفاع چاله ها (میلی متر)

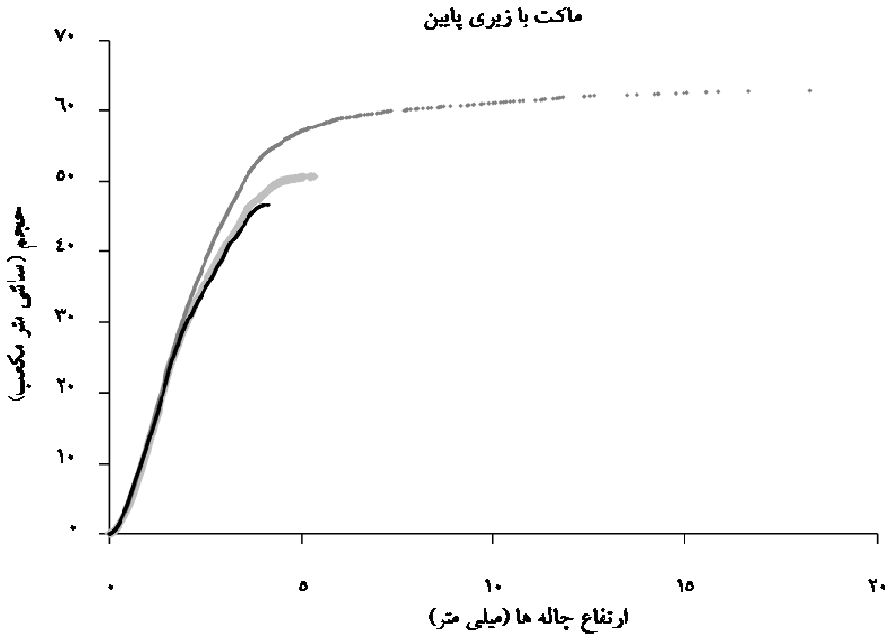
ماکت با زیری پایین
حجم (سانتی متر مکعب)
۷۰
۶۰
۵۰
۴۰
۳۰
۲۰
۱۰
۰
۰
۵
۱۰
۱۵
۲۰
ارتفاع چاله ها (میلی متر)

14

می‌توان جایگزین هم قرار دارد. از طرفی میزان نگهداشت سطحی نیز بسیار نزدیک به واقعیت می‌باشد. در این مطالعه بر خلاف اظهار جستر و کلیك (11) میزان نگهداشت سطحی در یک مورد 24 درصد بیش از میزان واقعی آن بدست آمد. علت اصلی تخمین بالا و یا پایین تر از میزان واقعی را می‌توان در تعداد چاله های با ارتفاع بالا مشاهده کرد.

هر کدام از این روشها دارای مزایای مربوط به خود می‌باشند. روش لیزری زمان زیادی می‌برد (به عنوان مثال برای یک ماکت 1 متر مربع در حدود 2 ساعت وقت نیاز است که البته با پیشرفتهای حاصل شده کمتر شده است) در حالی‌که روش فتوگرامتری روشی سریعتر می‌باشد. به عنوان نمونه ممکن است بتوان از این روش در حین بارندگی برای بررسی بیشتر فرآیند رواناب – نفوذپذیری و تغییرات آب نگهداشت سطحی استفاده کرد که به نظر می‌رسد تا کنون مقاله‌ای در این مورد ارائه نشده است. در هر دو روش داده‌ها بعد از برداشت باید پردازش شوند که زمان زیادی مخصوصا در روش فتوگرامتری می‌طلبد. استفاده از روش لیزری به‌صورت میدانی بسیار مشکل است در حالیکه روش فتوگرامتری را می‌توان در تمامی فضاها استفاده کرد.

در نهايت با توجه به نتايج اين تحقيق روش فتوگرامتري داراي دقت و صحت مورد نياز براي مطالعه خصوصيات سطحي خاك مي‌باشد كه تاييد كننده مطالعه تاكونه و سيارليتي (24) نيز مي‌باشد. البته به علت فقدان مطالعات گسترده در اين روش آناليز اين روش در حال حاضر ميسر نمي‌باشد و نياز به مطالعات بيشتر ي وجود دارد.

با توجه به اینکه در اکثر مطالعات نیاز به ارتفاع نسبی می‌باشد، نتایج بدست آمده رضایت بخش می‌باشد. البته احتمال داده می‌شود که خطای سیستماتیک موجود به علت ناکافی بودن نقاط شاهد می‌باشد. بنابراین در مطالعات بعدی بایستی تعداد نقاط کافی برای تمامی سطح با دقت بالا تعیین شود.

در آخر پیشنهاد می‌شود برای بررسی دقت این روش بر روی خاك لخت و پارامترهای مختلف خاك در مزرعه مورد آزمایش قرار گیرد. از طرف دیگر تاکنون این روش در شرایط بارندگی به منظور بررسي فرآیند تشکیل رواناب و فرسایش مخصوصا بررسی تغییرات نگهداشت سطحی در حین بارندگی مورد مطالعه قرار نگرفته است که زمینه مناسبی برای ادامه تحقیقات می‌باشد.

منابع

1- Allmaras, R.R., R.E. Burwell, W.E. Larson, and R.F. Holt. 1966. Total porosity and random roughness of the interrow zone as influenced by tillage. USDA Conservation Research Report 7.

2- BOIFFIN, J. and P. F. 1988. Influence des systèmes de culture sur les risques d'érosion par ruissellement concentré: II - Evaluation des possibilités de maîtrise du phénomène dans les exploitations agricoles. Agronomie:745-756.

3- Darboux, F. and C. Huang. 2003. An instantaneous-profile laser scanner to measure soil surface microtopography. Soil Science Society of America Journal 67:92-99.

4- Fox, D.M., Y. Le Bissonnais, and A. Bruand. 1998. The effect of ponding depth on infiltration in a crusted surface depression. CATENA 32:87-100.

5- Jester, W. A. Klik, G. Hauer, B. Hebel, and C.C. Truman. 2001. Rainfall and Surface Roughness Effects on Soil Loss and Surface Runoff ASAE International Symposium, Soil Erosion Research for the 21st Century, Honolulu.

6- Gascuel-Odoux, C., and P. Bruneau. 1990. A morphological assessment of soil microtopography using a digital elevation model on one square metre plots. CATENA 17:315-325.
7- Govers, G., I. Takken and K. Helming. 2000. Soil roughness and overland flow. Agronomy 20:131-146.
8- Huang, C. and J. M. Bradford. 1990. Depressional storage for Markov-Gaussian surfaces. Water Resour. Res. 26 2235–2242.
9- Huang, C., W. E.G., T. E.G. and B. A. 1988. A noncontact laser system for measuring soil surface topography. Soil Science Society of America Journal. 52:350-355.
10- Huang., C. and B. J.M. 1992. Applications of a laser scanner to quantify soil microtopography. Soil Science Society of America Journal 56:14-21.
11- Jester, W. and A. Klik. 2005. Soil surface roughness measurement--methods, applicability, and surface representation. CATENA 64:174-192.
12- Jetten, V., J. Boiffin, and A. DeRoo. 1996. Defining monitoring strategies for runoff and erosion studies in agricultural catchments: A simulation approach. European Journal of Soil Science. 47, 579-592.
13- Kamphorst, E.C. and Y. Duval. 2001. Validation of a numerical method to quantify depression storage by direct measurements on moulded surfaces. CATENA 43:1-14.
14- Kamphorst, E.C., V. Jetten, J. Guerif, J. Pitkanen, B.V. Iversen, J.T. Douglas and A. Paz. 2000. Predicting depressional storage from soil surface roughness. Soil Science Society of America Journal 64:1749-1758.
15- Kuipers, H. 1957. A reliefmeter for soil cultivation studies. . Netherland Journal of Agricultural Sciences 5:255-262.
16- Linsley, R.K.J., M.A. Kohler and J.L.H. Paulhus. 1947. Applied hydrology, p. 269 Applied Hydrology, New-York, USA.
17- Mitchell, J.K. and J. B.A. 1976. Micro-relief depression storage: analysis of models the depth-storage function Water Resources Association 12:1205-1221.
18- Onstad, C.A. 1984. Depresional storage on tilled soil surfaces. Transactions of the ASAE 27:729-732.
19- Planchon, O. and F. Darboux. 2001. A fast, simple and versatile algorithm to fill the depressions of digital elevation models. CATENA 46:159-176.
20- Robichau, P.R. and M. Molnau. 1990. Measuring soil roughness changes with an ultrasonic profiler. Transactions of the ASAE 33:1851-1858.
21- Römkens, M.J.M., S. Singarayar, and C.J. Gantzer. 1986. An automated non-contact surface profile meter. Soil and Tillage Research 6:193-202.
22- Saleh, A. 1993. Soil Roughness Measurement - Chain Method. Journal of Soil and Water Conservation 48:527-529.
23- Taconet, O. and V. Ciarletti. 2007. Estimating soil roughness indices on a ridge-and-furrow surface using stereo photogrammetry. Soil and Tillage Research 93:64-76.
24- Ullah, W. and W.T. Dickinson. 1979. Quantitative description of depression storage using a digital surface model, I. Determination of depression storage. Journal of Hydrology 42:63-75.
25- Ziarati. T., S. Ruy.,M. Mirzaei.,. On Juin, 2007, Caractériser les possibilités de la stéréophotographie pour le suivi de différents indices de rugosité sous l'action des pluies, Rapport de Stage M1 TSA,INRA d'Avignon ., 55.
26- Zribi, M. 1998. Développement de nouvelles méthodes de modélisation de la rugosité pour la rétrodiffusion hyperfréquence de la surface du sol, Thèse de l'Université Paul Sabatier, Toulouse.

Annexe 4 : publication (poster) dans EGU General Assembly (Vienne, 2008)

Geophysical Research Abstracts,
Vol. 10, EGU2008-A-03762, 2008
SRef-ID: 1607-7962/gra/EGU2008-A-03762
EGU General Assembly 2008
© Author(s) 2008

Evaluation of the precision of close-range photogrammetry to assess DEM of the soil surface.

M. Mirzaei (1,2), T. Ziarati (3), J.C. Gaudu (1), S. Ruy (1)
(1) UMR EMMAH, INRA, Avignon, France (mmirzaei@avignon.inra.fr / Fax: +33(0)4 32 72 22 12), (2) Yasuj University, Yasuj, Iran, (3) University of Avignon, Avignon, France

Close-range photogrammetry is a quick and flexible tool to assess digital elevation model (DEM) of the soil surface on small scale in the order of 1m2. Moreover, it can be used under rainfall and may be helpful to monitor rainfall induced changes of the soil surface roughness or to quantify erosion at a local scale. However, this method relies (i) on a very precise calibration procedure of the system of 2 cameras (to get the interior and exterior geometric parameters and to allow the process of epipolar rectification) and (ii) on a statistical correlation between every pixels of both images to obtain the disparity map. Therefore it is necessary (i) to check the stability of the interior parameters of both cameras, (ii) to study the sensitivity of the computed DEM to the interior and exterior parameters, (iii) to propose an optimal configuration for the data acquisition in the field. This study deals with the interior parameters only.We used a pair of Nikon D100 digital cameras (6 Mpixels CCD, 35 mm lens), a commercial software (Halcon, MvTec, Germany) and the associated calibration target composed of 49 black spots equally distributed on a 500 mm x 500 mm white plate, with a precision of 0.1 mm. Interior parameters (focal length /m, coefficient of radial distortion /m^{-2}, cell size of the CCD /m, pixel coordinates of the principal point Cx and Cy/pixel), are estimated with an iterative non linear optimization method. The objective function to minimize is the distance between the projection of the calibration marks onto the image plane and the marks locations extracted from the image (RMSE). 9 optical settings were studied (3 camera-to-target distances (1.5m, 3m, 4.5m) x 3 apertures (F4, F8, F16)). For each optical setting, 30 images of the calibration plate were taken. The calibration process was then conducted on the whole images set and on 3 sub-samples of 5, 10 and 20 images respectively (50 samplings for each subset). Finally, the calibration process was performed x(3x50+1)=1359 times. For each calibration, we obtained the interior parameters and the RMSE on the X axis (RMSE_X) and on the Y axis (RMSE_Y). A statistical analysis was performed on the parameters, on their correlation and on the RMSE. Interior parameters are not correlated except RMSE_X and RMSE_Y that are equal: no anisotropy can be found in the image acquisition process. The RMSE is always less than 0.2 pixel on the image plane (which corresponds to 65 µm on the target plane), but the fitted parameters are not unique and their variability decreases with the size of the image subset. In some cases (subsets of 5 and 10 images), fitted parameters have no physical meaning. The aperture and the camera-to-target distance have only a limited influence on the calibration process, but a distance of 3m and a F8 aperture yield to the smallest RMSE and to the best defined parameters when associated with a set of more than 20 images. This study was useful to check the stability of the interior parameters and to determine optimal configuration for the data acquisition in the field. The influence of the interior parameters on the precision of the reconstructed DEM still needs to be assessed through further study.

Annexe 5 : Effect of rainfall on soil microtopography evaluated using photogrammetry (soumis à SSSAJ)

Title: Effect of rainfall on soil microtopography evaluated using photogrammetry

Mirzaei, M.R. and Ruy, S.,

Date recieved : 06/09/2008

Abstract:

The aim of this paper was to test the ability of a photogrammetric method to monitor soil micro-relief using different roughness indices. Laser scanning and photogrammetric methods were used as non-contact techniques to acquire data on soil surface elevations. A field rainfall simulator was used on two experiment plots (100 x 100 cm) with two different initial levels of roughness (seedbed and harrowed plots). Three rainfall simulations were performed on each plot. Laser data were obtained for 11 profiles on each plot, before the first and after the last rainfall simulation.

The following indices calculated with the laser method were compared with those generated by photogrammetry: random roughness (RR, RR_rd, RR_cr), tortuosity (Tb), 1D second order variogram ( ), Linden's index (LD and LS), mean upslope depression (MUD) and fractal (D, l) indice. The roughness index calculated with photogrammetry was usually lower than that calculated with laser method, but from a qualitative point of view, the initial and final indices calculated on both plots with photogrammetry were in agreement with those calculated with laser method. We thus showed that (i) for both methods, the *RR_cr*, T_b, *LD*, *MUD* and *l* roughness indices were able to detect microtopography changes due to rainfall, and (ii) among all indices, the *LD* indice (limiting elevation difference) calculated using photogrammetry didn't show significant difference in comparison to reference method (laser) in all case. Moreover, it exhibited a high degree of sensitivity to rainfall and could therefore be considered as a highly promising indice.

Introduction

Runoff and soil erosion (by wind and water) are one of the environmental threats in the world. In order to diminish their negative effects, it is important to understand the processes underlying the development of runoff, and its spatial distribution. In the context of an Hortonian process, the development of runoff is mainly influenced by soil surface characteristics, including soil surface roughness which is an important parameter when determining the mechanisms of soil erosion. Surface roughness is the configuration of the soil caused by a random arrangement of soil clods. Generally of the small scale, surface runoff is borne out of the plot by the microtopography of the soil surface. Numerous erosion-related surface processes, such as depression storage, raindrop or wind shear detachment, and sediment transport, have characteristic lengths at the millimetre scale. It is therefore

important to monitor soil roughness at a small scale (roughly 1 m²) in order to understand the processes of runoff and erosion.

A wide range of measurements techniques can be used to determine soil surface roughness. They can be classified into contact and non-contact methods. In the former case, measurement devices are in direct contact with the soil surface, and it may thus changes soil surface elevation records. The most widely-used contact techniques are pin meters (Cremers et al., 1996) and the chain method (e.g., Saleh, 1993; Saleh, 1994): they are cheap and simple to implement but they provide measurements in one dimension only. Planchon et al. (2002) developed a contact relief-meter that operates in two directions. Non-contact techniques such as laser scanning (Bertuzzi and Stengel, 1988; Huang et al., 1988; Huang. and Bradford, 1992; Darboux and Huang, 2003) and photogrammetry or stereo-photography (Kirby, 1991; Clegg et al., 1999; Taconet and Ciarletti, 2007) have recently been developed. Laser scanning ensures high resolution and precision (sub-millimetre) while the photogrammetry is acknowledged as exhibiting sub-millimetre precision for horizontal planes and of about a millimetre for elevation acquisitions.

Laser scanners enable the highly accurate acquisition of elevation data, but the time required for a scan normally exceeds several minutes even with a rapid laser scanner, while soil surfaces may change within much shorter periods of time. Furthermore, it is not usually possible to use laser scanning techniques under rainfall conditions. Photogrammetry enables more rapid data acquisition, better versatility and rapid monitoring, and is considered to constitute an ideal surveying method. The system is not in contact with the soil surface, and can be used under rainfall conditions. However, photogrammetry is still under evaluation, and few studies have been published (Jester and Klik., 2005; Taconet and Ciarletti., 2007).

Soil surface microtopography can be characterized by roughness indices calculated by means of elevation data. Elevation data can be used to calculate indices for surface roughness. In most cases, these indices such as the random roughness indice (Allmaras et al., 1966) or the tortuosity factor (Boiffin., 1984) are single-dimension and are only measured along transects. Govers et al. (2000) and Kamphorst et al. (2000) reviewed on different soil surface roughness indices. However, some parameters of value in hydrology (e.g., surface storage capacity) cannot be derived from 1D measurements and usually require the acquisition of 3D data such as the digital elevation model (DEM) of the soil surface. Moreover, soil surface microtopography is usually anisotropic and the calculation of soil roughness indices derived from 1D measurements is questionable.

The scale dependence of roughness is not fully understood, although it remains clear that roughness occurs at a number of scales, and natural roughness may well have a fractal or similar structure (Kamphorst et al., 2000; Kirkby, 2002). It is therefore necessary to acquire soil elevation data with a small space step so that short-range spatial structures can be detected.

Several experiments in the laboratory or field have shown that photogrammetry generates reliable data (in the form of a DEM) to characterize erosion and soil surfaces (e.g. Taconet and Ciarletti., 2007). They stated that DEMs generated by stereo-photography enabled accurate study of the

geometrical properties of soils that would be of considerable interest to hydraulic and erosion studies. However, Jester and Klik (2005) showed that the DEMs from stereophotos were smoothed between major aggregates, which led to skewed distributions of elevations and inclinations as well as to lower surface areas and lower depression volumes and areas by comparison with the laser method. Mirzaei et al. (2008) compared DEMs and roughness indices of polyester reproduction of rough and smooth soil surfaces obtained with laser method and photogrammetry. Local surface slopes were lower (respectively higher) in the DEM obtained from photogrammetry than in the laser generated DEM method on rough (respectively smooth) surfaces. RR and Maximum depression storage were slightly underestimated by photogrammetry compared to the laser method (between 5% and 15%). However, this study needs to be done on real soils and on various roughness indices.

The aim of this paper is to investigate the ability of photogrammetric system to obtain accurate estimates of roughness indices, and to determine suitable roughness indices to hydrological study using photogrammetry in future. For that, 1D indices calculated from DEMs obtained by photogrammetry are compared with those calculated by means of a reference 1D method, namely the laser profile-meter developed by Bertuzzi et al (1990a).

Materials and Methods

Test sites

All measurements were carried out on an experimental site at the INRA Centre in Avignon, in the south of France.

The field study was performed from June to August, 2007. The soil was classified as Calcolsol of alluvial origin. The A horizon (0_60 cm) was highly structured, the texture being clay-loam at the surface (44.8% clay, 49% silt, 6.2% sand). We considered two kind of soil roughness, seedbed plot and harrowed plot. The slope was about 1% for the seedbed plot and 5% for the harrowed plot. The field was cultivated with wheat. After a manual harvest, the soil was tilled with a plough share and then with a circular spike harrow combined with a cultipacker (a weighted clod crusher) in order to obtain a more or less smooth soil surface representative of seedbed preparation (roller surface). On the second plot, the ridges of a furrowed surface were created manually at 30 cm intervals and a height of 8 cm.

A 100 cm x 100 cm square steel frame was levelled on the soil surface, and several points were marked precisely. This frame remained on the plot throughout the experiments. The points thus marked were necessary to orient the cameras. This frame was thus used to perform absolute comparisons between DEMs obtained at different times using the stereo-photography and laser methods.

Rainfall simulation

A sprinkler irrigation system was used to simulate rainfall. The intensity of rainfall could be controlled by a barometer and spatial distribution could be adjusted using the sprinkler head. Four sprinklers were installed at the four corners of a 1.8 x 1.8 m square plot. Three rainfall simulations were imposed separately for each plot. Irrigation intensities were sequentially 60, 80 and 80 mm h^{-1}. During all experiments, the spatial distribution of water on the subplot surface was determined by 8 rain gauges located at the four corners and in the middle of each side of a 1.1 x 1.1 m square surrounding the subplot. No rain gauge was placed in the centre of the plot, so as to avoid any artefacts when calculating soil roughness or DEMs. The homogeneity of the irrigation rate was studied; this was nearly homogeneous within the 1 x 1 m square subplot located at the centre of the irrigated plot, with a average standard deviation of 8 mm. The coefficient of variation changed within the range of about 8% to 13%.

An overview of calculated roughness indices

Five roughness indices and variogram analyses were taken into account in this study.

Elevation standard deviation (*RR, RR_rd, RR_cr*)

This is the most basic type of surface profile description (Taconet and Ciarletti, 2007; Zhixiong et al., 2005; Kamphorst et al., 2000). This index has a purely statistically basis and does not consider spatial distribution. Allmaras et al. (1966) defined random roughness as the standard deviation of elevations. We calculated three standard deviations for each profile: (i) with all height readings (*RR*), (ii) after eliminating 10 percent upper and lower of the data (*RR_rd*) and (iii) applying a correction of the height reading using the surface linear trend (*RR_cr*) as described by Currence and Lovely (1970). These authors showed that random roughness is more sensitive to roughness changes, thus it is calculated without any transformation.

Bertuzzi et al. (1990b) showed that this indice is sensitive to surface evolutions caused by rainfall.

Tortuosity (T_b)

Tortuosity describes tortuosity indices were defined in the literature (e.g. Boiffin, 1984; Helming et al., 1993). The former authors were the first to use tortuosity as a roughness indice. T_b is defined as the ratio between the length of a profile of ground (L_1: real length) and the horizontally projected length of the same profile of ground (L0: projected length):

$$T_b = \frac{L_1}{L_0} \geq 1 \quad [1]$$

This indice is frequently measured using the chain method (Saleh, 1993) but can also be estimated by means of surface elevations obtained by a laser scanner or a DEM. According to Bertuzzi et al. (1990b) and Eltz and Norton (1997), the tortuosity indice is able to detect soil surface roughness changes as a function of rainfall.

Variogram (γ)

The variogram, or second order variogram, characterizes the spatial continuity of a data set. In most cases, one-dimensional statistics (like average) for two data sets may be almost identical, but the spatial continuity can be quite different. A variogram is defined as:

$$\gamma(l) = \frac{1}{2N}\sum_{i}\left[Z_i - Z_{i+l}\right]^2 \qquad [2]$$

where γ is the semivariance, l is the distance between points, N is the number of all paired points within a distance class and Z_i is the elevation at location (i). To remove general slope effects and to satisfy the variogram hypothesis (stationarity and ergodicity), the elevation Z_i is taken as the distance from the soil surface to the mean plane. Computations for each profile were performed using a regular distance lag of 1 mm, ranging from 1 to at most 250 mm in steps of 1 mm.

Limiting Elevation Difference and Slope (LD and LS)

Linden and Van Doren (1986) described new indices, the Limiting elevation Difference (*LD*) and the Limiting Slope (*LS*), that are sensitive to roughness changes. These indices are the configuration parameters based on geostatistical analysis and they account for the spatial structure of elevation data.

The calculation of *LS* and *LD* are based on the mean absolute elevation difference, or the first order variogram

$$\Delta Z_l = \sum_{i=1}^{N}\left|\frac{Z_i - Z_{i+l}}{N}\right| \qquad [3]$$

where Z_i is the elevation of point i, and Z_{i+l} is the elevation of a point some lag numbers l from point Z_i.

The relationship between ΔZ_l and the lag distance ΔX_l, was obtained using a linear regression of their reciprocals:

$$\frac{1}{\Delta Z_l} = a + b\left(\frac{1}{\Delta X_l}\right) \qquad [4]$$

where a and b are fitted constants.

Horizontal spacing ΔX_l was limited to a maximum of 200 mm. The reciprocals of the parameters *a* and b, were designated Limiting elevation Difference (LD) and Limiting Slope, (LS), respectively:

$$LD = \frac{1}{a}, \qquad LS = \frac{1}{b} \qquad [5]$$

The Linden and Van Doren (1986) procedure was successfully tested by Bertuzzi et al. (1990b) as showed that LD and LS are highly sensitive in the morphology and magnitude of roughness due to rainfall.

Mean Upslope Depression (MUD)

The Mean Upslope Depression (*MUD*) was developed by Hansen et al (1999) in order to predict depression storage. It is based on the differences in elevation $\Delta Z_{r-a} = Z_r - Z_a$ between a reference point (X_r) and points (X_a) on a line segment positioned upslope from the reference point (i). Within each line segment, the calculation procedure is iterated for a number of sub segments (j), taking a new upslope point each time as the reference point:

$$MUD = 1/m \cdot \left(\sum_{i=1}^{m} \left(\sum_{j=1}^{n_i} \Delta Z / n_i \right) \right) \qquad [6]$$

The *MUD* is the mean value of all sub-segments, *n* is the number of points in a line sub-segment and *m* is the number of line sub-segments.

Fractal dimension (*D*) and crossover length (l)

Fractal geometry or self-similarity is a useful tool to analyse the topography of different surfaces types such as soil surface roughness (Huang and Bradford, 1992; Vazquez et al., 2005; Vazquez et al., 2007). Fractal indices have been shown to be the most promising to describe evolutions to roughness due to the effects of rainfall, vegetation cover or both factors concurrently (McDonald et al., 1999; Vazquez et al., 2005).

Huang and Bradford (1992) showed that the fractal model to describe soil roughness was only appropriate within a limited scale range (pseudofractal), contrary to the common belief that fractal processes should not have any scale limitations. These authors first used the concept of fractional Brownian motion (fBm), introduced by Mandelbrot and Van Ness (1968), to characterize soil surface microtopography, emphasizing that the fBm process should be quantified by two parameters, the fractal dimension (*D*) and the crossover length (*l*). After calculating semivariograms, *H* and *l* are the regression parameters obtained using the equation below:

$$\log(\gamma(h)) = 2H\log(h) + l \quad [7]$$

where γ is the semivariance and h is the lag distance. The fractal dimension D is:

$$D = 3 - H \quad [8]$$

Experimental database

Two techniques were employed to obtain elevation data from the soil surface: a laser profiler and photogrammetry. Both techniques produced high resolution data.

Laser profiler

A laser profiler was used to measure the roughness of bare agricultural soil. The profiler is a non-contact micro-laser relief meter developed by INRA (Avignon) and described by Bertuzi et al. (1990) This profiler measures one point elevation at a time (point to point), so its speed is relatively slow (about 20 s/m). It is equipped with two lenses with different focal lengths f (50 cm and 100 cm) so that the resolution can be adjusted to the elevation range. We used the lens with f=100 cm, because it is able to measure distances that are 250 to 640 mm between the lens and the soil surface. The profiler was calibrated prior to each plot experiment using two black and white targets to take account for the effect of reflectance on calibration. The different colours exerted no significant influence. The measuring range of the laser profiler is 2 metres, its horizontal resolution 1 mm and its vertical resolution less than 1 mm; it is thus suitable for soil surface roughness measurements and served as reference method in this study.

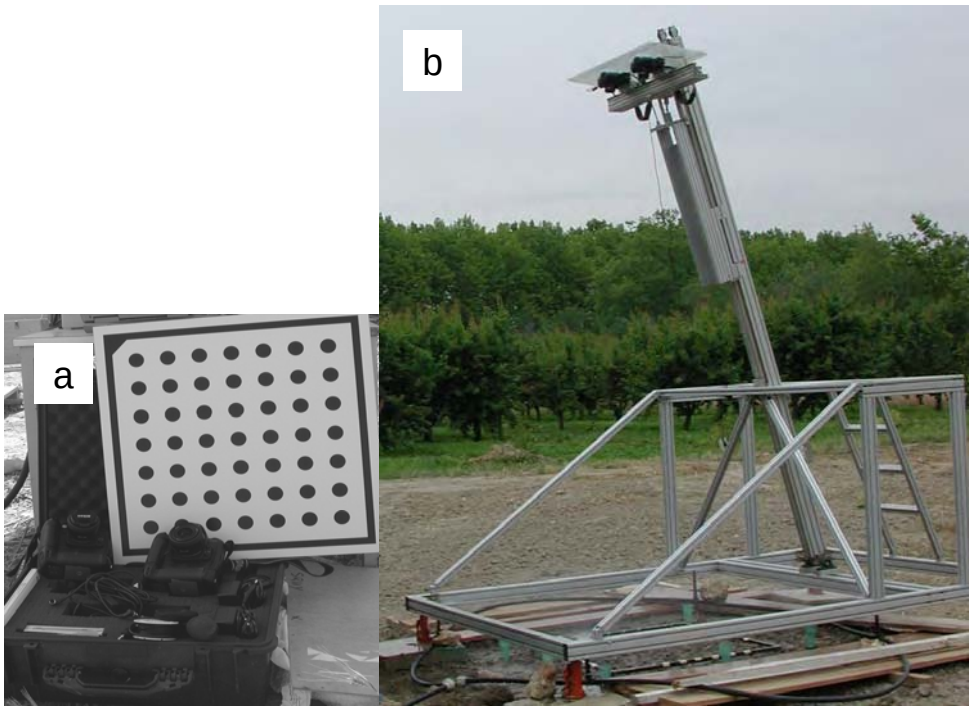

Fig.1: Equipment used for stereo-photogrammetry: a) two cameras with the calibration plate (50 cm x 50 cm), (b): support.

Data acquisition with a laser scanner was always performed in one direction (horizontal or *X*) on 11 transects of the seedbed plot and on the harrowed plot perpendicular to the direction of tillage. Each profile was scanned twice, before rainfall simulation (initial state) and after the last simulated rainfall event (final state). Transects were equally spaced every 10 cm.

Photogrammetry data

The camera system (Fig. 1) was mounted on a stable support (made by INRA in Avignon).

The height of photographs could be changed within a range of 1 to 4 metres above the soil surface. Stereo-photos were taken using a pair of Nikon D100 digital cameras with a constant theoretical focal length of 35 mm, and a CCD sensor of 3000 x 2008 pixels.

The optimal experimental setup was determined from a preliminary study by Ziarati et al. (2007). We used an F8 aperture and a soil-cameras distance between 3.5 to 4 m. Horizontal distance between the cameras was 40 cm while the optical axes were parallel and vertical to the ground surface. The resulting image resolution was about 0.65 mm pixel^{-1}. The stereo-photogrammetry system was calibrated according to Ziarati et al. (2007).

DEM reconstruction was based on a matching process between each pixel of the left photography and of the right photography. For this we used the Normalized Cross Correlation (NCC) method; this compensated for the mean gray value and its variance within the matching window. NCC is more

time-consuming than other methods but is preferable if the two images differ in terms of their brightness and contrast. Calibration, matching and DEM reconstruction were performed using commercial software (Halcon; MVTec, 2006).

Results and Discussion

All roughness indices were computed initially for all the profiles obtained using the laser profiler, and were then averaged. For comparative purposes, they were also computed on the same profiles extracted from the DEMs obtained by stereophotography and averaged.

Soil elevation profiles

For the seedbed plot, the elevation profiles obtained by laser profiler and stereo-photogrammetry were very similar (Fig. 2). For the harrowed plot, differences are more pronounced particularly regarding the final state. Stereo-photogrammetry generated smoother soil elevation profiles than laser profiler. Because roughness is a function of elevations, photogrammetry was expected to produce lower roughness indices than the laser method.

For a given plot, a clear difference between the soil surface profiles before (initial) and after (final) rainfall simulation was detected by both method. After 220 mm of cumulative rainfall, aggregates were broken down by rainfall simulation, and the morphology of the soil surface changed.

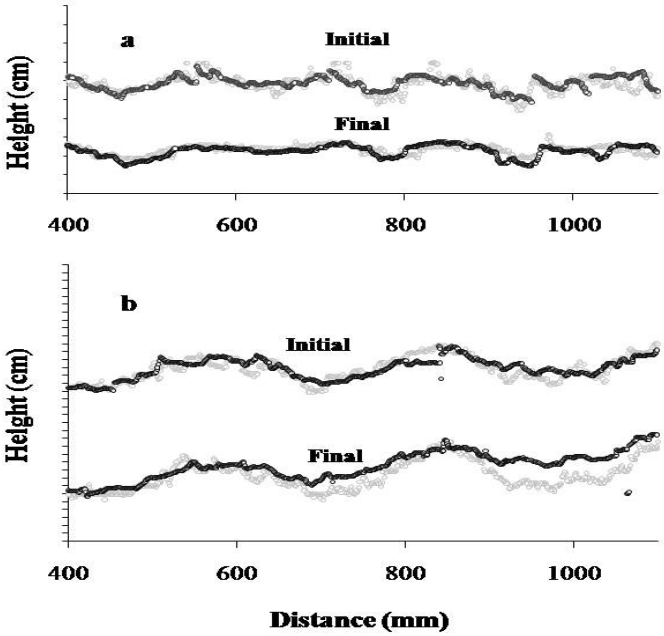

Fig. 2: Comparison of soil surface elevation profiles obtained by laser method profiler (gray points) and stereo-photogrammetry (black points), on the seedbed plot (a) and on the harrowed plot perpendicular to the direction of tillage (b).

Table 1: Average (M) of and standard deviation (σ) of different roughness indices obtained using the two methods on the two plots, before the first rainfall (initial) and after the last rainfall simulation (final). σ is the standard deviation for roughness indices. Profile number n =11, except for the seedbed plot at the initial state with the stereo method (n=9).

Plot	State		Laser profiler			Photogrammetry		
			RR	RR_rd	RR_cr	RR	RR_rd	RR_cr
Seedbed	Initial	**M**	**15.6**	**7.1**	**7.0**	**13.4**	**8.0**	**7.6**
		σ	3.5	1.6	1.6	1.4	1.5	1.6
	Final	**M**	**16.7**	**5.1**	**4.8**	**13.0**	**6.9**	**5.5**
		σ	2.0	1.6	1.4	1.3	1.9	1.1
	ratio		1.07	0.72	0.69	0.97	0.86	0.72
Harrowed	Initial	**M**	**37.3**	**28.1**	**23.9**	**31.2**	**25.8**	**21.1**
		σ	3.4	3.2	2.4	5.2	4.0	3.4
	Final	**M**	**28.5**	**21.9**	**14.5**	**46.8**	**36.7**	**15.4**
		σ	3.0	2.9	1.5	5.1	4.3	1.5
	ratio		0.76	0.78	0.61	1.50	1.42	0.73

From a qualitative point of view, photogrammetry appeared to be an appropriate method to survey soil elevation profiles and their variation due to rainfall. However, it is necessary to quantify such surveys by means of roughness indices.

Standard deviations of elevation data

In order to prevent any bias due to the different spatial resolutions applied with the two methods, the same spatial resolution of 1 mm was used in both cases.

First, we checked the assumption concerning the normal distribution of elevation data. This assumption, which is required for standard statistical analyses such as the calculation of random roughness turned out to be invalid for many of the profiles, particularly on the harrowed plot. This was in contradiction with the results of several other authors who had shown that the distribution of soil surface elevation data is normal (e.g. Currence and Lovely, 1970). We examined the data distribution for 46 of 86 profiles graphically but also using two classic tests: the Kolmogorov-Smirnov and the chi-square tests for normal and lognormal distributions, respectively. It appeared that these curves had normal distribution visually, but when using these tests the normal or lognormal assumptions were not accepted (only six cases exhibited a normal distribution at the level of 1%). It is thus possible that the calculated statistics failed to describe adequately the data set, because of a poor fit of the normal model (Linden. and D.M., 1986). These data are not presented here. A log-normal transformation had only a slight effect and only improved the Gaussian type distribution in certain cases. It was therefore not useful to use a log transformation, contrary to other observations (Allmaras et al., 1966; Burwell et al., 1963). Moreover Currence and Lovely (1970) had shown that random roughness without a log transformation was more sensitive to roughness changes.

The elimination of 20% of height data (as suggested by Burwell et al., 1963, and Allmaras et al., 1966), had a strong influence on the calculation of standard deviations (compare *RR* and *RR_rd*, Table 1), whereas removing the slope and tillage effect exerted little influence on the calculation (compare *RR_rd* and *RR_cr*, Table 1). The results of ANOVA showed that *RR_rd* and *RR_cr* differed significantly from *RR* (*P*=5%) in all cases. Similar results could be obtained regarding the initial and final states on both plots. *RR_cr* indices were identical in three cases for the seedbed but in only one case on the harrowed plot (*P*=5%). The reason for this difference between *RR_rd* and *RR_cr* is discussed below.

The estimates for M (average) revealed a good correspondence between the tillage state and this parameter using both methods (see values before and after rainfall, Table 1). According to Table 1 two principal outcomes can be made:

- (i) the *RR* index was not able to detect roughness changes due to rainfall. These changes were not regular and the evolutions of *RR* values due to rainfall depended on the surveying method (laser vs. photogrammetry). After eliminating the top and bottom 10% of the elevation data, the estimated roughness index (*RR_rd*) showed a monotonous decrease in line with rainfall amounts, as expected. However, the tillage and slope effects were incorporated in the calculation of *RR_rd*, and depended on the surveying method (particularly regarding the harrowed plot). Corrections for tillage and slope (*RR_cr*), resulted in a decrease of the roughness index *RR_cr* regardless of method and plot. The change was more marked for the harrowed plot than for the seedbed plot, but the final/initial *RR_cr*

ratio was about the same. This may have been due to a difference in the slope (1% for the seedbed plot and 5% for the harrowed plot) and tillage operations. However, the estimated *RR_cr*, showed a satisfactory agreement between the two methods, with similar relative evolutions and values;

- (ii) we observed that *RR_cr* values decreased as a result of rainfall impact. Comparing the three random roughness indices, *RR_cr* responded most sensitively to the roughness changes. Inspecting the ratios (Table 1) of these changes (final/initial) shows very similar results in case of the seedbed plot and a 15% discrepancy between the two methods for the harrowed plot.

We expected *RR_cr* estimated by stereo-photogrammetry to be lower than those estimated by laser profiler as mentioned by Jester and Klik (2005). However, this was only true for the harrowed plot in the initial state (Fig. 3). This could be explained by shadow effects to which the photogrammetric method was more sensitive than the laser method, or by the outlier points generated during the photogrammetric process. Nevertheless, the trends were the same with both methods.

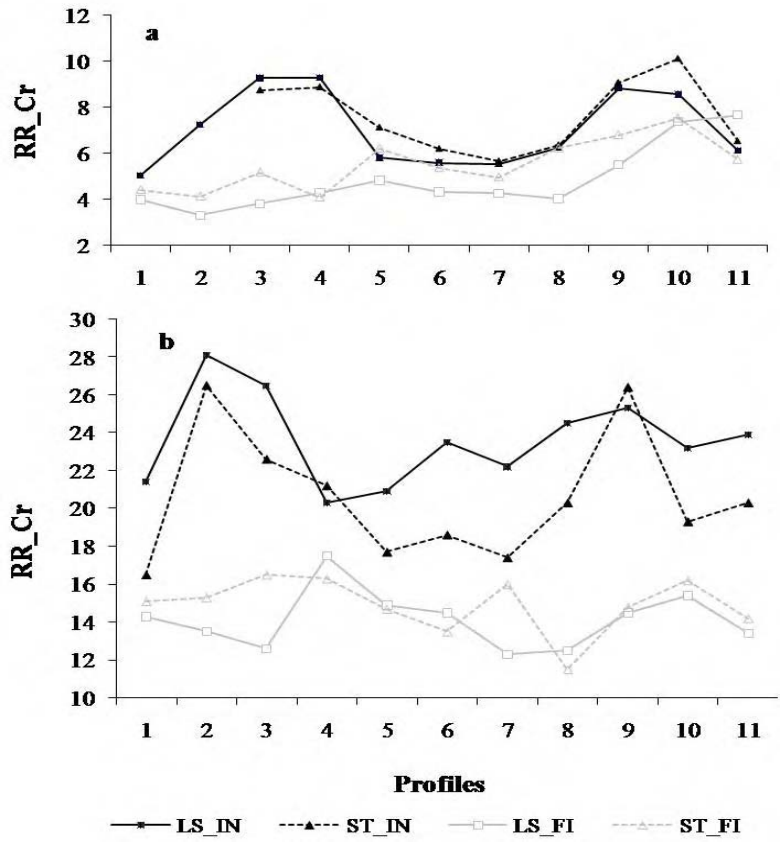

Fig. 3: Computed RR_cr values for all profiles acquired by laser profiler (LS) and stereo-photogrammetry (ST), before (Initial) and after (Final) rainfall, on (a) seedbed and (b) harrowed plots (perpendicular to the direction of tillage); IN: initial state, FI: final state

Table 2: Computed average (M) and standard deviation (σ) for the tortuosity roughness indice, T_b obtained using the two techniques on the two plots, before (initial) the first and after (final) the last rainfall simulation. (n=11 except Initial State – Seedbed Plot – Photogrammetry: n=9)

State		Seedbed Plot			Harrowed Plot		
		Laser	Stereo	Ratio (ST/LS)	Laser	Stereo	Ratio (ST/LS)
Initial	M	**2.41**	**1.64**	**0.68**	**3.17**	**2.21**	**0.70**
	σ	0.19	0.25		0.41	0.30	
Final	M	**1.99**	**1.34**	**0.67**	**2.63**	**1.94**	**0.74**
	σ	0.20	0.12		0.32	0.30	
Ratio (FI/IN)		0.82	0.82		0.83	0.88	

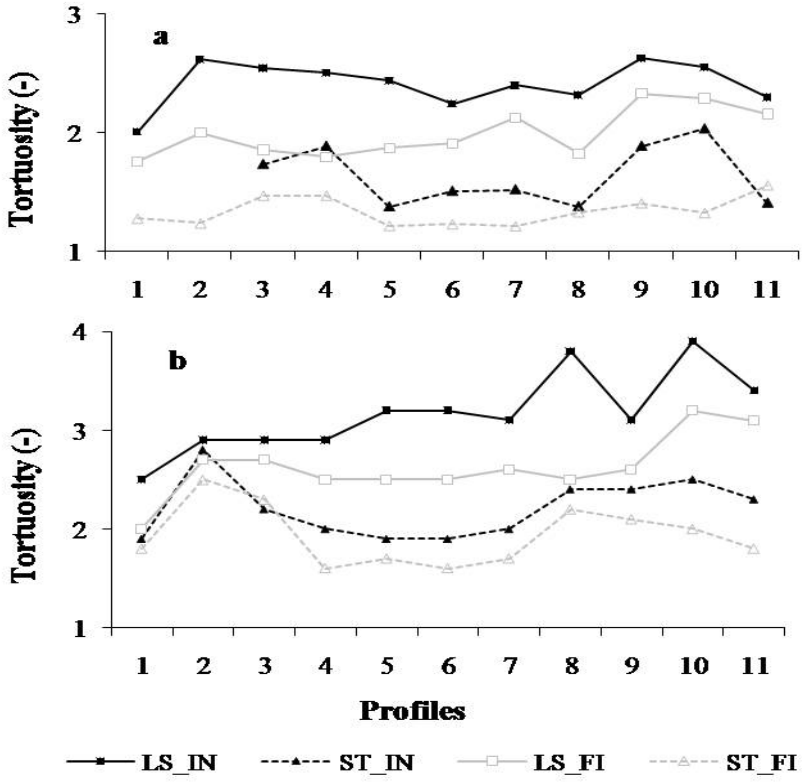

Fig. 4: Calculated tortuosity for different profiles for (a) seedbed and (b) harrowed plot, for captions see the one of Fig. 3.

Tortuosity (T_b)

Regarding the initial state of the seedbed plot, the average of T_b was 2.41 for laser profiler and 1.64 for photogrammetry. In the final state, the values were 1.99 (laser) and 1.34 (photogrammetry) indicating a decay of 18% with the laser method and 17% with photogrammetry (see Table 2). Similar results were found on the harrowed plot. On average, Table 2 shows that: (i) T_b was higher for the harrowed plot than for the seedbed plot, as expected, and (ii) T_b was always lower for photogrammetry compared to laser profiler. This accorded with the fact that the profiles obtained by stereo-

photogrammetry were always smoother than those obtained by laser profiler (see Fig. 4). (3) T_b fell after rainfall while this effect was more pronounced for laser profiler (Fig. 4). Nevertheless, both methods detected changes to roughness using the T_b index.

Variograms

Variograms were computed in the direction of rows for the seedbed plot and in the direction of columns on harrowed plot (perpendicular to the direction of tillage).

Several theoretical variogram models (spherical, exponential, Gaussian, power and circular) were fitted to our experimental data using the ILWIS software. Exponential and power expressions exhibited poor fitting. The best fit was obtained with the spherical model for the seedbed plot and the circular model for the harrowed plot. The expression of the spherical model is

$$\gamma(h) = C_0 + C * \left(\frac{3h}{2a} - \frac{h^3}{2a^3} \right) \qquad \text{for } 0 < h \le a$$
$$\gamma(h) = C_0 + C \qquad \text{for } h > a \qquad [9]$$

and for the circular model

$$\gamma(h) = C_0 + C * \left(1 - \frac{2}{\pi} * \arccos\left(\frac{h}{a}\right) + \frac{2h}{\pi a}\sqrt{1 - \frac{h^2}{a^2}} \right) \qquad \text{for } 0 < h \le a$$
$$\gamma(h) = C_0 + C \qquad \text{for } h > a \qquad [10]$$

where $\gamma(h)$ is the theoretical semi-variogram (mm^2), h is a lag distance (mm), C_0 is the nugget value (mm^2), C is the sill value (mm^2), and a is the range value (mm).

The agreement between the experimental data and the best fitting model was good for both experimental plots (see Fig. 5 for example): R^2 coefficients were usually higher than 0.85 and sometimes close to the value of 0.99.

Sill and range values were clearly lower for the seedbed plot than the harrowed plot in all profiles (Fig. 6). The low variance observed at close spacing contrasted with uniform total variance over the entire range, indicating spatial dependence over the range 30 to 75 mm for the seedbed plot versus 105 to 180 mm for the harrowed plot. The small range values for the seedbed plot demonstrated a correlation at short distances. Spatial variances ranged from 23 to 313 mm² for the seedbed plot versus 405 to 2000 mm² for the harrowed plot, or a very considerable difference. Thus the two plots had distinctive variograms with respect to tillage operations.

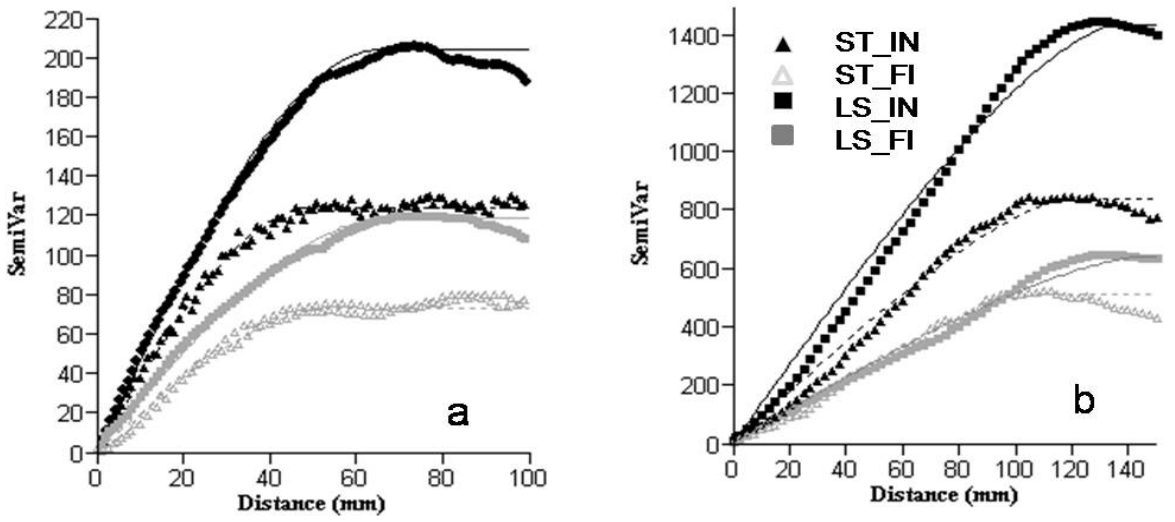

Fig. 5: Experimental (points) and theoretical (lines) variograms, a) spherical model on seedbed plot b) circular model on harrowed plot obtained from a profile perpendicular to the direction of tillage.

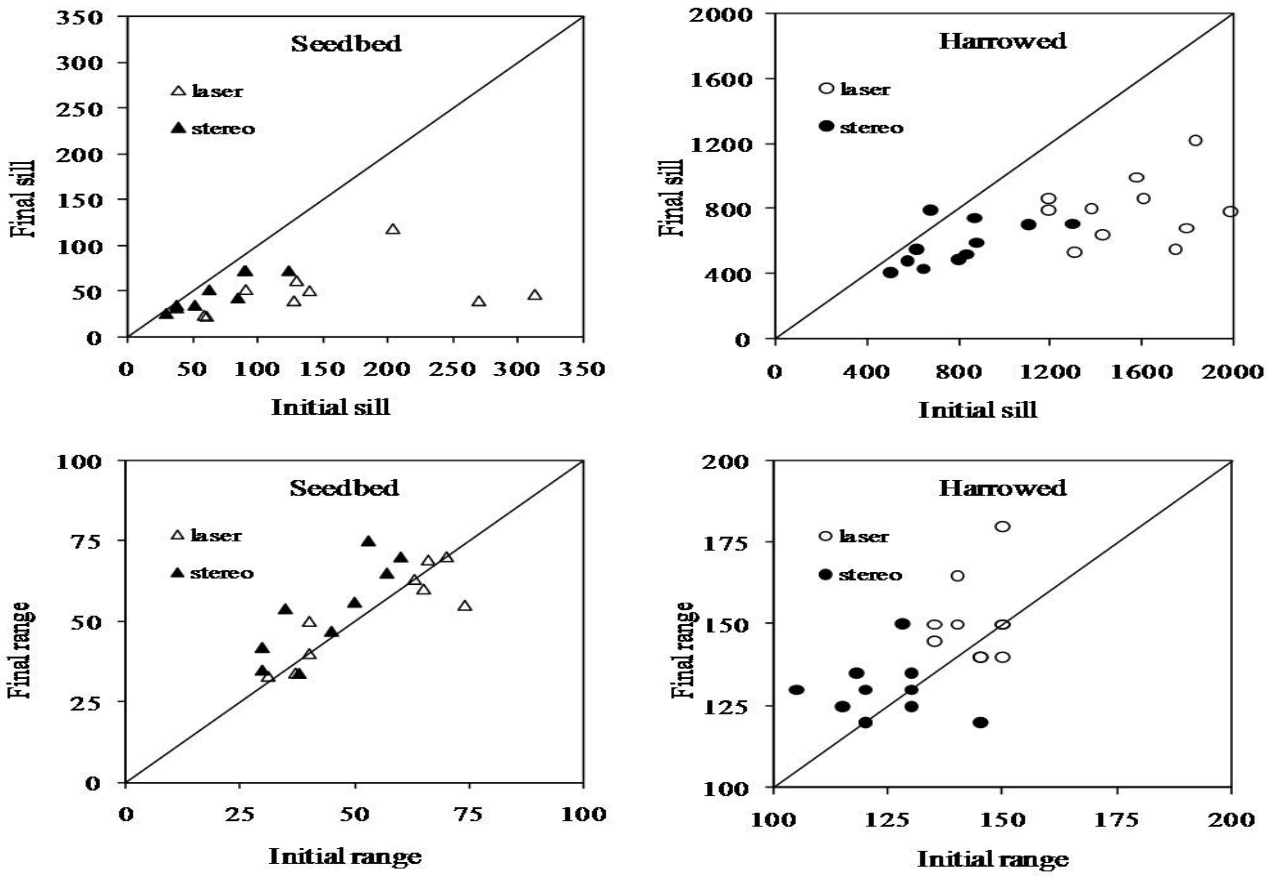

Fig. 6: Theoretical variogram parameters (sill and range) for the final state versus initial state for each profile.

At the initial state, sill values calculated using laser data were higher than those calculated with photogrammetry data. After rainfall sill values were lower for both methods and plots. For the seedbed plot, the range values calculated from laser data remained constant between the initial and final states, whereas they showed a slight increase when calculated from photogrammetric data. Range value also increased for harrowed plot due to rainfall. We expected range values to remain rather constant throughout the experiments, because in this setting any changes to the soil surface were mainly due to minor range effects due to splash phenomena on a relatively flat surface. Moreover, runoff was more or less homogeneous (sheet flow) and followed a direction perpendicular to that applied when calculating variograms.

During the studies performed by Darboux and al. (2001), experimental variograms revealed a gradual and homothetic reduction in semivariances after each additional period of rainfall that was similar to our findings.

Limiting Elevation Difference and Slope (*LD* and *LS*):

Linden and Doren (1986) presented two new indices, *LD* and *LS*, where *LD* is the sill and *LS* is the slope of the first-order variogram at the origin (Kamphorst and al, 2000). These two parameters define the shape of the variogram. An example of the experimental relationship first order variance (ΔZ) and lag distance (ΔX) and the fitted theoretical model is presented in Fig. 7.

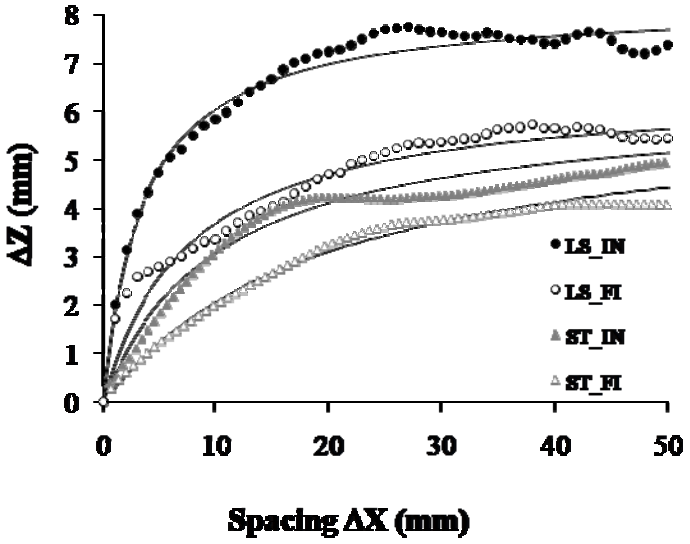

Fig. 7: Experimental and theoretical variograms (first order) calculated on profile using the Linden and Doren (1986) method to obtain the limiting elevation difference (*LD*) and slope (*LS*). ST1: Stereo; LS1: laser method, H60: profile number in Harrowed plot, IN and FI: initial and final states, respectively.

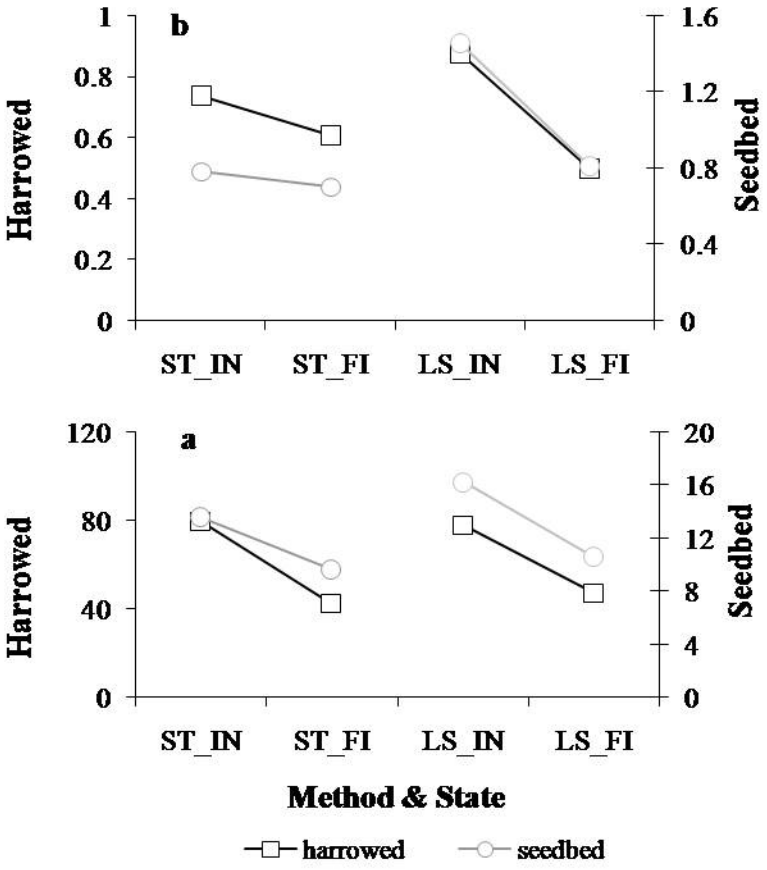

Fig. 8: Rainfall-induced changes to average values of (a) limiting elevation difference (*LD*) and (b) limiting slope (*LS*) estimated by laser profiler (LS) and the photogrammetry method (ST). IN: initial state, FI: final state.

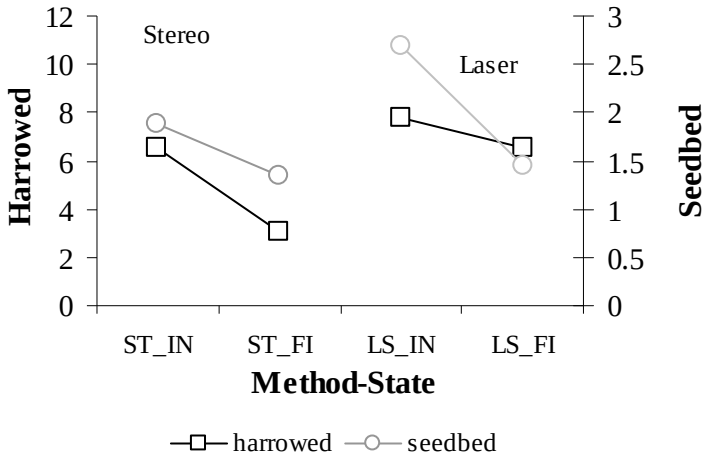

Fig. 9: Calculated mean upslope depression (MUD) for initial (IN) and final (FI) states, obtained using the laser (LS) and photogrammetry (ST) methods.

LD values obtained by laser profiler were comparable to those estimated by stereo-photogrammetry (Fig. 8). By contrast, *LS* values differed as a function of method, especially regarding

the seedbed plot. *LD_IN* (initial value of *LD*) and *LD_FI* (final value of *LD*) were approximately 15 and 10 respectively for the seedbed plot, whereas they are about 78 and 45 for the harrowed plot. These results show that the correlation length of elevation data was greater on the harrowed plot than on the seedbed plot, which is in line with the analysis of 2^{nd} order variograms (see previous section).

Another interesting point was the high sensitivity of *LD* values to rainfall: on average, *LD* values were reduced by 32% for the seedbed and by 55% for the harrowed plot, regardless of the method applied.

Mean Upslope Depression (*MUD*)

Once again, the *MUD* values revealed a clear difference between the two types of plot and a reduction during rainfall simulation (Fig. 9). In all cases, photogrammetric values were lower than those obtained using the laser profiler.

Fractal Dimension (*D*) and crossover length (*l*)

In order to obtain parameters *D* and *l*, lag distances and semivariograms were plotted on a logarithmic scale (Fig. 10). The results are summarized in Table 3 and 4 for parameters *l* and *D*, respectively.

These showed that parameter *D* was similar for the two plots and using the two methods, before and after rainfall. This parameter is not efficient in either monitoring roughness changes or under rainfall (initial vs. final), nor in terms of tillage operations (seedbed vs harrowed plot). According to Huang and Bradford (1992), the fractal dimension *D* is an index for the proportional distribution of different-sized clods in a relative scale, and a constant *D* value means that the probability density function of clods size is simply translated during rainfall (or tillage operations) but its shape does not change.

The *l* parameter is the intercept of the linear model with the lag distance axis. Higher *l* values are indicative of greater roughness (Table 3): this was the case regarding the initial state of both plots (*l*= 1.59 for the harrowed plot, *l*=1.14 for the seedbed plot) when *l* was calculated from laser data. Lower values were obtained for the same plots using photogrammetry (*l*=1.51 for the harrowed plot and *l*=0.72 for the seedbed plot). In the final state, significant differences could also be seen. *l* values decreased during rainfall by about 38% (laser method) and 25% (stereo method). Thus changes to roughness were reflected to a significant extent by the *l* parameter. In general, the stereo method generated lower *l* values than the laser method, but the stereo method was still able to detect these changes.

In summary regarding comparisons between roughness indices calculated using laser profiler (reference method) and photogrammetry by inspecting of the results of ANOVA test (Table 5) it can be concluded:

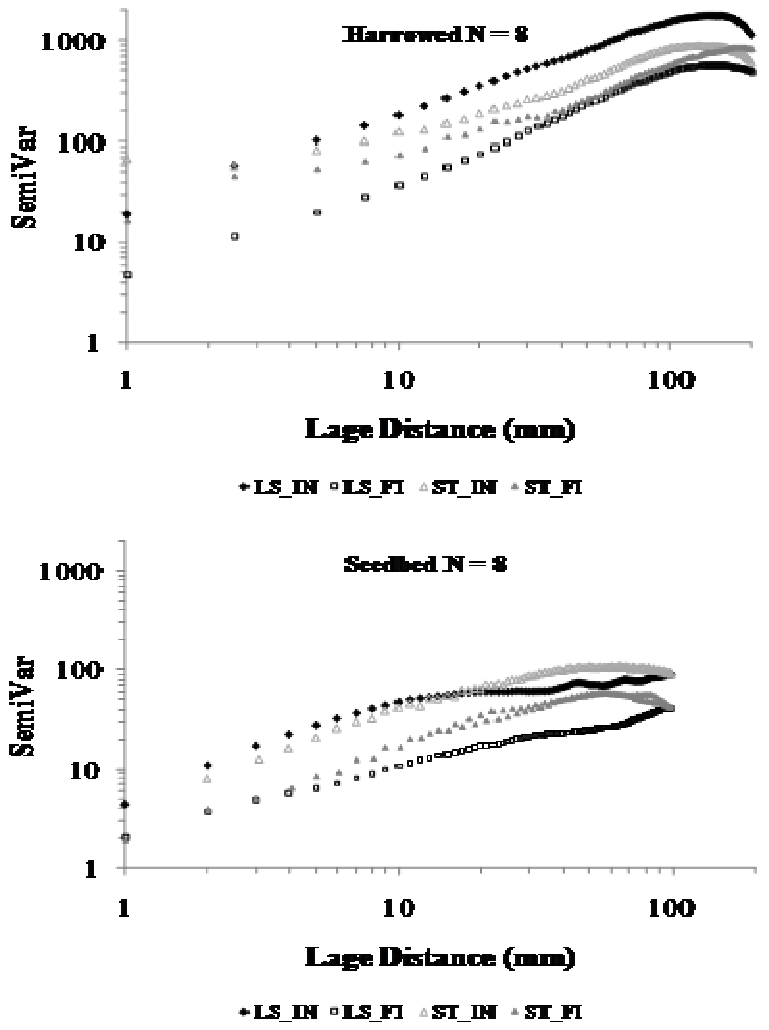

Fig.10: Roughness function from two plots (harrowed and seedbed), for profile number 8, before the first rainfall (IN) and after the last rainfall (FI) simulations, calculated using the laser data (LS) and stereo data (ST).

Table 3: Average over all profiles for the parameter *l*, calculated using laser data and stereo data.

State		Seedbed Plot			Harrowed Plot		
		Laser	Stereo	Ratio (ST/LS)	Laser	Stereo	Ratio (ST/LS)
Initial	M	**1.14**	**0.72**	**0.63**	**1.59**	**1.51**	**0.95**
	σ	0.19	0.22		0.18	0.19	
Final	M	**0.63**	**0.48**	**0.76**	**1.10**	**1.29**	**1.12**
	σ	0.22	0.15		0.32	0.3	
Ratio (FI/IN)		0.55	0.66		0.69	0.86	

Table 4: Average over all profiles for the parameter *D*, calculated using laser data and stereo data.

State		Seedbed Plot			Harrowed Plot		
		Laser	Stereo	Ratio (ST/LS)	Laser	Stereo	Ratio (ST/LS)
Initial	M	**2.72**	**2.70**	**0.99**	**2.67**	**2.70**	**1.01**
	σ	0.06	0.06		0.05	0.05	
Final	M	**2.71**	**2.65**	**0.98**	**2.61**	**2.63**	**1.01**
	σ	0.05	0.06		0.04	0.06	
Ratio (FI/IN)		1.00	0.98		0.98	0.97	

(i) roughness values for seedbed plot are significantly different in comparison to harrowed plot;

(ii) comparing among the initial and final states corresponding to each plot and method usually showed significant difference before and after rainfall. *RR_cr*, T_b, *LD*, *MUD* and *l* indices detect evolution of microtopography due to rainfall in all cases. So these roughness indices can be used to monitor soil surface microtopography evolutions.

(iii) laser method and photogrammetry gave similar value for *LD* in all cases and RR_cr, rang parameter (variogram) and fractal dimension (*D*) in three case. Whereas *Range value* (variogram parameter) didn't change due to rainfall in seedbed plot and the sensitivity of the *D* indice did not adequate. The low variance of this parameter caused that the statistic test show a significant difference whereas the value are really close together (Table 4). *RR_cr* also showed a good estimation in comparison to the reference method (it is only different in initial state on harrowed plot).

Table 5: Summary results of one-way analysis of variance of data for different variables

	Comparaison Initial and final state				Comparaison Laser to Stereo				Treatement (seedbed & Harrowed)
	Seedbed Plot		Harrowed Plot		Seedbed Plot		Harrowed Plot		
	Laser	Stereo	Laser	Stereo	IN	FI	IN	FI	
RR_cr	S	S	S	S	N	N	S	N	S
T_b	S	S	S	S	S	S	S	S	S
Vrg_Sill	S	N	S	N	S	N	S	S	S
Vrg_Range	N	N	S	S	N	N	N	S	S
LD	S	S	S	S	N	N	N	N	S
LS	S	N	S	N	S	N	N	S	S
MUD	S	S	S	S	S	N	S	S	S
L-Fractal	S	S	S	S	S	S	N	N	S
D-Fractal	N	S	S	S	N	N	S	N	S

S: Significant difference at level 5%; N: Non-significant at 5% level

(iv) the best roughness indices have two conditions. It change due to rainfall and give similar value using two methods. According Table 5 only *LD* guarantied these conditions and RR_cr also can be present a good estimator.

Conclusion

Surface micro-topography is one of the principal factors in numerous hydrologic processes. Recent developments in roughness measurement techniques have now made it possible to collect data with a sub-millimetre precision.

Five roughness indices, together with variogram analysis, were employed. Photogrammetry was able to reflect the general form of the soil surface and aggregates, but produced a smoother surface than the laser technique. For this reason, the roughness indices calculated using this method, were generally lower than those calculated with the laser technique.

Both methods were able to detect different soil surface roughness (seedbed and harrowed plots). Although photogrammetry showed a smoother surface, this method was still able to reveal roughness changes. The range of changes reflected by laser methods was broader. For this reason, it is possible to suggest that the two techniques each have a specific field of application (e.g.T_b). The *RR_cr*, T_b, *LD*, *MUD* and *l* roughness indices indice were able to detect microtopography changes due to rainfall. The *RR* indice should be calculated after elimination of the 10 % upper and lower data, and correcting for the slope. The *LD* indice (limiting elevation difference) calculated using photogrammetry was very similar to that calculated with the reference (laser) method in all case. Moreover, it exhibited a high degree of sensitivity to rainfall and could therefore be considered as a highly promising indice.

This study shows that the photogrammetric method is suitable for the monitoring of the soil surface roughness and that it gives the good information from soil surface and its change during the rainfall in qualitative and quantitative point of view.

References

Allmaras, R.R., R.E. Burwell, W.E. Larson, and R.F. Holt. 1966. Total porosity and random roughness of the interrow zone as influence by tillage. USDA Conservation Research Report. 7.

Bertuzzi, P., and P. Stengel. 1988. Measuring effects of tillage implements on soil surface geometry with a laser reliefmeter, pp. 7-12 Proc. 11th Int. Soil and Tillage Res. Organization, Vol. 1, Edinburgh.

Bertuzzi, P., J.M. Caussignac, P. Stengel, G. Morel, J.Y. Lorendeau, and G. Pelloux. 1990a. An automated, noncontact laser profile meter for measuring soil roughness in situ. Soil Science. 149, 169-178.

Bertuzzi., P., G. Rauws., and D. Courault., 1990b. Testing roughness indices to estimate soil surface roughness changes due to simulated rainfall, Soil Tillage Res. 17, 87-99.

Boiffin, J. 1984. Structural degradation of the soil surface by the action of rainfall. (In French.) Ph.D. diss. Inst. Natl. d'Agronomie Paris-Grignon, Paris, France.

Burwell, R.E., R.R. A1lmaras, and M. Amemiya. 1963. A field measurement 0f total porosity and surface microrelief of soils. Soil Sci. Soc. Am. Proc. 27.

Clegg, Z., P.J. Farres, and J.W. Poesen. 1999. Soil surface drip point features: an integrated approach using analytical photogrammetry and soil micromorphology. Catena. 35, 303-316.

Cremers, N.H.D.T., P.M.V. Dijk, A.P.J.D. Roo, and M.A. Verzandvoort. 1996. Spatial and temporal variability of

soil surface roughness and the application in hydrological and soil erosion modeling. Hydrol. Process. 10 . 1035–1047.

Currence, H.D., and W.G. Lovely., 1970. The analysis of soil surface roughness. Trans. ASAE. 13, 710–714.

Darboux, F., P. Davy, C. Gascuel-Odoux, and C. Huang. 2001. Evolution of soil surface roughness and flowpath connectivity in overland flow experiments. Catena. 46, 125-139.

Darboux, F., and C. Huang. 2003. An instantaneous-profile laser scanner to measure soil surface microtopography. Soil Science Society of America Journal. 67, 92-99.

Eltz, F.L.F., and L.D. Norton. 1997. Surface roughness changes as affected by rainfall erosivity, tillage, and canopy cover. Soil Science Society of America Journal. 61, 1746-1755.

Govers, G., I. Takken, and K. Helming. 2000. Soil roughness and overland flow. Agronomie. 20, 131-146.

Hansen, B., P. Schjonning, and E. Sibbesen. 1999. Roughness indices for estimation of depression storage capacity of tilled soil surfaces. Soil and Tillage Research. 52, 103-111.

Helming, K., C.H. Roth, R. Wolf, and H. Diestel., 1993. Characterization of rainfall—microrelief interactions with runoff using parameters derived from Digital Elevation Models (DEMs). Soil Technology. 6, 273–286.

Huang, C., E.G. White, E.G. Thwaite, and A. Bendel., 1988. A noncontact laser system for measuring soil surface topography. Soil Sci. Soc. Am. J., 52, 350-355.

Huang., C., and J.M. Bradford., 1992. Applications of a laser scanner to quantify soil microtopography. Soil Sci. Soc. Am. J., 56, 14-21.

Jester, W., and A. Klik. 2005. Soil surface roughness measurement--methods, applicability, and surface representation. Catena, 64, 174-192.

Kamphorst, E.C., V. Jetten, J. Guerif, J. Pitkanen, B.V. Iversen, J.T. Douglas, and A. Paz. 2000. Predicting depressional storage from soil surface roughness. Soil Science Society of America Journal. 64, 1749-1758.

Kirby, R.P., 1991. Measurement of surface roughness in desert terrain by close range photogrammetry. Photogrammetric record. 13, 855-875.

Linden., D.R., and V.D. D.M., 1986. Parameters for characterizing tillage-induced soil surface roughness. Soil Sci. Soc. Am. J. 50, 1560-1565.

McDonald, A.; Crossley, S.; Bennet, J.; Brown, S.; Cookmartin, G.; Morrison, K.; Quegan, S., 1999. Stereo vision measurements of soil surface characteristics and their use in model validation. SAR Workshop: CEOS Committee on Earth Observation Satellites; Working Group on Calibration and Validation, 26-29 October 1999, Toulouse,

Mirzaei, M.R., S. Ruy, G. Ghazavi, and C. Boaner. 2008. Soil microtopography studies using Stereophography and Laser-Scaning methods. Journal of Science and Technology of Agriculture and Natural Resources, *in press*.

MVTec, S.G., (ed.) 2006. HALCON application note "Machine Vision in World Coordinates" version 7.1, pp. 1-144. München, Germany.

Planchon, O., M. Esteves, N. Silvera, and J.-M. Lapetite. 2002. Microrelief induced by tillage: measurement and modelling of Surface Storage Capacity. Catena, 46, 141-157.

Saleh, A., 1993. Soil Roughness Measurement - Chain Method. Journal of Soil and Water Conservation. 48, 527-529.

Saleh, A., 1994. Measuring and predicting ridge-orientation effect on soil surface roughness. Soil Sci. Soc. Am. J., 58, 1228-1230.

Taconet, O., and V. Ciarletti. 2007. Estimating soil roughness indices on a ridge-and-furrow surface using stereo photogrammetry. Soil and Tillage Research. 93, 64-76.

Vazquez, E.V., J.G.V. Miranda, and A.P. Gonzalez. 2005. Characterizing anisotropy and heterogeneity of soil surface microtopography using fractal models. Ecological Modelling. 182, 337-353.

Vazquez, E.V., J.G.V. Miranda, and A.P. Gonzalez. 2007. Describing soil surface microrelief by crossover length and fractal dimension. Nonlinear Processes in Geophysics. 14, 223–235.

Zhixiong, L., C. Nan, U.D. Perdok, and W.B. Hoogmoed. 2005. Characterisation of Soil Profile Roughness. Biosystems Engineering. 91, 369-377.

Ziarati, T., S. Ruy, and M.R. Mirzaei. 2007. Caractériser les possibilités de la stéréophotographie pour le suivi de différents indices de rugosité sous l'action des pluies. INRA, Avignon.

Annexe 6 : Monitoring roughness changes caused by rainfall using photogrammetry (Soumis à Catena)

Monitoring roughness changes caused by rainfall using photogrammetry.

Mirzaei, M.R., Ruy, S., Ziarati, T., Rist, A. and Khaledian, M.R

Date received: 02 Jul 2008

Abstract:

Microtopography of the soil surface strongly affects various hydrological processes such as water infiltration, surface water storage, surface runoff and erosion. It is thus important to quantify soil surface microtopography. This is classically done using roughness indices which are calculated by means of roughness profiles. However, as a profile is two-dimensional (along one axis), this approach is only valid for isotropic conditions, which is rarely the case in agricultural systems. A new method to easily generate three-dimensional digital elevation models (DEM) under field conditions is stereo-photogrammetry.

In this study we tested stereo-photogrammetry under field conditions to detect changes of soil surface roughness due to rainfall on two agricultural soils surfaces - a seedbed plot and a harrowed plot. Three rainfalls were simulated on the two plots of $1m^2$ with intensities of 60, 80 and 80 mm/h respectively and DEMs were generated before and after each rainfall. Three groups of roughness indices were calculated for each situation by means of the DEMs: (1) random roughness (*RR*), reduced random roughness (*RR_rd*) and corrected random roughness (*RR_cr*), (2) Tortuosity (T_b) as well as (3) limiting elevation difference (*LD*) and limiting slope (*LS*). In addition, surface variograms were calculated to characterize the microtopography at the beginning and end of the rainfall experiment.

A detailed analysis of the factors influencing the stereophotogrammetry process and the calibration of the system showed the importance of a stable support bearing the two cameras and calm weather conditions. It was further necessary to consider the effect of the correlation window size to optimize the DEM quality.

All investigated roughness indices decreased as a result of rainfall on both plots; especially *LD* and *RR_cr* were found to be highly negatively correlated to cumulative rainfall. Rainfall has thus a smoothening effect on the soil surface. However, due to some difficulties in estimating T_b, no statement on its usability for the detection of roughness changes due to rainfall could be made in this study. The analysis of the surface variograms showed that the heterogeneity of the soil surface can be decreased by rainfall, while the spatial correlation can be increased.

This study showed that if some basic provisions are considered to guarantee the image quality, stereo-photogrammetry is a promising method to monitor soil surface roughness and its changes caused by rainfall.

Keywords: soil surface roughness indices; digital elevation model; stereo-photogrammetry; surface variogram; rainfall simulation

1 Introduction

The micro-relief or roughness of a ground surface refers to elevations differences at the scale of centimeter to decimeter (Kamphorst, 2000) and can be measured at the scale of meters (Soil Survey Manual, 1993). This soil surface characteristic strongly affects hydrological processes such as infiltration, surface water detention and soil erosion; thus, monitoring of soil micro-relief is important for the prediction of runoff or erosion.

In a field scale two types of roughness can be distinguished, (i) random roughness and (ii) oriented roughness. The first one is due to the random distribution of the soil aggregates on the surface at a small scale, while oriented roughness is the result of agricultural operations carried out by humans.

Surface roughness characterisation is limited to different indices. The must commonly used indices are random roughness and tortuosity. These indices generally have been defined for profiles (1D) whereas soil elevation is usually anisotropic and the calculation of soil roughness indices from (1D) measurement can be called into question. However these indices can easily be extended to surface (e.g. tortuosity, Helming *et al.*, 1993).

To calculate the roughness indices, first the soil surface micro-relief has to be recorded. For this purpose, different techniques were developed which can be divided into two main groups, (i) contact method such as a pin meter (Kuipers, 1957; Podmore and Huggins., 1981) or a chain meter (Saleh, 1993; Saleh, 1994; Merrill, 1998) and (ii) non-contact method like photogrammetry (Jester and Klik, 2005; Mirzaei et al., in press). Taconet and Ciarletti, 2007; Zribi et al., 2000), laser in the form of point or line scanning (Bertuzzi et al., 1990a; Darboux and Huang, 2003; Huang et al., 1988 and 1992; Pardini et al., 1995; Römkens et al., 1986) and radar or remote sensing (Moran et al., 1997; Rahman et al., 2008; Sano et al., 1998). The contact methods are widely used under field condition because of their easy handling and low costs. However as they require to be in direct contact with the soil surface its micro-relief could be disturbed. This method is replaced gradually by laser method. The great progress in roughness studies was made by apparition of laser meters at the end of the 1980s. Laser scanners have high spatial resolution (vertical: 0.1-0.5 mm and horizontal: 0.1-2 mm). They thus allow for the accurate recording of soil surface properties and erosion processes. This major advantage faces the difficulty of being fragile and unhandy for the use in the field. However field operation is possible but very elaborate and is supposed to be associated with loss of accuracy (e.g. reflection of sunlight and movement of the device), and needs a relatively short measurement time faced quite much effort for data preparation (Jester and Klik, 2005; Mirzaei and Ruy, 2008). In comparison with laser method, photogrammetry is not yet commonly used for the recording of soil surface micro-relief and is still in experimental phase. However, this method could be used more and more in practice by improving the method for automatic stereo-correlation and continual progress of CCD-cameras. The disadvantages of this method are time-consuming and requiring computing procedures and needs an extensive knowledge about image processing. The great advantage of this method is quick data acquisition, because roughness can change rapidly during rainfall where laser meter can not be used. Accuracy and

resolution of this technique should usually be checked by a laser scanner (as reference method). The horizontal accuracy of a digital elevation model (DEM) generated by photogrammetry is comparable to this one generated by laser meter, while the vertical accuracy does not reach to submilimeter.

Recently photogrammetry was used as a soil surface monitoring tool and several studies in the laboratory and field have shown that it generates reliable data (presented in the form of a DEM) to characterize erosion and soil surfaces (Kirby 1991, Rieke-Zapp and Nearing, 2005a; Rieke-Zapp and Nearing, 2005b; Taconet and Ciarletti, 2007). Histogram of elevations data is similar for laser method and photogrammetry. In contrast, slope histogram shows more difference between two methods, as photogrammetry tends to lower slopes and the frequency of larger slops diminished and produce a DEM with a smoother surface (Jester and Klik, 2005; Mirzaei et al., in press). Taconet and Ciarletti (2007) used photogrammetry for the determination of soil surface roughness indices and showed that tortuosity is more suitable to detect important degree of soil degradation. Mirzaei et al. (in press) compared photogrammetry and laser method by means of DEMs and roughness indices. Their measurements were performed on rough and smooth soil surfaces reproduced by polyesters. They showed that random roughness index and maximum depression storage were slightly underestimated by photogrammetry compared to the laser method (between 5% and 15%). However, this study also continued by a field rainfall simulation study (Mirzaei and Ruy, 2008).Their results showed that limiting elevation difference (LD) was the most sensitive roughness indices that detect to the roughness change due to rainfall, moreover there was no difference (at P= 5%) between two methods.

A variety of natural processes modify soil surface roughness over time such as wind, rain splash and runoff. Microtopography is smoothed by these processes, as depressions tend to be filled at the expense of higher points. Dexter (1977) showed that random roughness decreased exponentially with cumulative rainfall. Similar results were obtained by other authors (Johnson et al., 1979; Zobeck and Onstad, 1987; Guzha, 2004; Eltz and Norton, 1997), all these studies being performed in the context of different tillage treatments.

This paper deals with the quantitative characterization of different small-scale soil roughness indices on bare agricultural soils. The overall aim was to analyze the ability of a stereo-photographic to detect changes to soil surface roughness due to rainfall as a monitoring tool. A further objective was to work out technical recommendation on the use of photogrammetry to guaranty reliable results in field conditions.

2. Materials and Methods

2.1 Study site

This study was performed on an experimental site of the INRA centre in Avignon (south of France). The soil was classified as Calcolsol of alluvial origin. The A-horizon (0-60 cm) is very structured; texture is a clay-loam at the surface. The experiments were carried out on two square

measuring plots (area: $1m^2$) with two different soil roughness, a seedbed plot (slope: 1%) and a harrowed plot (slope: 5%). The field had been cultivated with wheat. After a manual harvest, the soil was tilled with a plough share and then with a circular spike harrow combined with a cultipacker (a weighted clod crusher) in order to obtain a more or less smooth soil surface representative of seedbed preparation. On the second plot, the ridges of a furrowed surface were created manually at 30 cm intervals and a height of 8 cm.

2.2 Rainfall simulation

A sprinkler irrigation system was used to simulate rainfall whose intensity could be controlled by a barometer. In order to achieve a uniform spatial distribution of the rainfall four sprinklers were installed at the four corners of a 1.8 m x 1.8 m square plot surrounding the measurement plot in the centre. Three successive rainfall simulations were imposed separately on each plot with intensities of 60, 80 and 80 mm h^{-1} respectively. During all experiments, the spatial distribution and intensity of the applied water on the surface of the measuring plot was controlled by 8 rain gauges located at the four corners and in the middle of each side of a 1.1 x 1.1 m square surrounding the measuring plot.

2.3 An overview of calculated roughness indices

2.3.1 Elevation standard deviation (RR, RR_rd, RR_cr)

Standard deviation of a surface roughness describes variations in surface elevation. This is the most basic type of profile description (Taconet and Ciarletti, 2007; Zhixiong et al., 2005; Kamphorst et al., 2000). This index has a purely statistically basis and does not consider spatial distribution.

Allmaras *et al.* (1966) defined Random Roughness as the standard deviation of elevations. In this method, the original height reading is first transformed by the natural logarithm. The effects of slope and tillage are then removed by correcting each reading for the average of the row and the column containing the reading. RR is calculated after eliminating the upper and lower 10 percent of data.

We calculated three standard deviations for each DEM: (i) with all height readings (*RR*), (ii) after eliminating 10 percent of the data (*RR_rd*) and (iii) applying the corrected height (*RR_cr*) as described by Currence and Lovely (1970). These authors showed that when random roughness is calculated without any logarithm transformation, it is more sensitive to roughness changes. We thus applied this method during our study.

Several studies showed that this indice is sensitive to surface evolutions caused by rainfall (Bertuzzi *et al*., 1990a; Mirzaei et al., in press).

2.3.2 Tortuosity (T_b)

Boiffin (1984) were the first to use T_b as a roughness indice. T_b is defined as the ratio between the length of a profile of ground (L1: real length) and the horizontally projected length of the same profile of ground (L0: projected length):

$$T_b = \frac{L_1}{L_0} \geq 1 \qquad 1$$

This indice is frequently measured using the chain method (Saleh, 1993) but can be estimated with data elevations obtained by a laser meter or DEM, depending on its spatial definition. This definition extends to a three-dimensional DEM as the ratio of the total surface area to the projected map area (Helming et al., 1993). This indice also is suitable for microtopography changes due to rainfall (Bertuzzi *et al*., 1990b; Eltz and Norton., 1997; Mirzaei and al 2008).

2.3.3 Surface Variogram

Contrary to profiles data, photogrammetry prepares the 3D elevation data (DEMs) which allow calculating surface variogram. These variograms were calculated using ILWIS-GIS package to analyse the anisotropy in the spatial correlation of elevation data. This operation calculates a surface of semi-variogram values where each pixel in the surface represents a directional distance class. Distance and optionally direction is calculated between all points of possible point pairs. Semi-variogram values are calculated from the values of those point pairs which fall within the same lag, i.e. the same distance (and direction) class.

The output of the Variogram surface operation is a plot, depicted as a raster map, with the origin in the center (with a zero value). Each pixel in the output map has the size of the user-specified lag spacing. The maximum number of lags allowed under the ILWIS software is 45, so in this case only a plot with a surface area of 45*45 mm^2 (area of 90*90 mm) was considered.

2.3.4 Limiting Elevation Difference and Slope (LD and LS)

Linden and Van Doren (1986) described new indices (*LD* for Limiting elevation Difference and *LS* for Limiting Slope) that are sensitive to roughness changes. These indices are the configuration parameters based on geostatistical analysis and they account for the spatial structure of elevation data.

The calculation of *LS* and *LD* are based on the mean absolute elevation difference, or the first order variogram,

$$\Delta Z_l = \sum_{i=1}^{n} \left| \frac{Z_i - Z_{i+l}}{n} \right|, \qquad 2$$

where Z_i is the elevation of point i, and Z_{i+l} is the elevation of a point some lag numbers l from point Z_i.

The relationship between ΔZ_l and the lag distance, ΔX_l, was obtained using a linear regression of their reciprocals:

$$\frac{1}{\Delta Z_l} = a + b(\frac{1}{\Delta X_l}), \qquad 3$$

where a and b are fitted constants.

Horizontal spacing ΔX_l was limited to a maximum of 200 mm. The reciprocals of the constants a and b, were designated as Limiting elevation Difference, *LD*, and Limiting Slope, *LS*, respectively:

$$LD = 1/a \qquad LS = 1/b \qquad 4$$

The Linden and Van Doren (1986) procedure was successfully tested by Bertuzzi et al. (1990b) as showing changes to the morphology and magnitude of roughness due to rainfall.

Because the spatial structure could exhibit some degree of anisotropy (see above), these parameters were obtained separately in perpendicular and horizontal directions, i.e. rows (X) and columns (Y). Linden and Van Doren (1986) had shown that 50 samples with segments of 20 cm in both directions were sufficient to calculate *LD* and *LS* indices parameters. First of all, we chose at random 50, 200 and 500 segments for the three DEMs. The test results only changed slightly with an increase in sample size. This is in accordance with Linden and Van Doren (1986). However to guarantee the sample size to be sufficient 200 samples were used for each DEM. Another consideration was the length of the segments. From analysis of some of the variograms, their ranges in all cases (seedbed and harrowed plot) were found to be less than 15 cm. It was therefore decided to use 15 cm segments to calculate these parameters. The lag distance thus ranged from 1 mm to 150 mm. A single segment was then chosen at random from a selected row or column. Finally, the means of rows and columns was calculated.

2.4 Photogrammetry data

Table 1: Employed dataset and labelling of different trials during rainfall

	Conditions						
State / plot	Initial*	Rain1	Rain2		Rain3		Final*
Seedbed	S_IN	S1_AF	S2_BE	S2_AF	S3_BE	S3_AF	S_FIN
Harrowed	H_IN	H1_AF	H2_BE	H2_AF	H3_BE	H3_AF	H_FIN

*** In the initial and final states, the soil surface was dry. BE: before rainfall and AF: after rainfall.**

The stereo-camera system was mounted on a rigid support (made by INRA in Avignon). The height of photographs could be changed within a range of 1 to 4 meters above the soil surface. Photos

were taken using a pair of Nikon D100 cameras with a constant theoretical focal length of 35 mm, and a CCD sensor of 3000 x 2008 pixels.

During a preliminary study, the optimum setup for photography was determined (Ziarati et al., 2007) which turned out to be an F8 aperture and a distance of 3 to 4.5 m from the stereo-camera system to the soil surface. Before each rainfall simulation, the photogrammetry system was calibrated by taking at least 20 photos of the calibration plate in different positions. The calibrated parameters were applied to obtain the DEMs before and after rainfall (Table 1).

2.5 Calibration process and stability of the frame

The photogrammetry process in the field condition contrary to the laboratory condition could be disturbed by some uncontrollable and undesired factors (such as wind) causing the instability of the stereo-camera system. For this reason it is necessary to calibrate the stereo-camera system before and after rainfall in a field condition. There was no problem to calibrate the system prior to rainfall. However, after rainfall, the soil was very damp; the calibration plate could not be placed directly on the soil surface, because it would have changed its roughness. The calibration plate was thus hold manually without touching the soil surface, resulting in undesired vibrations of the calibration plate during the photography. These vibrations can disturb the calibration process. As mentioned by Mirzaei et al. (in press) in stable condition, the same calibration parameters obtained before rainfall could be used for after rainfall. So in this case we supposed that the stereo-camera system was stable in period of a rainfall event and the images taken before rainfall were used to calibrate the stereo-camera system.

2.6 DEM reconstruction

One of the most difficult and important steps in the 3D reconstruction of an object using binocular-stereo vision is the matching of homologous points, i.e. the projection of one object point into the two images. When homologous points have been identified, a disparity map is generated by the software (Halcon, MVTec, 2006). Disparity is the difference between the coordinate of these points on the x and y axes. In fact, disparities are an indicator of the distance of object points from the stereo camera system, because points with equal disparities will also have equal distances (MVTec, 2006). However before the identification of homologue points the two images first have to be rectified to obtain the epipolar geometry. After image rectification, homologous points are in the same row in two images ($row_1 = row_2$). This facilitates the matching process between two points which is established by measuring the similarity of neighbouring points. This similarity is calculated as the correlation between gray values of the pixels surrounding the two candidate points. Each pixel in the left-hand image is considered to be the centre of a fixed window with the dimensions of M*N pixels. A motion window of the same size moves in the right-hand image with the centre pixel over the same row number of the left-hand window.

Several parameters can be used to control the behaviour of the matching process in order to determine homologous points such as windows size and method of similarity choosing. In order to demonstrate the effect of window size on the DEMs obtained during the study, one DEM was calculated using three different window sizes (5*5, 11*11, and 21*21).

Calibration, matching process and DEM reconstruction were performed using commercial software called Halcon (MVTec, 2006). For the matching process the Normalized Cross Correlation (NCC) method was employed which compensates for the mean gray value and its variance within the matching window. NCC is more time-consuming than other methods but is markedly preferable if the two images differ in terms of their brightness and contrast.

DEMs obtained using the triangulation process (stereo-photogrammetry) were not regular and the space lag between two adjacent points could also vary from less than 0.5 mm to more than 0.8 mm depending on the distance between the soil surface and the focal plane of the cameras. So the elevations were linearly interpolated on a regular grid, with a space lag of 1 mm in both directions and for all DEMs. So, they were transformed to raster maps with a pixel size of 1mm. These DEMs were used to estimation of roughness indices without any image processing such as median filtering.

2.7 Checking Usability of the generated DEMs

Highly accurate ground control points are necessary to validate the generated DEM which are not available in this study. However a criterion was therefore necessary to check the validity of the DEMs in micro topographical scale and to decide whether to retain or remove the DEM from the database. To achieve this, each DEM was analysed using a pattern filter, and it was thus possible to detect areas where pixels were more or less of the same value, and outliers where the values of all neighbours were markedly different from the central pixel. This was achieved with a 3 * 3 pixel window. A threshold of 10 mm was determined for the seedbed plot and 30 mm for the harrowed plot. These thresholds were representative of the maximum diameter of clods at the soil surface of both plots.

3 Results and Discussion

3.1 Calibration parameters and windows size effect

When the images taken after rainfall were used to obtain calibration parameters, all of calibration parameters were unusable as a result of calibration plate vibrations. The intrinsic parameters obtained with these images differed only slightly from those obtained from the set taken before rainfall, but these slight changes were sufficient to nullify the rectification process. So the calibration parameters before rainfall were used to obtain the DEM after rainfall for each rainfall simulation.

The generated DEMs differed markedly using different correlation window size (Figure 1). Using

the dimensions 5*5, matching process was unsatisfactory and numerous noise points, or outliers, were present. With an 11*11 window size, we obtained acceptable DEM values despite the existence of some outliers. Using a 21*21 window, the achieved DEM was very smooth and outliers had disappeared; this may have influenced the roughness indice. We therefore applied the 11*11 window size, which had also been used by Taconet and Ciarletti (2007).

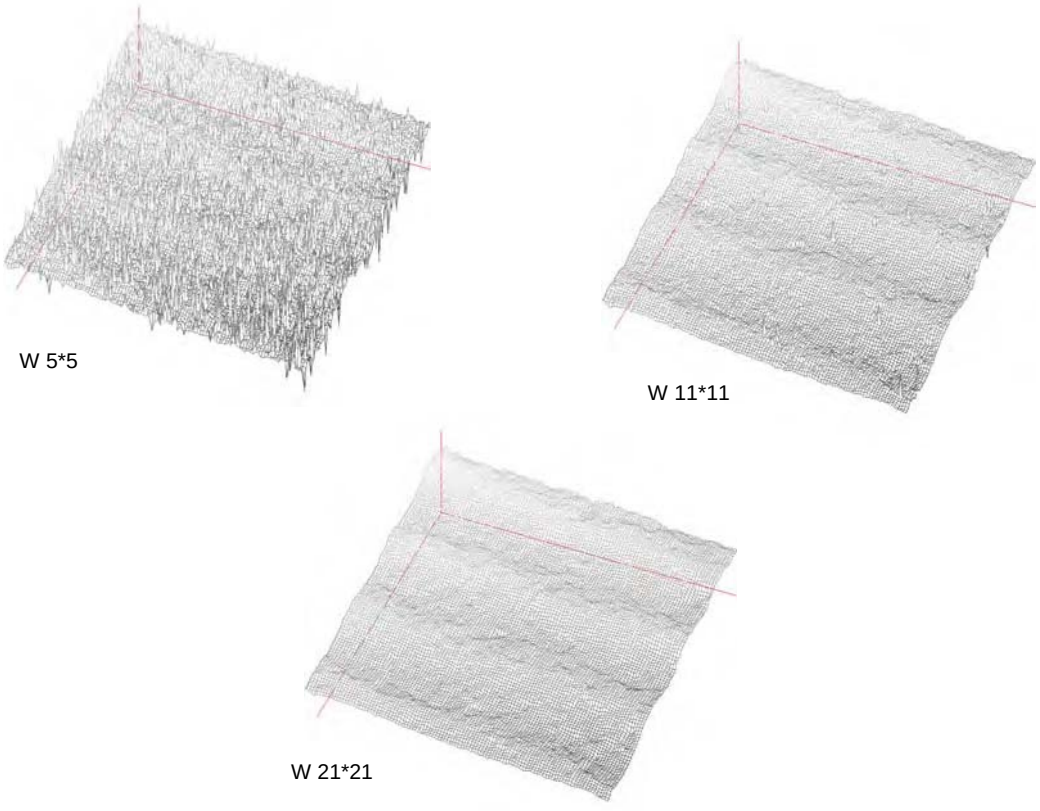

Figure 1: Effect of using different sizes of correlation window

3.2 Usability of the generated DEMs

The overall shape of each DEM, and several statistical parameters of elevation data (e.g. averages) were checked. As shown in Figure 2, the values appeared to be reliable from a qualitative point of view on the plot scale such as the main aggregate position, agricultural treatments, ridge and furrows for harrowed plot. However, a pattern filter was used to check the usability of the DEMs.

For the seedbed plot the DEMs S2_AF and S3_BE were very similar (as expected, since they represent the same surface), with a few outliers situated in the same areas on both plots (Figure 2). It was expected that S3_AF would be smoother than S3_BE with fewer outliers due to rainfall effect. However this was not the case. The large number of outliers and their distribution throughout the surface of S3_AF were attributed to erroneous calibration. Similar results could be obtained for the

harrowed plot: while the DEM H2_BE was of good quality, many outliers appeared on H1_AF or H2_AF. Moreover, the density of outliers on H2_AF could only be seen in the bottom left-hand corner of the image. These results showed that before calculating roughness indices a DEM, its usability has to be checked. We suppose that outliers can be ascribed to oscillations of the frame bearing the two cameras resulting from high wind speed during the data acquisition for the DEMs S3_AF, H1_AF and H2_AF. These 3 DEMs were therefore removed from our data set. We have nonetheless presented the results of the roughness indices calculated by these DEMs in order to demonstrate the influence of erroneous calibration.

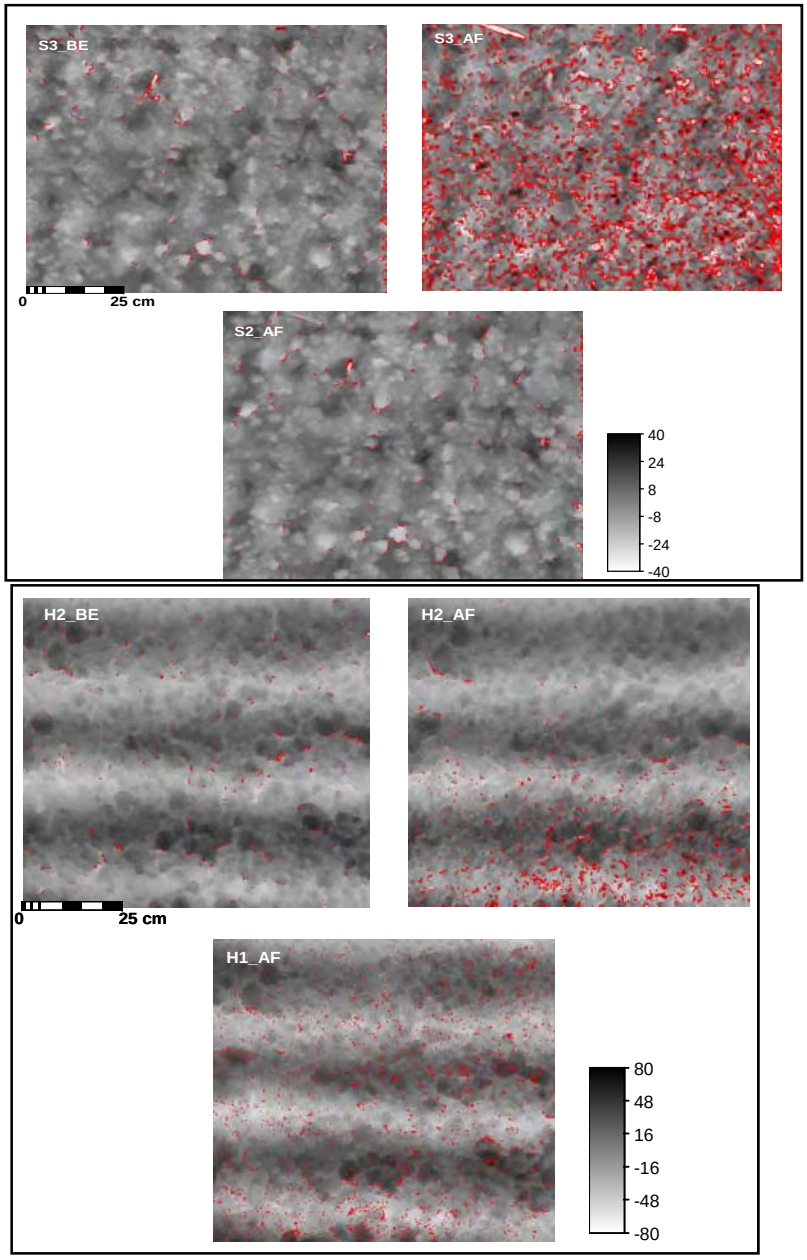

Figure 2: outliers (in red) detection using a pattern filter on generated DEMs. Elevation scale is in mm. For abbreviation see Table 1

To gain a visual impression of the soil surface under different conditions, DEMs were visualized three dimensionally. Figure 3 shows that the surface of the seedbed plot was initially rough and became smoother towards the end of the experiments due to rainfall, on the harrowed plot, we observed a reduction in the amplitude of furrows as well as a smoothing of the surface.

After each movement or displacement of the cameras or the support, the stereo system must be calibrated. Once the camera-system is stable, one calibration using a single set of photos is sufficient for the entire period of experiment. Moreover, multiple photos can be easily and quickly captured during the experiment, providing additional information on runoff and erosion processes.

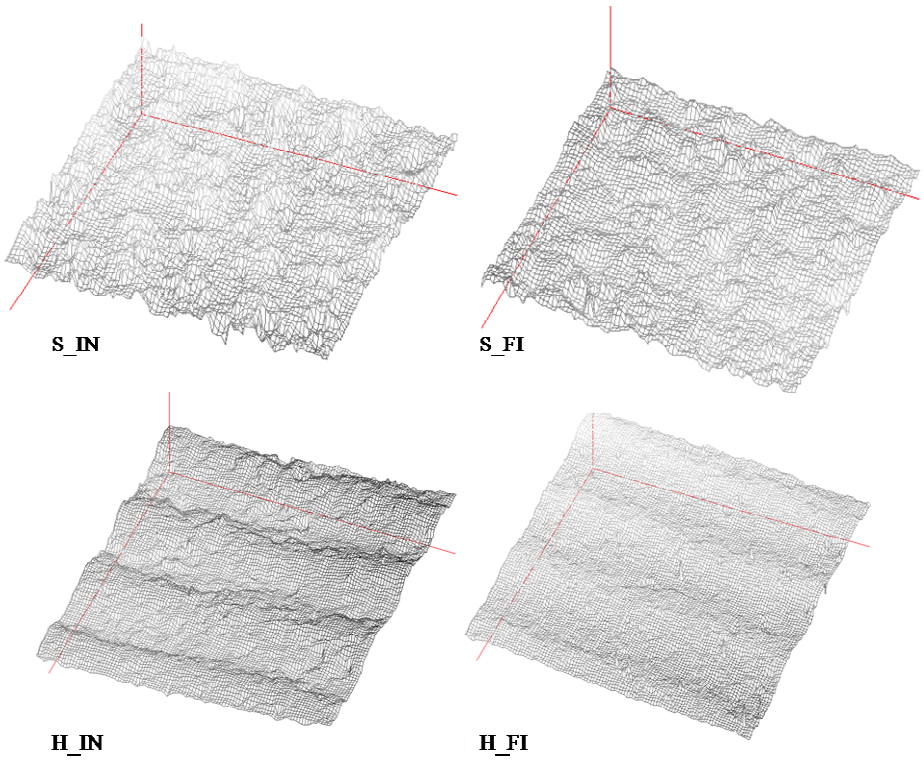

Figure 3: Four examples of three dimensional DEMs obtained under different conditions on the two plots. For abbreviation see Table 1.

3.3 Random Roughness indices

The random roughness indices *RR*, *RR_rd* and *RR_cr* were calculated for each DEM.

The results of one-way ANOVA tests showed that *the* three random roughness indices differed significantly for the two plots (P = 5%). In some cases, *RR* did not reveal the same trend as *RR_rd* and *RR_cr* (for the same data): for instance in S1, *RR* increased but *RR_cr* decreased (Figure 4). Roughness generally decreased as a result of rainfall energy, whereas *RR* indice showed an increasing trend specifically on the seedbed plot, so it is not a reliable indicator of roughness changes. The *RR_rd* and

RR_cr indices indicated a monotonous decrease over successive rainfall periods on the both plots (without considering unusable DEMs), except for *RR_rd* on the seedbed plot (compare S2_BE to S2_AF) which showed an increase during second rainfall, contrary to our observations. Therefore, in our view, the *RR* and *RR_rd* indice was not a reliable indicator of roughness changes using photogrammetry, and preference should be given to the *RR_cr* indice.

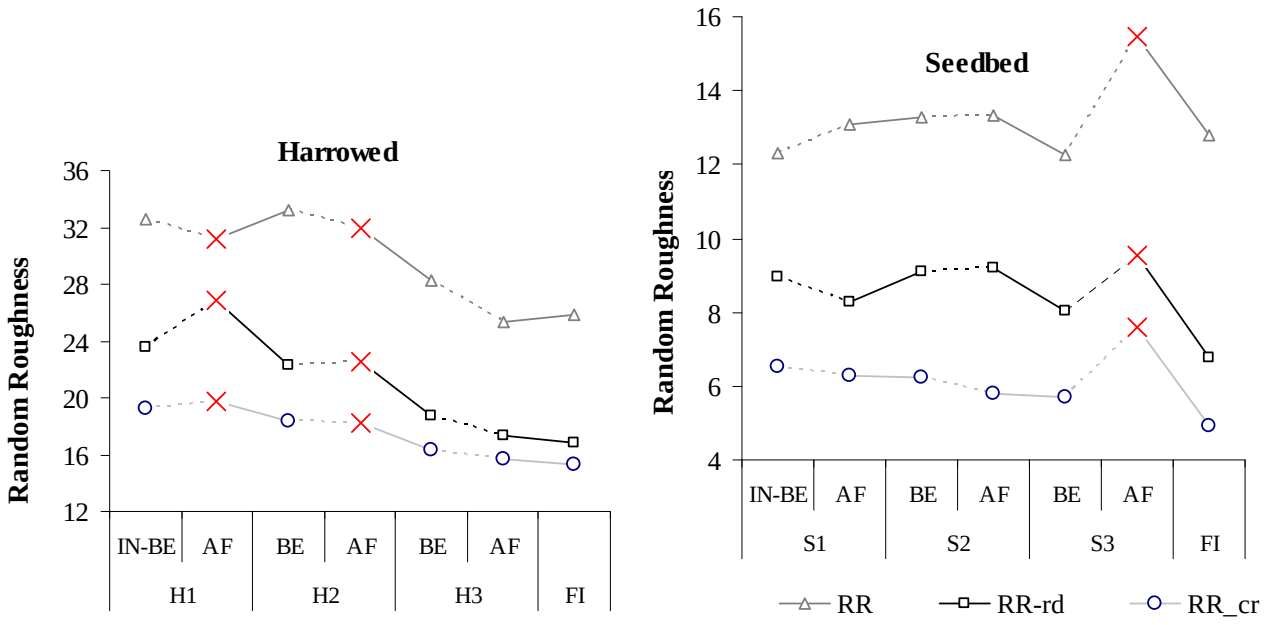

Figure 4: Changes to random roughness indices during the course of the experiment on the harrowed and seedbed plot. Corrupted DEMs are indicated by ×. For abbreviation see Table 1.

On the seedbed plot (harrowed plot), *RR_cr* values decrease from an initial level of 6.54 (19.27) to a final value of 4.93 (15.34), representing a ratio of 0.75 (0.79). The increase in random roughness values during rainfall for the H1_AF and S3_AF could be ascribed to the unusable DEMs.

The values levels for these three roughness indices always were higher on the harrowed plot than the seedbed plot. The three indices are thus capable to distinguish different types of tillage operations.

The interesting characteristic of *RR_cr* was its ability to compare roughness estimates for two rainfall simulations. For example, on the harrowed plot, the *RR_cr* value obtained on H1_BE decreased to H2_BE, and this could be seen even more clearly on the seedbed plot, where it fell from S1_AF to S2_BE and from S2_AF to the final state S3_BE. During soil drying it was observed that the *RR_cr* remained relatively stable (slight increase for the seedbed plot). It was therefore possible to monitor roughness changes by calculating the *RR_cr* indice by photogrammetry which also reported by Mirzaei and Ruy (2008) over soil surface profiles obtained by photogrammetry compared to the laser meter.

3.4 Tortuosity (Tb)

Except for the unusable DEMs (S3_AF, H1_AF and H2_AF), T_b values decreased during rainfall (Figure 5).This overall decrease was only slight for the seedbed plot, as indicated by the ratio of the initial and final value of 0.88. On the harrowed plot, the ratio of 0.74 indicates a stronger overall decrease, whereas in this plot the interpretation for the successive rainfall events was difficult because of an increase from H2_BE to H3_BE.

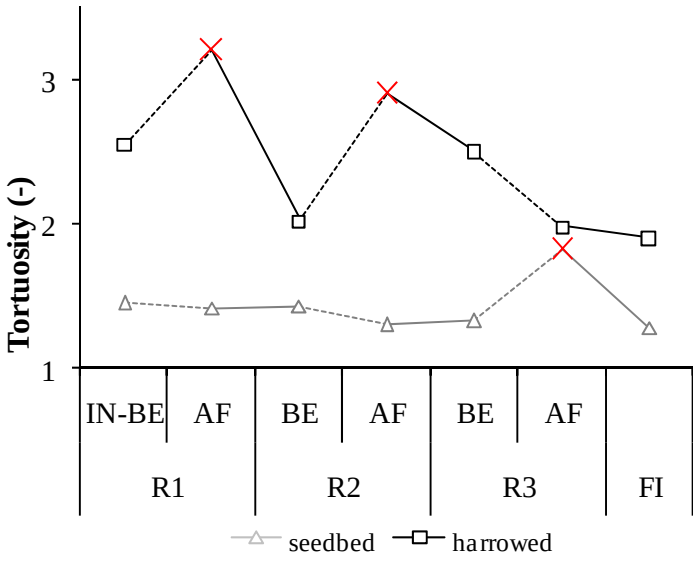

Figure 5: Changes to the tortuosity index calculated during the rainfall simulations. For abbreviation see Table 1.

For the seedbed plot, changes to T_b during a single rainfall event were very slight, for example during the first event, whereas for the harrowed plot showed a marked decrease for the equivalent rainfall. Taconet and Ciarletti (2007) studied this indice using photogrammetry and found it is suitable to detect soil degradation due to rainfall contrary to our study and we don't propose using this factor by photogrammetry.

3.5 Surface variogram analysis

Figure 6 shows the surface variograms computed with ILWIS software. Semi-variogram values close to the origin of the output map were expected to be low (blue colour), because the values for points very close to each other were expected to be similar.

For the seedbed plot, a circle-like shape from the origin outwards was observed, with the colour changing gradually from blue at the origin to green or red at distance from the origin in all directions. This indicates mainly isotropic conditions (S_IN); the slight flatting of the yellow ring in the surface variogram for S_FI indicates a slight anisotropy. The value of semivariogram decreased after rainfall and the correlation distance increased slightly (S_FI).

The harrowed plot is characterized by an ellipse-like shape in the lower (blue) domain in the direction of harrow operation (right to left), reflecting anisotropy. The spatial correlation is greater in the tillage direction than in the perpendicular direction. However, perpendicular to harrow operation, the semi-variogram clearly increased from blue at the origin to green or red as the distance to the origin increased. After rainfall, the spatial correlation increased and the semivariogram values decreased like for the seedbed plot. For the harrowed plot, semi variogram values exhibited the same trends, i.e. a reduction at the origin and at a distance of 45 mm (restricted by used software).

As roughness decreased under the impact of rain drops, the spatial correlation can also change slightly due to rainfall.

The equivalent value for the final state was higher for both plots which show heterogeneity decrease due to rainfall. From a qualitative point of view, it was easy to observe any change to the spatial structure of elevation data. It was thus possible to survey spatial evolutions due to rainfall using photogrammetric data by means of 2D variogram computations.

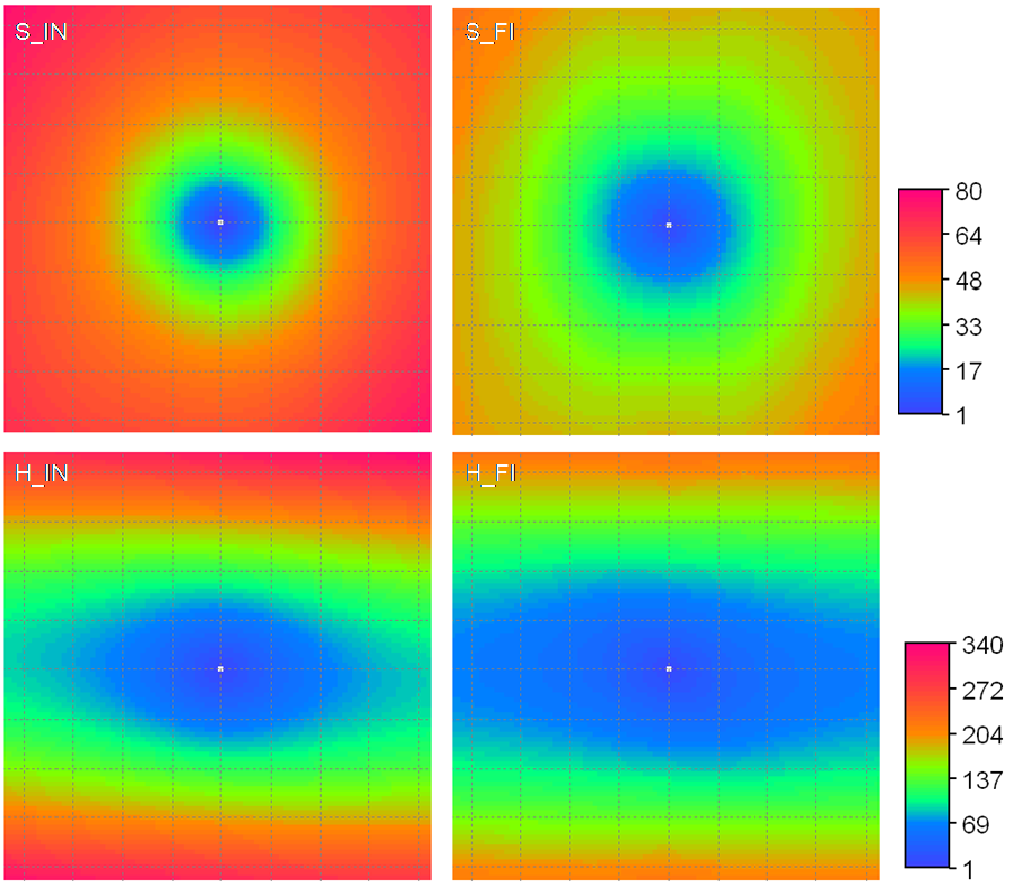

Figure 6: Semi-variograms of soil surface height (mm^2) calculated from directional distance classes for the seedbed (S) and harrowed (H) plots, at the initial (IN) and final (FI) states. Grid lines have a 10 mm scale. The value of centre pixel is zero.

3.6 LD and LS indices:

The experimental relation between the mean absolute elevation difference (ΔZ) and the lag distance agreed well with the theoretical model (Figure 7). For all plots and rainfall events values for the *LD* and *LS* indices are shown in Table 2.

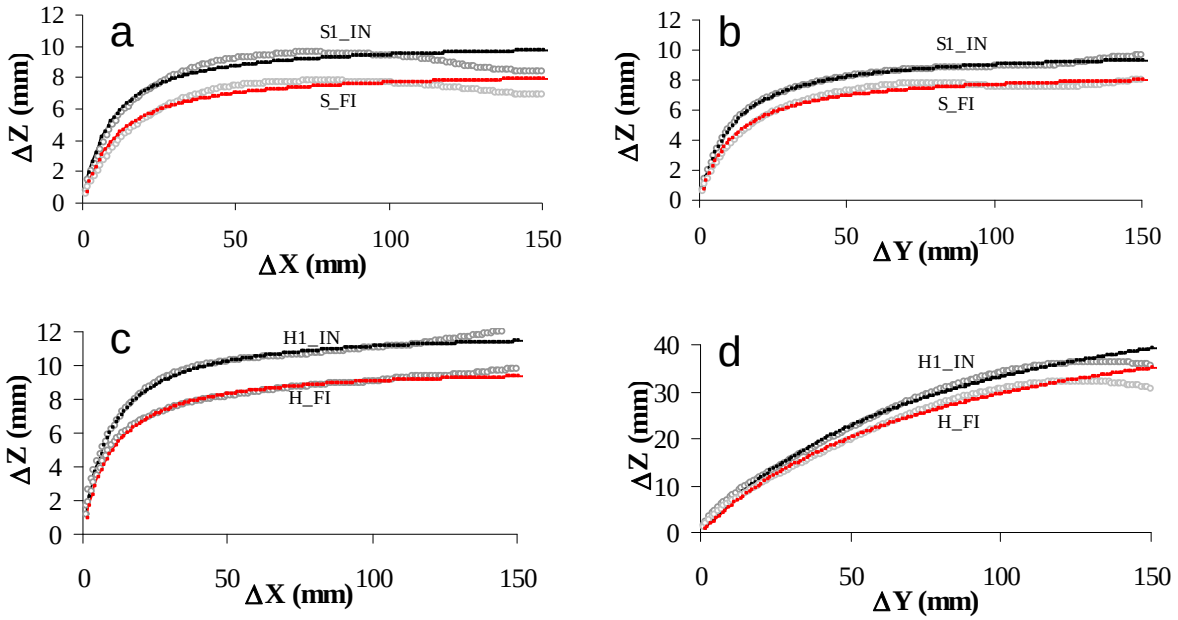

Figure 7: Experimental (gray circles) and theoretical (continuous lines) changes of the mean absolute elevation difference ΔZ with the lag distance for initial and final states. ΔX is the lag distance over row segments parallel to the direction of tillage (a, c), ΔY is the lag distance over column segments perpendicular to the direction of tillage (b, d). For abbreviations see Table 1

There was generally a reduction for *LD* and *LS* values with cumulative rainfall, that was in accordance with finding of Bertuzzi et al. (1990b) but in their study the decrease was more important for *LS* (about 70%) despite a lower cumulative rainfall amount (100 mm with intensity of approximately 40 mmh^{-1}). As soil tillage and soil type were very similar, the difference between the results of Bertuzzi et al. and our results can be attributed to the erosivity (kinetic energy) of the simulated rainfall and/or to the erodibility (structural stability of soil aggregates due to different soil organic matter status) of the soil clods, or to a different measuring device (data measured along transects with a laser meter). Usually photogrammetry gives smaller values for the roughness indices in comparison to the laser meter (Jester and Klik, 2005, Mirzaei et al, in press). However, Mirzaei and Ruy (2008) showed that *LD* values obtained by photogrammetry were similar with those obtained by the laser method. As expected, *LD* values in columns (perpendicular to tillage direction) are larger than row values (mean of 55.8 vs 10.0) in harrowed plot, whereas *LD* is isotropic in the seedbed plot. Whatever the plot, *LS* values along the X direction were always greater than those along the Y direction. By considering the ratio of initial and final value, the smallest change occurred on harrowed

plot in the perpendicular direction of tillage operation.

Table 2: Estimated limiting elevation difference (LD) and slope (LS) roughness parameters for the harrowed and seedbed plots, determined vertically (X) and horizontally (Y) to operation. The gray values were calculated from the unusable DEMs

		HARROWED (H)				SEEDBED (S)			
		ROW (X)		COL (Y)		ROW (X)		COL (Y)	
		LD	LS	LD	LS	LD	LS	LD	LS
Rain1	BE	12.13	1.31	61.10	0.72	10.29	1.16	9.98	0.91
	AF	11.96	1.30	59.33	0.75	8.95	1.16	9.23	0.81
Rain2	BE	11.16	1.27	58.44	0.70	9.16	1.01	9.08	0.97
	AF	12.12	2.12	63.56	0.81	8.46	0.86	8.28	0.63
Rain3	BE	11.12	2.12	56.08	0.81	8.48	0.80	8.57	0.74
	AF	10.83	1.20	52.62	0.74	12.20	3.11	12.89	3.51
	FI	9.95	1.00	51.09	0.64	8.01	0.72	7.38	0.65
Ratio = IN/FI		0.82	0.76	0.90	0.88	0.78	0.62	0.74	0.71

3.7 Correlation between Roughness Indices and Cumulative Rainfall

Correlations between roughness indices and with cumulative rainfall are shown on Table3. For directional indices such as *LD*, we used the average indice computed along the X and Y direction. High correlations between indices were obtained for the seedbed plot in all cases (Table 3), whereas only *LD* and *RR_cr* were highly correlated on the harrowed plot. The negative correlations with cumulative rainfall indicate a decrease of the roughness indices due to rainfall.

The high correlation between *LD* and *RR_cr* is in accordance with the finding of Bertuzzi et al. (1990b) and Linden et al. (1988), and allows these two indices to be used alternatively. The linear relationship between the two indices (Figure. 8) shows that their values are about 3 to 4 times higher for the harrowed plot than for the seedbed plot. *LD* and *RR_cr* are thus suitable to characterize and distinguish the two different plots. However, *LD* should be preferred as it has a physical signification and gives more information while *RR_cr* is only statistically based. *RR_cr* and T_b were only correlated on the seedbed plot but not on the harrowed plot (Figure 9). Regarding the seedbed plot, there was a linear relationship and *RR_cr* ($R^2 = 0.83$) values increased in line with those of T_b, whereas there was no correlation ($R^2 = 0.13$) for the harrowed plot.

Table 3: Calculated correlation coefficients between roughness indices and with rainfall amount

Index	RR_cr	Tb	LD	LS	Rainfall
Seedbed Plot					
RR_cr	1				
Tb	0.916**	1			
LD	0.871**	0.846**	1		
LS	0.846**	0.95**	0.845**	1	
Rainfall	-0.984**	-0.934**	-0.95**	-.92**	1
Harrowed Plot					
RR_cr	1				
Tb	0.37	1			
LD	.93**	.385	1		
LS	.029	.529	.282	1	
Rainfall	-.923**	-.674	-.956**	-.150	1

**** Correlation is significant at the 0.01 level (2-tailed). Dataset: 6 DEMs for the seedbed plot and 5 DEMs for the harrowed plot.**

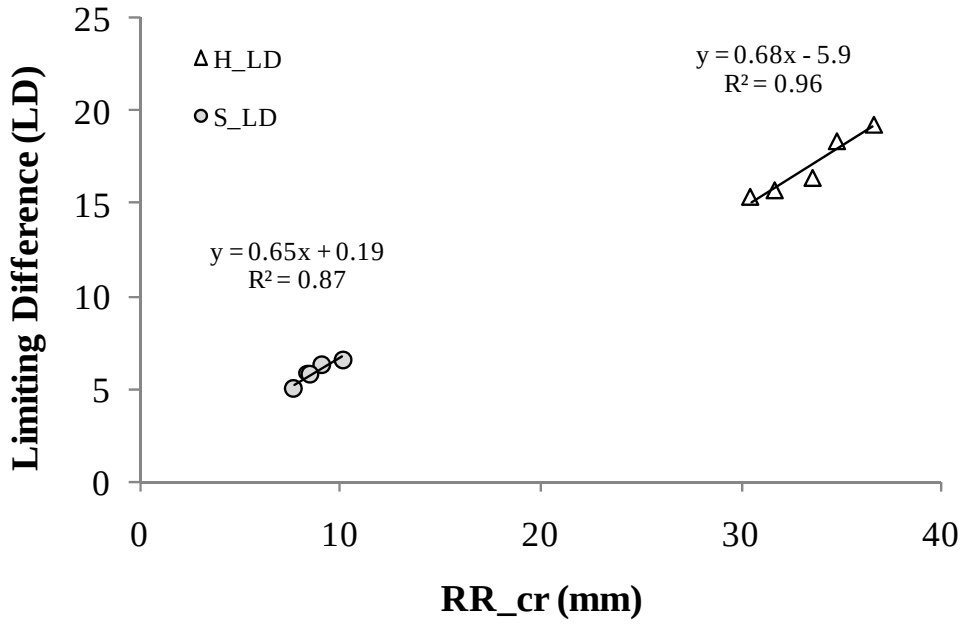

Figure 8: Linear relationship between corrected random roughness (RR_cr) and limiting elevation difference (LD). Circles are for seedbed. Triangles are for harrowed plot, continuous lines are for the linear regression.

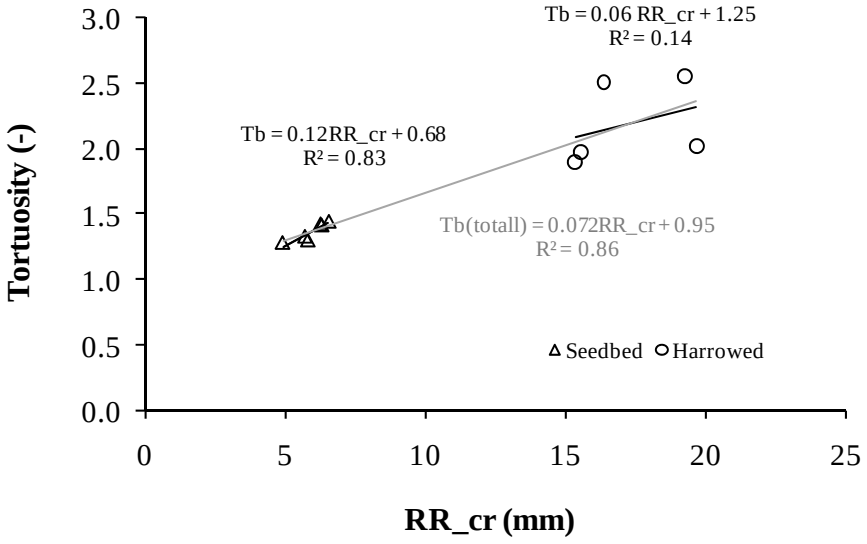

Figure 9: Correlation between the Tortuosity indice and corrected Random roughness (RR_cr)

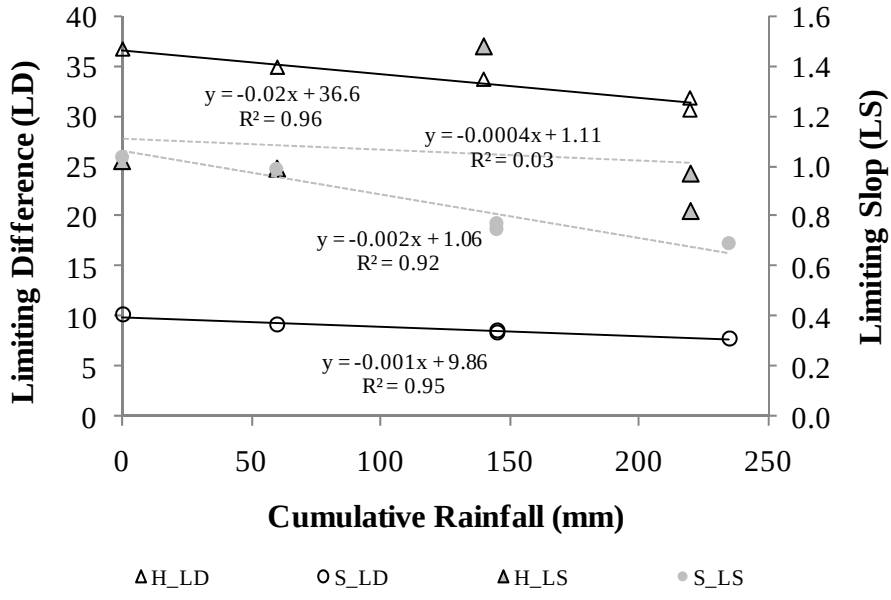

Figure 10: Relationship between limiting elevation difference (LD) and limitation slope (LS) indices with cumulative rainfall.

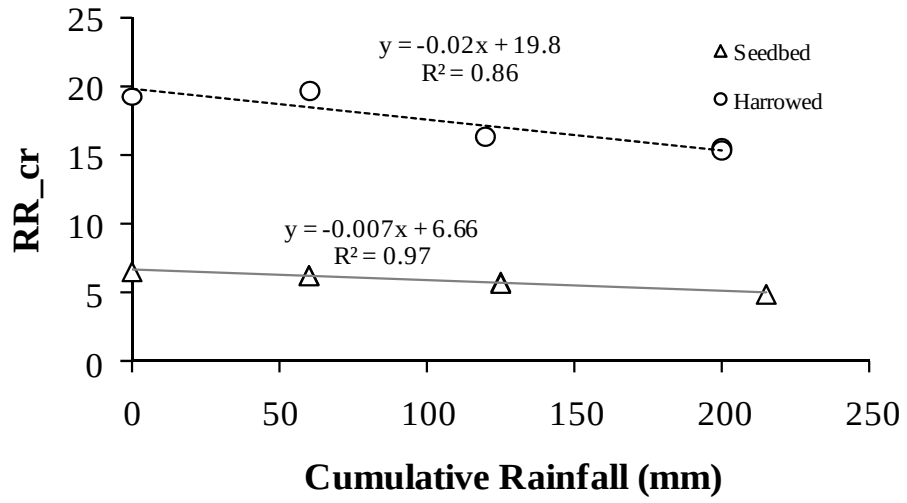

Figure 11: Correlation between cumulative rainfall as independent variable and the roughness index RR_cr.

In most cases, cumulative rainfall was found to be well correlated to roughness indices (see Table 3 and figures 10, 11, 12): this is the case for all indices computed on the seedbed plot, but Tb and LS are weakly related to rainfall on the harrowed plot. Because of the small number of experimental states, only general comments are made on the regression. In all cases the decrease of roughness indice with rainfall is more rapid on the harrowed plot than on the seedbed plot *LD* (Figure 10) and *RR_cr* indice (Figure 11) and T_b indice computed on the seedbed plot (Figure 12) are closely linked to cumulative rainfall, despite the minor erosivity of simulated rainfall.

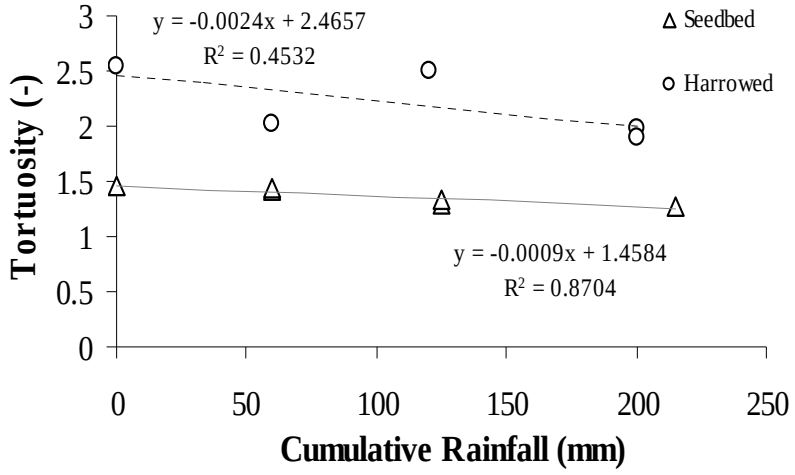

Figure 12: Correlation between cumulative rainfall as an independent variable vs. the Tortuosity indice.

4-Conclusion

Surface micro-topography is one of the principal factors in numerous hydrologic processes. Recent developments in roughness measurement techniques have now made it possible to collect data with a sub-millimetre precision. This study focused on rainfall-related changes to the soil surface microtopography, determined using 3D DEMs obtained with the stereo method.

The stereo-photogrammetry method used in this study was suitable to generate digital elevation models (DEMs) of the soil surface and to calculate various soil surface roughness indices. Seedbed and harrowed plot could be distinguished by means of these indices.

For the random roughness computation, it was showed that eliminating 10 percent over and lower of the data beside the slope correction (*RR_cr*) using trend linear surface gives more reliable response to rainfall simulation. It is also observed that roughness indices are negatively correlated with cumulative rainfall, which was expected

Most of the roughness indices are highly correlated between each other in the seedbed plot. High negative correlations between the roughness indices and cumulative rainfall demonstrate the suitability of these indices to detect changes in soil surface roughness due to rainfall. Spatial indices such as *LD* and *LS* have more physical meaning than statistical indices such as *RR_cr*. *LD* was found to give more reliable value using photogrammetry. The *LD* indice also was related to the *RR_cr* in both plots. We can tell now that these two indices can be obtained using photogrammetry but *LD* is preferred. In this study, T_b was not able to detect the soil surface changes on the harrowed plot.

We propose stereo-photogrammetry to be appropriate for the implication in field experiments. However the following recommendations should be taken into account: (1) A preliminary study must be performed to determine the characteristics of the cameras. (2) The support of the stereo camera system must be rigid and stable. (3) No measurement should be made during environmental conditions that could cause vibrations of the stereo-camera system; especially wind. (4) One of the important option in stereo method as presented here is the windows correlation size for the DEMs reconstruction and so for the calculation of the indices.

This study shows that photogrammetry can now be used as a monitoring tool to study soil surface roughness changes. 3D data are of great interest for hydrologic studies, for instance for the calculation of depressionnal storage capacity or for the validation of microwave remote sensing device (Zribi et al., 2002). This method should be used widely in the field under various pedoclimatic conditions. The scale of measurements can easily be changed from 1m² to 4m² by changing the height of the cameras.

References:

Allmaras, R.R., R.E. Burwell, W.E. Larson, and R.F. Holt. 1966. Total porosity and random roughness of the interrow zone as influence by tillage. USDA Conservation Research Report. 7.

Bertuzzi, P., J.M. Caussignac, P. Stengel, G. Morel, J.Y. Lorendeau, and G. Pelloux. 1990a. An automated, noncontact laser profile meter for measuring soil roughness in situ. Soil Science. 149, 169-178.

Bertuzzi., P., G. Rauws., and D. Courault., 1990b. Testing roughness indices to estimate soil surface roughness changes due to simulated rainfall, . Soil Tillage Res. 17, 87-99.

Boiffin, J. 1984. Structural degradation of the soil surface by the action of rainfall. (In French.) Ph.D. diss. Inst. Natl.

d’Agronomie Paris- Grignon, Paris, France.

Currence, H.D., and W.G. Lovely., 1970. The analysis of soil surface roughness. Trans. ASAE. 13, 710–714.

Darboux, F., and C. Huang. 2003. An instantaneous-profile laser scanner to measure soil surface microtopography. Soil Science Society of America Journal. 67, 92-99.

Dexter, A.R., 1977. Effect of rainfall on the surface micro-relief of tilled soil. Journal of Terramechanics. 14, 11-22.

Eltz, F.L.F., and L.D. Norton. 1997. Surface roughness changes as affected by rainfall erosivity, tillage, and canopy cover. Soil Science Society of America Journal. 61, 1746-1755.

Guzha, A.C., 2004. Effects of tillage on soil microrelief, surface depression storage and soil water storage. Soil and Tillage Research. 76, 105-114.

Hansen, B., P. Schjonning, and E. Sibbesen. 1999. Roughness indices for estimation of depression storage capacity of tilled soil surfaces. Soil and Tillage Research. 52, 103-111.

Helming, K., C.H. Roth, R. Wolf, and H. Diestel., 1993. Characterization of rainfall—microrelief interactions with runoff using parameters derived from Digital Elevation Models (DEMs). Soil Technology. 6, 273–286.

Huang, C., W. E.G., T. E.G., and B. A. 1988. A noncontact laser system for measuring soil surface topography. Soil Sci. Soc. Am. 52, 350-355.

Huang, C., and J.M. Bradford., 1992. Applications of a laser scanner to quantify soil microtopography. Soil Sci. Soc. Am. J. 56, 14-21.

Jester, W., and A. Klik. 2005. Soil surface roughness measurement--methods, applicability, and surface representation. CATENA. 64, 174-192.

Johnson, C.B., J.V. Mannering, and W.C. Moldenhauer. 1979. Influence of surface roughness and clod size and stability on soil water losses. Soil Sci. Soc. Am. J. 43, 772–777.

Kamphorst, E.C., V. Jetten, J. Guerif, J. Pitkanen, B.V. Iversen, J.T. Douglas, and A. Paz. 2000. Predicting depressional storage from soil surface roughness. Soil Science Society of America Journal. 64, 1749-1758.

Kamphorst, E.C. mai, 2000. Mesures et méthodes d'estimation de la capacité de stockage d'eau dans le micro-relief créé par les opérations de travail du sol, 'Institut National Agronomique Paris-Grignon.

Kirby, R.P., 1991. Measurement of surface roughness in desert terrain by close range photogrammetry. Photogrammetric record. 13, 855-875.

Kirkby, M., 2002. Modelling the interactions between soil surface properties and water erosion, Modelisation des interactions entre caracteristiques superficielles des sols et erosion hydrique. CATENA. 46, 89-102.

Kuipers, H., 1957. A reliefmeter for soil cultivation studies. . Netherland Journal of Agricultural Sciences. 5, 255-262.

Linden., D.R., and D.M. Van-Doren., 1986. Parameters for characterizing tillage-induced soil surface roughness. Soil Sci. Soc. Am. J. 50, 1560-1565.

Merrill, S.D., 1998. Comments on the chain method for measuring soil surface roughness: Use of the chain set. Soil Science Society of America Journal. 62, 1147-1149.

Mirzaei, M.R., and S. Ruy. 2008. Effect of rainfall on soil microtopography evaluated using photogrammetry. Soumis in Soil Sci Soc Am J

Mirzaei, M.R., S. Ruy, G. Ghazavi, and C. Boaner. in press (2008). Soil microtopography studies using Stereophography and Laser-Scaning methods. Journal of Science and Technology of Agriculture and Natural Resources.

Moran, M.S., A. Vidal, and D. Troufleau. 1997. Combining Mukifrequency Microwave and Optical Data for Crop Management. Remote Sensing of Environment. 61, 96-109.

MVTec, S.G., (ed.) 2006. HALCON application note "Machine Vision in World Coordinates" version 7.1, pp. 1-144. Mûnchen, Germany.

Pardini, G., R. Pini, R. Barbini, D. Regüès, F. Plana, and F. Gallart. 1995. Laser elevation measurements of a smectite-rich mudrock following freeze-thawing and wet-drying cycles. Soil Technology. 8, 161-175.

Podmore, H.T., and L.F. Huggins., 1981. AN automated profile meter for surface roughness measurements. transctions of the ASAE.

Rahman, M.M., M.S. Moran, D.P. Thoma, R. Bryant, C.D. Holifield Collins, T. Jackson, B.J. Orr, and M. Tischler. 2008. Mapping surface roughness and soil moisture using multi-angle radar imagery without ancillary data. Remote Sensing of Environment. 112, 391-402.

Rieke-Zapp, D.H., and M.A. Nearing. 2005a. Digital close range photogrammetry for measurement of soil erosion. Photogrammetric Record. 20, 69-87.

Rieke-Zapp, D.H., and M.A. Nearing. 2005b. Slope shape effects on erosion: A laboratory study. Soil Science Society of America Journal. 69, 1463-1471.

Römkens, M.J.M., S. Singarayar, and C.J. Gantzer. 1986. An automated non-contact surface profile meter. Soil and Tillage Research. 6, 193-202.

Saleh, A., 1993. Soil Roughness Measurement - Chain Method. Journal of Soil and Water Conservation. 48, 527-529.

Saleh, A., 1994. Measuring and predicting ridge-orientation effect on soil surface roughness. Soil Sci. Soc. Am. 58, 1228-1230.

Sano, E.E., A.R. Huete, D. Troufleau, M.S. Moran, and A. Vidal. 1998. Relation between ESR-1 synthetic aperture radar data and measurements of surface roughness and moisture content of rocky soils in a semiarid rangland. Water resources research. 34, 1491-1498.

Soil Survey Manual. 1993., (last modified 2006), Soil Conservation Service. U.S. Department of Agriculture Handbook 18, Now available online, http://soils.usda.gov/technical/manual/print_version/chapter3.html.

Taconet, O., and V. Ciarletti. 2007. Estimating soil roughness indices on a ridge-and-furrow surface using stereo photogrammetry. Soil and Tillage Research. 93, 64-76.

Zhixiong, L., C. Nan, U.D. Perdok, and W.B. Hoogmoed. 2005. Characterisation of Soil Profile Roughness. Biosystems Engineering. 91, 369-377.

Ziarati, T., S. Ruy, and M.R. Mirzaei. Juin 2007. Caractériser les possibilités de la stéréophotographie pour le suivi de différents indices de rugosité sous l'action des pluies. INRA, Avignon.

Zobeck, T.M., and C.A. Onstad. 1987. Tillage and rainfall effects on random roughness: a review. Soil Tillage Res. ,9 1–20.

Zribi, M., V. Ciarletti, O. Taconet, J. Paille, and P. Boissard. 2000. Characterisation of the Soil Structure and Microwave Backscattering Based on Numerical Three-Dimensional Surface Representation: Analysis with a Fractional Brownian Model. Remote Sensing of Environment. 72, 159-169.

Zribi, M., O. Taconet, V. Ciarletti, and D. Vidal-Madjar. 2002. Effect of row structures on radar microwave measurements over soil surface. International Journal of Remote Sensing. 23, 5211-5224.

Annexe 7: Depressionnal storage evolution during rainfall using photogrammetry combined with image processing (soumis à Journal of Hydrology)

Title: Depressionnal storage evolution during rainfall using photogrammetry combined with image processing.

M.R. Mirzaei[a, b,*], S. Ruy[a],

[a] *UMR EMMAH, INRA, Domain St Paul, Site Agroparc, 84914, Avignon, France,*

[*]Email : **mmirzaei@avignon.inra.fr** / Tel : +33 4 32 72 22 37 Fax: +33 4 32 72 22 12

Email : **ruy@avignon.inra.fr**

[b] Yasuj University, Yasuj, Iran,

Date recieved 25 Aug 2008

Abstract

Soil surface water storage and its variability during rainfall affect significantly infiltration rate. Over the past decades several methods were developed to derive maximum depression storage (MDS). Until present no study considered the evolution of depression storage (DS) during rainfall. For this purpose a methodology was developed. Three datasets were used, two from laboratory experiments and one from field experiment. Digital elevation models (DEM) from the soil surface were obtained before and after rainfall simulation using either laser method (LS) or photogrammetry (PGM) to be compared later. However, monitoring of DS during the entire rainfall simulation was only possible by mean of PGM. The proposed method for the monitoring of water storage during rainfall includes a combination of DEMs, obtained either from PGM or laser method, and of image processing. Image processing allowed the visualization of the location and topology of puddles. Coordinates of puddles contours and their area for each depression were obtained from the rectified image. Amount of water storage was determined crossing these coordinates with DEMs.

The comparison between the two measuring methods (LS and PGM) was performed using the water volume, the average height of water stored in the depressions, the area and digital elevation of DS. It showed a good correspondence. Acquiring puddles contours needs a good knowledge about image processing. Using this methodology can help to obtain useful information about DS evolution in micro scale during rainfall events.

Keywords:

depression storage, maximum depression storage, Laser scanner, stereophotogrammetry, image processing

1. Introduction

Runoff generation, erosion and infiltration rate can be affected by microtopography which referred to surface roughness (Helming et al., 1998; Monteith, 1974).

Depression storage (DS) and thus maximum depression storage (MDS) depend on microtopography which shows spatial and temporal changes due to different factors such as rainfall, tillage and canopy cover (Eltz and Norton, 1997). DS can be quite important: for example Moore and Larson (1979) reported DS values in the range of 5 to 27 mm for different ploughed surface with zero slope, these values were less than 8mm for unploughed plots. It can control runoff generation especially in small scale (m^2). In this scale, when the predominant mechanism of runoff formation is Hortonian (infiltration excess runoff), initialisation of surface flow is directly ordered by the soil roughness. Indeed DS or MDS act on the surface depression storage and infiltration rate.

In erosion models, runoff is supposed to begin after the MDS is reached. MDS in water erosion prediction project (WEPP) model is computed from a relationship derived by Onstad (1984) (Stone et al., 1995) and can impact runoff in a considerable way (De Jong van Lier et al., 2005). In the new version of the LISEM model (Jetten, 2002) MDS were also used and calculated by Kamphorst et al. (2000) relationship. However, runoff could also occur contemporary with depression filling in local scale (Darboux, 1999; Huang and Bradford, 1990; Kamphorst, 2000; Moore and Larson, 1979; Onstad, 1984). For this reason although the concept of MDS is widely used for hydrological models (Jetten et al., 1996), it is not appropriate to predict runoff in local scale.

Linsley et al. (1947) and Moore and Larson (1979) presented three stages of depressions filling due to spatial heterogeneity of the microtopography: i) all rainfall water is used to fill depressions and there is no runoff, ii) all of the depression don't have the same volume, and the depressions fill individually so some depressions overflow, while others continue to fill up so the runoff can be observed in some place and iii) the MDS is reached and the entire surface contributes to runoff. Sneddon and Chapman (1989) showed that the outflow from a depression is not only dependent to depression volume but also to the drained surface area.

One of the important aspects of the depressions effect on the infiltration rate can be explained by the height of water stored in depressions. Fox et al. (1998a) compared two ponding depths (0.5 and 4.0 cm) in a simple virtual depression and showed that infiltration rate increased with ponding depth. Fox et al. (1998b) concluded that the increase in infiltration with rainfall intensity may be due to small changes in surface ponding depth caused by the spatial variability of the crust. Small changes in runoff depth can significantly increase infiltration rate when structural crusts of lower hydraulic resistance are inundated (Fox et al., 1998b). So ponding water can affect infiltration either by i) increasing the pressure head or ii) because of the spatial variability of the soil infiltrability due to structural crusts located preferentially in the depressions. Until now there is no method to measure water storage in situ. Only MDS parameter can be obtained from different methods:

The different methods to calculate MDS can be divided in two main groups:

i) Direct methods: water depression can be directly measured by adding water in the soil depression. In this method a) either an impermeable soil surface or b) a reproduced soil surface using impermeable material is needed. The impermeable surface can be obtained by

adding bitumen (Langford and Turner, 1972), polyester resin (Gayle and Skaggs, 1978), plastic film (Mwendera and Feyen, 1992) or plaster (Garcia-Sanchez L., 1997). (Kamphorst and Duval, 2001) created a precise impermeable reproduction of a soil surface in polyester, using a silicone mould.

ii) Indirect method: MDS can be obtain i) from statistical relations between MDS and roughness indices (Hansen et al., 1999) and sometimes with other factors such as surface slope (Kamphorst et al., 2000; Onstad, 1984); or ii) from filling algorithms of digital elevation models (DEM) which represent the soil microtopography (Mitchell and Jones, 1976; Moore and Larson, 1979; Onstad, 1984; Planchon and Darboux, 2001; Ullah and Dickinson, 1979). Jenson and Domingue (1988) proposed a depression-filling algorithm which is used routinely. The depression-filling algorithms are all based on a two-stage principle (Planchon and Darboux, 2001), 1) to identify local minima and 2) to fill them from the bottom to the top by exploring the neighbourhood of each minima to find their outlets. Planchon and Darboux (2001) also proposed an emptying algorithm which runs more rapidly and is more suitable for studying soil surface microtopography.

Direct methods can face some difficulties such as those described by Garcia-Sanchez (1997) where the impregnated surfaces tended to crack while hardening and when coming into contact with water.

Nowadays using DEM is accepted as a standard method, as mentioned by Kamphorst and Duval (2001). In that case, the DEM must be obtained precisely with a small spatial step and with a reliable method.

Photogrammetry (Jester and Klik, 2005; Mirzaei et al., in press; Rieke-Zapp and Nearing, 2005; Taconet and Ciarletti, 2007) and laser-meter method (Abedini et al., 2006; Darboux et al., 2001; Darboux and Huang, 2003; Kamphorst et al., 2005) were recently applied to obtain high resolution DEMs from soil surface. By considering limitations and disadvantages of the laser-meter despite of its accuracy, photogrammetry could be a more practical and flexible alternative on the field conditions (Mirzaei et al., 2008b). However, DEM obtained from photogrammetry are usually smoother than those obtained from laser method (Jester and Klik, 2005; Mirzaei et al., in press), which may influence the calculation of the DS. Our aims in this study are to develop and to validate (using laser-meter as a reference method) a methodology to monitor water storage at the soil surface and its evolution during rainfall using photogrammetry.

2. Material and Methods

2.1 The study dataset

Two techniques were employed to obtain elevation data from the soil surface: laser scanner (LS) and photogrammetry (PGM). Both methods produce a high resolution data. Elevation data were obtained before and after water supplying, and also during rainfall using PGM only.

Three experiments were performed in different times and conditions considering their complexities, i) a simple wavy surface with known depressions dimension, ii) two moulded surfaces with different random roughness, iii) an additional experiment under field condition with seedbed roughness surface using only PGM.

The first experiment was done on the “maquette-a” (Figure 1-a) in INRA (Orleans, France) filled with a loamy soil (Villamblain). This maquette was used to obtain data necessary for validating a 2D infiltration-runoff model (Mirzaei et al., 2008a) but only data related to the monitoring of DS are presented in this paper. A 50cm long x 10cm wide x 20 cm high model of soil with a wavy surface was first built. The wavy surface created 3 depressions of increasing depth (0.2 to 2.5 cm) from upstream to downstream. The acquisition of soil surface microtopography data was achieved by using a high speed instantaneous-profile laser meter described by Darboux and Huang (2003) and a stereophotography system and camera characterization described by Mirzaei et al (2008c) and Mirzaei and Ruy (2008). Rainfall was simulated using a rainfall simulator described by Le Bissonnais Y. et al. (online) with an intensity of 52 mm/h for about 80 minutes until achieving the runoff steady condition.

The second experiment was conducted on two impermeable moulded surfaces which were used before by Kamphorst and Duval (2001). The two surfaces differed in roughness and are named “rough-maquette” and “smooth-maquette” (Figure 1-b). Laser data was obtained by Kamphorst and Duval (2001) and photogrammetry was done in INRA (Avignon). Water was supplied manually two times with known water volume for each maquette.

The third data acquisition was performed in a field cropped with wheat. The soil was classified as Calcolsol of alluvial origin. After a manual harvest, the soil was tilled with a plough share and then with a circular spike harrow combined with a cultipacker (a weighted clod crusher) in order to obtain a more or less smooth soil surface representative of seedbed preparation. A wheel trace of a tractor was incorporated in the middle of plot (Figure 1-c). Rainfall was applied with a small simulator (Bogner et al., 2008). The rainfall was in form of powder (very small droplets) with a very low energy kinetic of rainfall.

The image of the study area and dataset are given in Figure 1 and

Table 1 respectively.

Figure 1: Dataset used in this study a) maquette A b) moulded surface (rough and smooth) c) field plot

Table 1: Used dataset for this study

N° experiment	Name	Dimension (cm)	Resolution (mm)		Comparison Resolution (mm)
			Laser	PGM	
a	Maquette a	10*50	0.5	0.2-0.4	0.5
b-1	Smooth-Maquette	50*50	2	0.5-0.7	2
b-2	Rough-Maquette	50*50	2	0.5-0.7	2
c	Field	100*100	*	0.5-0.7	0.6

* No laser profile meter was used in the field.

2.2 Photogrammetry system

The camera system (Figure 2) was mounted on a support (made by INRA in Avignon). This support was stable, and the height of cameras could be changed within a range of 1 to 4 meters from the soil surface along a shaft of support. Photos were taken using a pair of Nikon D100 cameras with a constant theoretical focal length of 35 mm, and a CCD sensor of 3000 x 2008 pixels. During a preliminary study, the optimum setup for photography was determined (Mirzaei et al., 2008c; Ziarati et al., Juin 2007).

For each rainfall simulation, the photogrammetry system was first of all calibrated by taking more than 20 photos of the calibration plate in different positions before rainfall simulation. This calibration was performed also after rainfall without water of the soil surface. The parameters thus calibrated were used to obtain initial and final DEM values for the plot for every rainfall simulation.

During rainfall, photos were taken at different times to enable a possible comparison of surface depression storage at different time points.

For the “smooth-” and rough-maquette, only one calibration procedure was performed as the surface is made of polyester with no change of the soil surface during rainfall.

The calibration parameters for the intermediate photos (during rainfall) were obtained in two different conditions. For maquette-a, we were obligated to setback (draw back) the shaft of support because rainfall simulator was above the camera system installation. Required time for pushing the shaft above the maquette, taking a photo and setting it back was of several second (about 10 s). For this experiment we supposed that the calibration parameters obtained either before or after rainfall could be used for reconstruction of DEM using intermediate photos as we used a rigid support. For other experiments, shaft of support was fixed in place so calibration parameters before or after rainfall could be used.

Figure 2: Support and camera system used for stereoscopic vision.

2.3 Algorithm and computational procedure:

Initially two methods were considered to compute water storage in the soil surface depression:

1) **Photogrammetry**: obtaining the DEM directly from the images intermediate. By subtracting this DEM from the one obtained before or after rainfall, depression storage can be calculated. We assumed that surface puddles were sufficiently opaque and textured to be recognized by the PGM algorithm. It would be the best option if this method works.

2) **Combination of photogrammetry with image processing**:

In this procedure an algorithm was determined which is summarized as below (Figure 3 and Figure 4):

1. cameras calibration to obtain a set of calibration parameters,
2. DEM reconstruction,

During rainfall:

3. separating water region and soil surface, using different image processing such as different filters and texture analysis,
4. determining the contours of puddles (see 0),
5. deriving the coordinates of the contours and the area for each closed water region
6. crossing the water contours with the DEMs generated using PGM or LS,
7. obtaining the average altitude of a contour crossed by a DEM. In this part 20 percent lower and upper of elevation data were eliminated to filter outliers points,
8. setting averages values obtained for each region (in precedent step) as the average of water altitude (named Dep-H). It is supposed that the surface of water is flat so for a closed region the altitude of the water surface is the same),
9. crossing the surface (area) of the water regions with its corresponding DEM to obtain elevation data of soil surface inside individual puddles (named POLY-DEM because of polygon shapes of the water regions).
10. Amount of water storage (named WSD-DEM) was calculated by subtracting Dep-H and POLY-DEM.

All steps for PGM can be performed by programming in the Halcon software (MVTec, 2006a).

In this study, steps 1 to 5 must be done in a stereo-photogrammetric and image processing software (e.g. Halcon) and 6 to 10 can be done in any GIS package software (e.g. ILWIS) as explain in Figure 4.

Pixel size is an important factor which affects the results and soil characteristics. Its effect is known as grid spacing (Kamphorst et al., 2000) or spatial resolution (Abedini et al., 2006). Thus for comparing laser method and PGM, a common pixel size was used according to accessible laser elevation resolution (

Table 1). Output data from Halcon software also was in irregular distances. Thus we used interpolation between irregular points to get a DEM with a regular grid. Different interpolation methods are available in the GIS package among which moving average interpolation was performed using Integrated Land and Water Information System (ILWIS). This part of the process was time consuming.

2.4 Image processing for water puddles recognition

In the following some technical image processing terms used in this study will be defined.

Rectified image shows no radial and no perspective distortions.

Supervised classification: first a classificator was created, after it was trained using a color image with three channels (RGB) with the gray values of color photo. This training is done using the points in the training samples for different objects. We used several training samples for water region and soil region separately used to obtain water regions. The classificator trained for different objects (regions) can thus be used in the next step to segment multi-channel images.

Texture filters: they are kind of filters which are used to analyse the texture of an image. Two kinds of them were used and are presented here: *Texture-laws and fuzzy-entropy.*

Texture-laws filter an image using a Laws texture filter. *Texture-law*s operator (MVTec, 2006b) applies one or more *texture transformations* using a determined filter according to the laws (on the rows or/and columns) to an image. This is done by convolving the input image with one (or more) filter masks. *Texture transformations* are linear filters that intensify certain frequencies which are typical for the requested texture. We had to specify the filter size (7*7 pixels) and type ("ee", "ss"). Both attributes determine the frequency properties. The name of these filters is composed of the letters of the two vectors used, where the first letter denotes convolution in the column direction while the second letter denotes convolution in the row direction. We present two vectors of these filters that we used in the examples presented here in the results section.

e =[-1,-4,-5,0,5,4,1]and s=[-1,-2,1,4,1,-2,-1],

fuzzy-entropy: calculates the fuzzy entropy of a fuzzy set. To do so, the image is regarded as a fuzzy set. The entropy then is a measure of how well the image approximates a white or black image.

Median-separate is a kind of smoothing filter which carries out a non-linear smoothing of the gray values of all input images.

Min-gray (respect. Max-gray): determines the smallest (respect. the largest) gray value in a region.

Threshold: selects the pixels from the input image whose gray values (g) fulfill the following condition: $MinGray \leq g \leq MaxGray$.

The algorithm used to obtain puddles boundaries (Figure 3) can be summarized as the following procedure using Halcon package.

First the image of soil surface taken during rainfall (with water in the depressions), was rectified using the calibration parameters before or after rainfall (depending on which DEM would be used). Depending on the experiment, two until four cm of the surface was eliminated from the borders before defining a region of interesting (ROI) for each plot. To obtain water contours, different methods such as supervised classification, texture analyzing or simple filtering were used.

Extracting segmentation parameters can be achieved usually using fixed (or dynamically for each image) threshold values. One example for this is a gray value histogram that has multiple peaks, one for each object class (Figure 13-c-2).

Usually in the next stage, the segments of the different regions have been obtained using a global threshold. Sometimes obtained region are not only puddles, other object such as shadow regions can be chosen in this step, so using some other characters are necessary to separate water regions. In this case some useful characters were used particularly selecting regions based on gray value features. Each image has a number of regions which for each of them, the calculated features were investigated. From the features, *minimum* and *maximum gay* values within regions, *fuzzy-entropy* of regions and *standard-deviation* of gray values within regions or a combination of them were sufficient to determine the water region. Finally the coordinate of water region contours (named polygons) and all pixels within

polygons regions were acquired. Each polygon represents a water depression. Some examples are showed in the results (Figure 15 and **Erreur ! Source du renvoi introuvable.**).

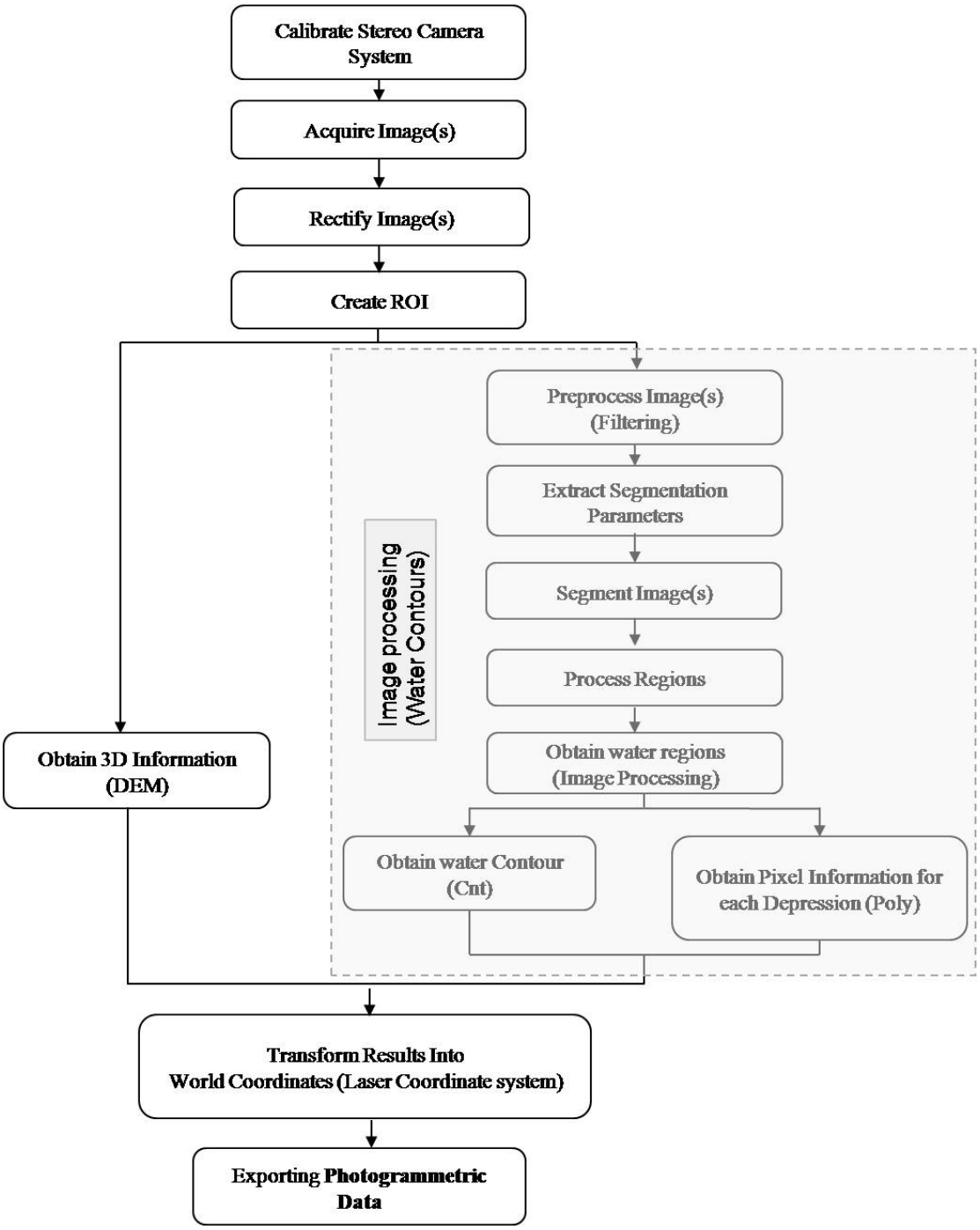

Figure 3: Flowchart for Obtaining Photogrammetric Data and water region coordinates (x,y) , ROI: Regions Of Interest, Gray part shows the image processing flowchart to determine water regions.

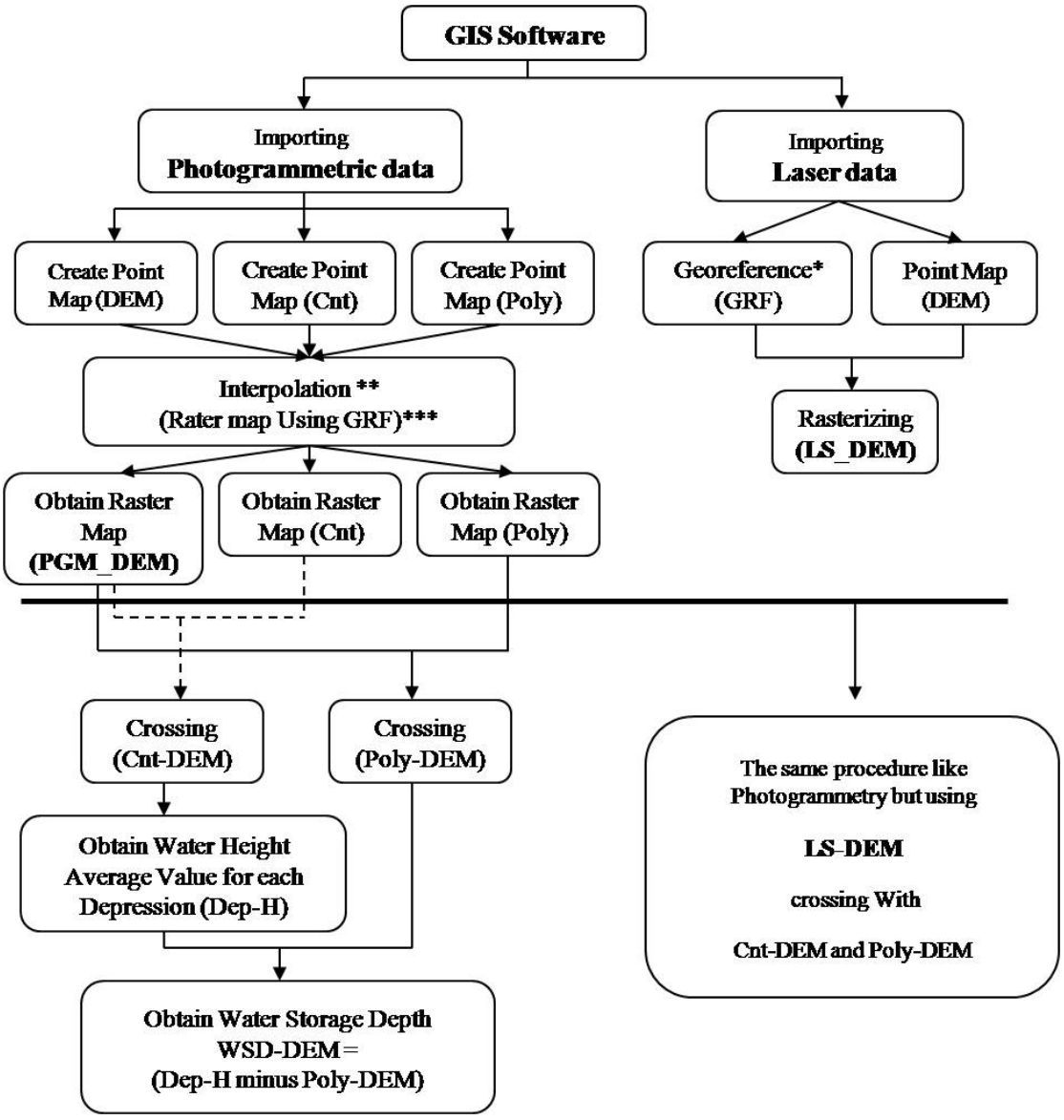

Figure 4: Algorithm for obtaining the Water Storage Depth,

*** A georeference defines the relation between rows and columns in a raster map and XY-coordinates. The location of pixels in a raster map is thus defined by a georeference. It is advised that raster maps of the same area use the same georeference. Pixel size was always equal to the one of laser data**

***** Georeference is the same which is used by laser data**

3. Results and discussion

Recently studies have proved that photogrammetry can be used as a reliable method to obtain soil surface characteristics (Jester and Klik, 2005; Mirzaei and Ruy, 2008; Mirzaei et al., in press; Taconet and Ciarletti, 2007). We compared PGM and LS methods by means of the first two experiments which will be presented first, and after this depression storage is discussed separately.

3.1 Comparison between laser and photogrammetry

3.1.1 Maquette-a

The DEMs were obtained before and after rainfall simulation using two methods (LS, PGM) and are presented in Figure 5. Both methods had a good agreement visually. For more quantitative comparison, cumulative frequencies of the heights were plotted in Figure 6: they are found to be very similar. After rainfall depression heights were diminished under the impacts of raindrops, erosion and aggregates transportation, and the shape of depressions has changed (Figure 5) particularly the third depression (black part on the right side of each image). After rainfall the height frequencies in small heights (which usually shows depression) were decreased which could be attribute to depression filling by sediment deposition, and the slight decrease of frequencies in overtop heights is attributed to erosion of the mounds which is in agreement with other observations (Courault et al., 1993; Fox et al., 1998b; Onstad et al., 1984).

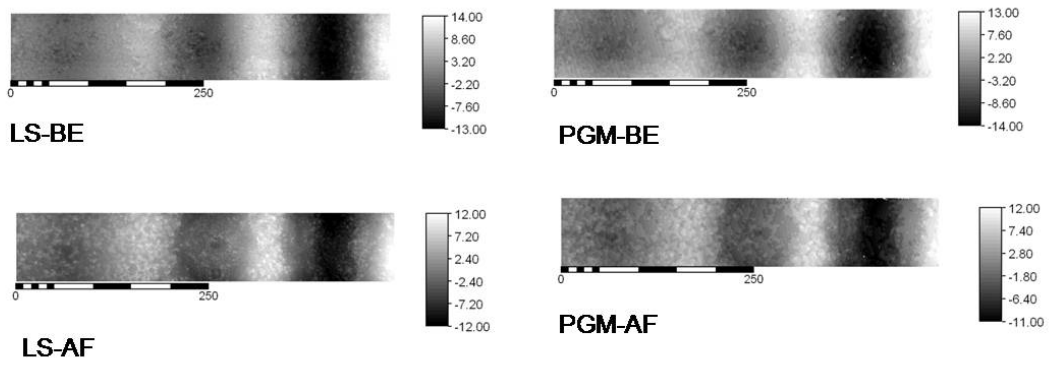

Figure 5: DEMs obtained before (BE) and after (AF) rainfall simulation using photogrammetry (PGM) and Laser method (LS). Vertical scale (mm) represent the altitude above and below a mean horizontal plane. All scales are in mm.

Results regarding surface depressions prepare easy way to investigate the effect of two methods on the calculation of factors as maximum depression storage (MDS) and ponded area. MDS was calculated using depressions-filling-algorithm. Also the possibility of being able to map depression storage spatially can be providing a good context to compare two methods. Visual inspection of Figure 7 show that both methods can detect changes carry out by rainfall. Moreover the spatial distribution of depressions is almost the same with both methods. The ponded area and MDS decreased respectively of about 50 % and 19 % due to rainfall for LS and about 54 % and 26 % for PGM (Table 2).

Contrary to what was expected MDS computed from LS-DEMs were less than those calculated from PGM-DEMs before and after rainfall. Other studies have shown that PGM give a smoother DEM than LS (Jester and Klik, 2005; Mirzaei et al., in press) and so a smaller MDS (Mirzaei et al., in press). Two reasons could be cited. Firstly, this may be produced because of changing the pixel size for PGM which was about 0.3 mm before interpolation with more details than with the LS method where the pixel size was of 0.5 mm. Abedini et al. (2006) showed that the grid spacing treatment (changing pixel size) significantly changes the average depth of depression and total ponded area. Secondly some points which close a depression may not be detected with LS because of its larger pixel size. To our knowledge, there is no study which compared the drainage network obtained by photogrammetry and

laser. However, despite these small differences, both values are very close to each other.

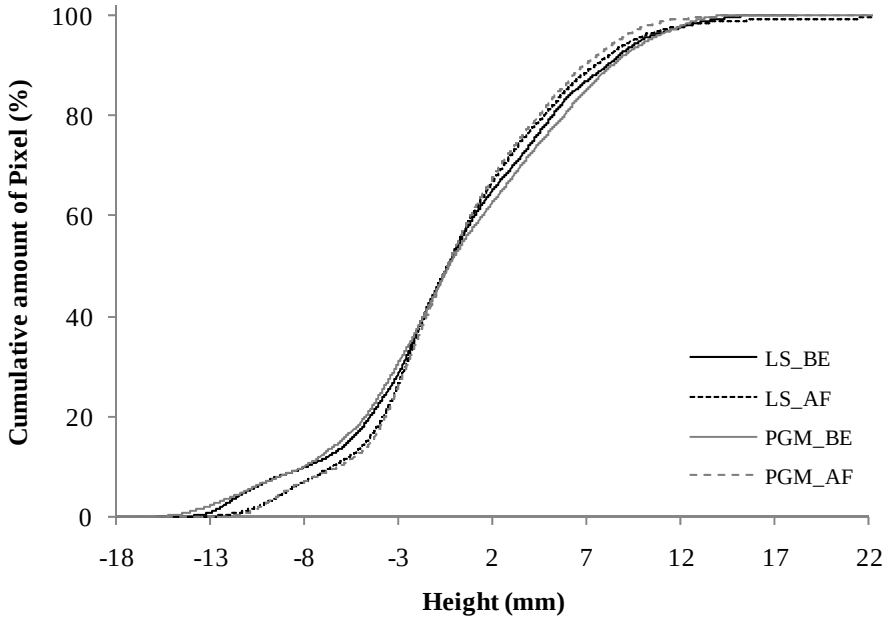

Figure 6: Cumulative frequencies of heights for both methods (LS stand for Laser scanner, PGM is for photogrammetry), before (BE) and after (AF) rainfall simulation.

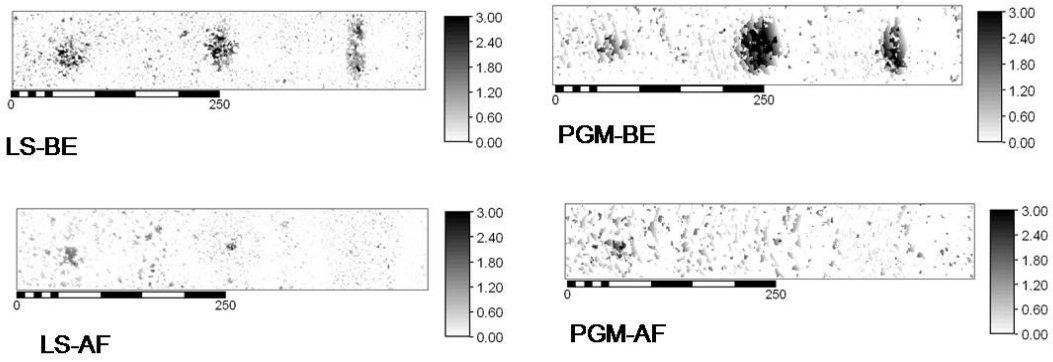

Figure 7: Spatial distribution of the depressions after calculation of MDS before and after rainfall, LS: Laser method and PGM: photogrammetry

Table 2: Maximum detention storage (MDS) calculated on Maquette-a before and after rainfall, for both methods

	Laser			Photogrammetric	
	Before	After		Before	After
MDS (mm)	0.16	0.08		0.22	0.10
Ponded Area (%)	0.27	0.22		0.26	0.19

3.1.2 Maquettes-b

Several profiles are provided in X and Y axes (Figure 8) for a direct comparison between laser and photogrammetry results for both maquettes after acquiring DEM, whereas a general overview is presented on Figure 9. A good agreement between both methods can be seen and the shapes of the soil aggregates are well reproduced by PGM. But the PGM has always a larger value. For more investigation, difference among DEMs obtained by two methods was calculated. The difference map showed two interesting results: first as showed in Figure 9 this map has relatively uniform colour (colours are representation of elevation) for both maquettes which shows that the difference is uniform and proved a systematic error or bias. This error can be due to benchmark points used (only three points) to transform the coordinate system of PGM to the LS. Another interesting result of this comparison is that the difference is more important in the aggregate borders. PGM produced also the aggregates with smoother borders.

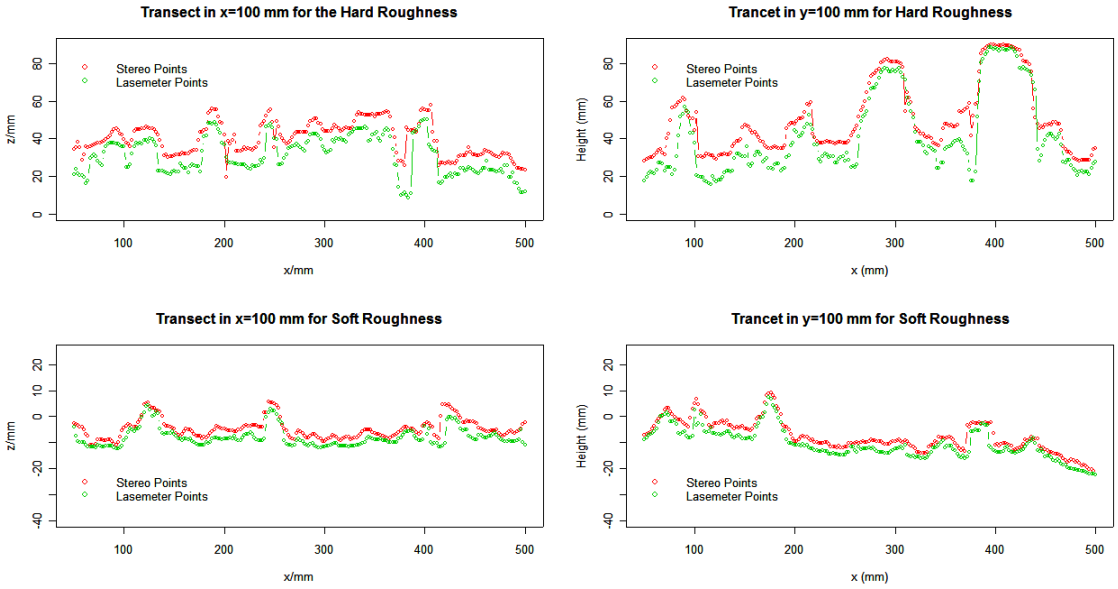

Figure 8: Comparison of surface elevation profiles obtained using the laser method (green points) and photogrammetry (red points), on the smooth maquette (low) and on the rough maquette (above)

A visual comparison of spatial mapping of the depressions depth showed a good correspondence between two methods (Figure 10) especially for the smooth maquette. In that case, general shapes of depression can be reconstructed by PGM contrary to results of Jester and Klik (2005) who showed very clear differences in depression representation between two methods. On the rough maquette as it is marked in Figure 10, some depressions were not reproduced on the PGM-DEM and the calculated MDS (see Table 3) was larger by laser method (0.78 mm) in regard to PGM (0.61mm). On the smooth maquette calculated MDS using LS (0.23 mm) was very similar but slightly smaller than the value calculated with PGM (0.25 mm).

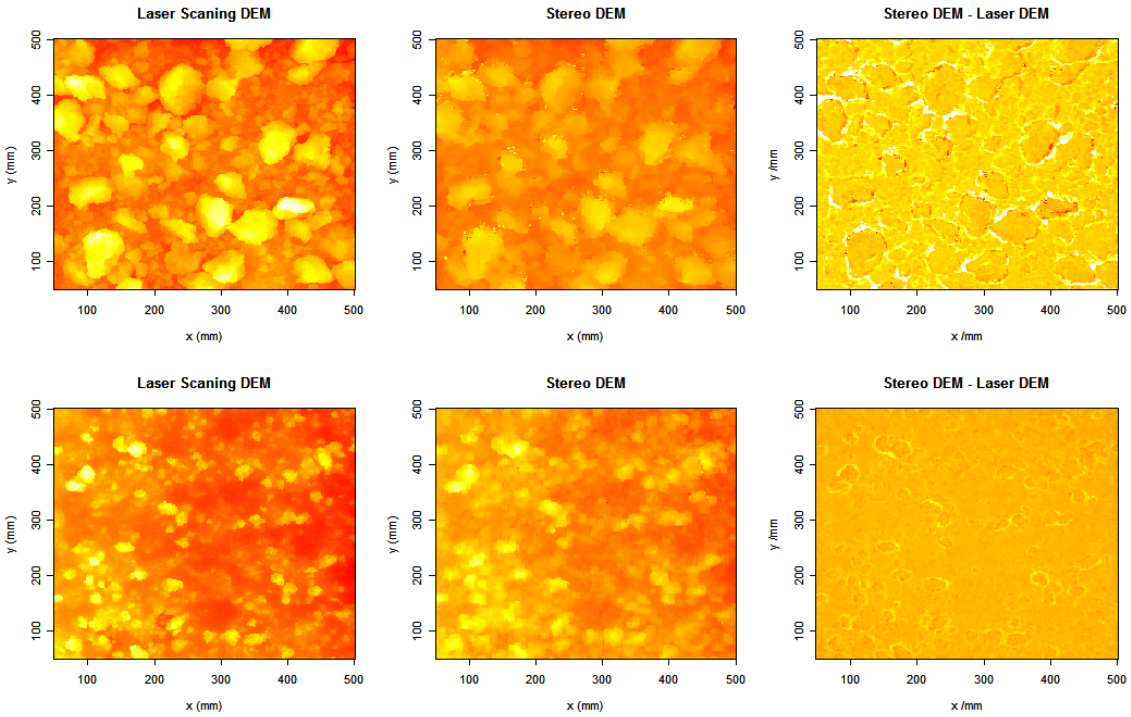

Figure 9: DEMs obtained for the rough-maquette (upper row) and the smooth-maquette (lower row) with the laser scanner (left column), PGM (middle column) and differences between both methods (Stereo-DEM minus Laser-DEM , right column)

	LS	PGM	PGM - LS (%)
	Rough-maquette		
MDS (mm)	0.78	0.61	-22
Ponded Area (%)	21.4	19.8	-1.6
Area of depressions (%) > 10 mm	1.37	0.45	-0.92
	Smooth-maquette		
MDS (mm)	0.23	0.25	9
Ponded Area (%)	24	25.7	1.7
Area of depressions (%) > 4.18 mm	0	0.17	0.17

Table 3: calculated MDS, ponded area and area of depressions with hiegher depth

To understand why the MDS values differ between the two methods, first we calculated ponded area for each maquette (Table 3). It shows, the higher is the ponded area, the higher is the MDS value. However, for the rough-maquette, MDS is underestimated by about 22% when calculated with PGM; whereas this underestimate is only 1.6% for the calculation of ponded area. For the smooth-maquette,

PGM over estimates MDS by 9 % and ponded area by 1.7%. In the case of the smooth-maquette, the relationship between depressions height and their volumes (Figure 11) obtained by PGM is in good accordance with the one obtained by LS. Deepest depressions with a depth greater than 4.1 mm are absent in the LS-DEM and represent only a very small fraction of the PGM-DEM (see Table 3, Figures 11 and 12). These deepest depressions are responsible for the slight overestimation of MDS by PGM compared with LS. For the rough-maquette, the curves of water volume vs. depression height are similar for both methods until a height of about 10 mm, but they are very different for bigger depths (see Figure 12). In this range (> 10mm) the higher volumes obtained by LS are due to the higher value of the ponded area (Figure 12). As the volume is the product of area times depth, the small difference of the depression > 10 mm between two methods (Table 3) results in a 22% underestimation of MDS by PGM compared to LS. However, these values showed a good estimation of this parameter using PGM.

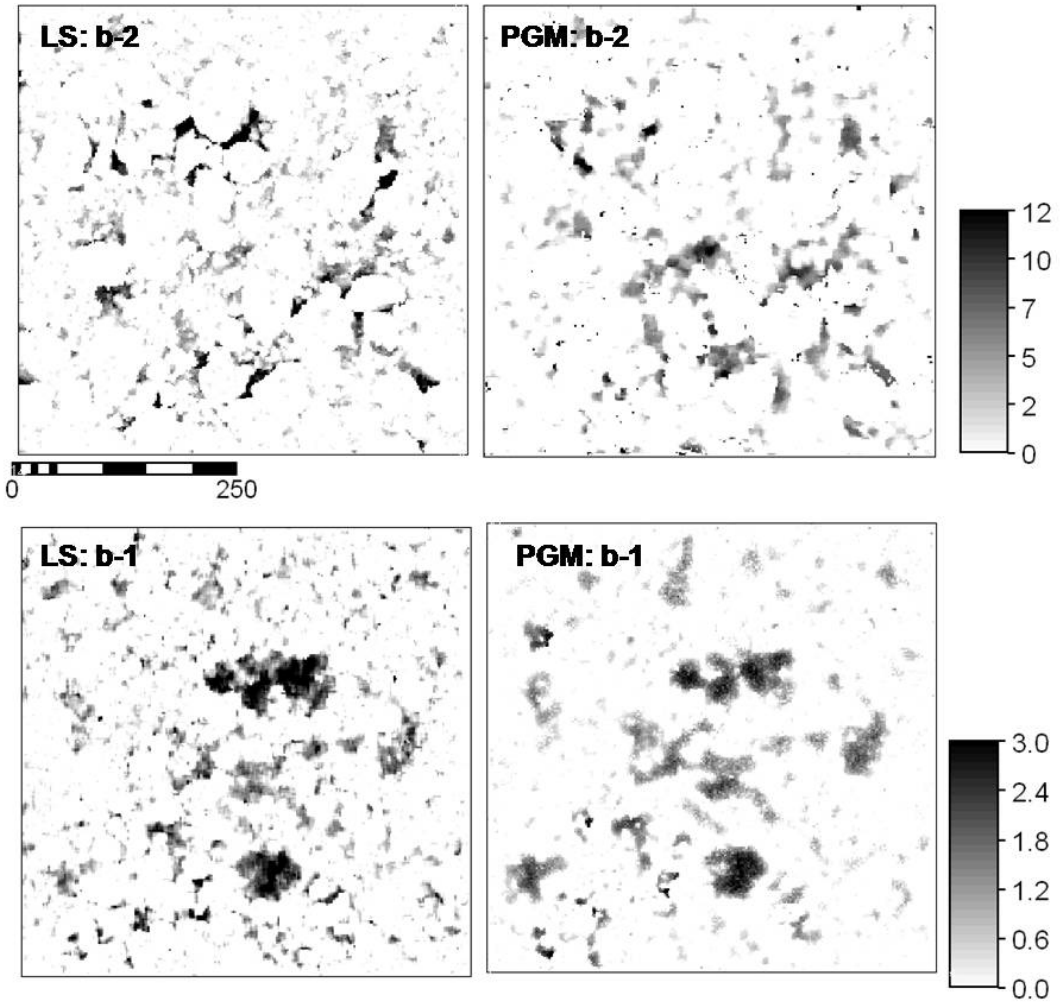

Figure 10: Spatial mapping of depressions for Laser (LS) and PGM, for maquette smooth (b-1) and maquette rough (b-2)

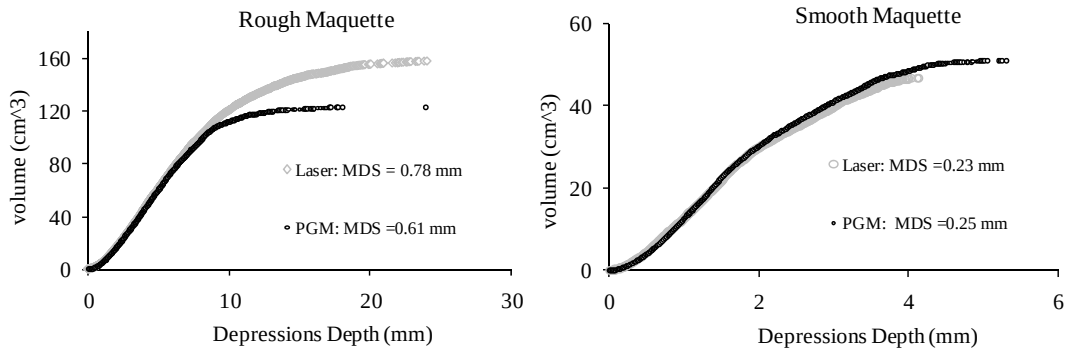

Figure 11: Water volume corresponding to the each depression height, for laser and PGM

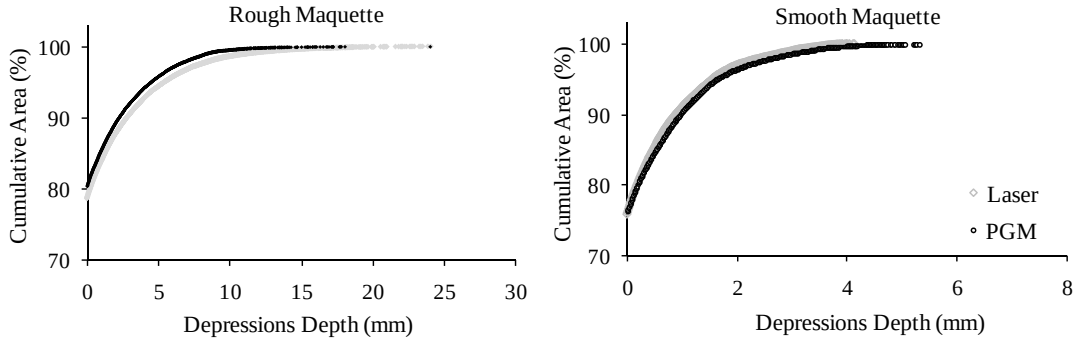

Figure 12: Covered area by different depression height

In this part comparison between laser method as a reference method and photogrammetry method was done. As a partial conclusion stereophotogrammetry can give a good estimation of water retention on the soil surface.

3.2 Depression storage during rainfall

The results are presented separately for each experiment.

3.2.1 Using photogrammetry

Maquette-a:

For maquette-a, 2 calibrations of the PGM devices were done throughout the experiment: one before and the other after rainfall simulation. As the experiment was conducted 4 times, a total of 8 calibrations were performed on the same device with a constant spatial configuration of the cameras. All of these calibrations were done when the soil surface was free of excess water.

Using current calibration parameters give a good representation of the DEM (Figure 13-a) for the soil without water. Conversely, DEM reconstruction process failed when water puddles appeared at the soil surface whatever the calibration parameters used (Figure 13-c, Figure 13-b). Two assumptions can be made to explain this failure. The first one is that the reconstruction algorithm of the DEM is

inappropriate: water puddles are not sufficiently opaque or the texture of the water surface is too homogeneous and the algorithm cannot find corresponding points on the left and right photos. The second one concerns an experimental problem: the shaft of the PGM device should be switched between pictures as it intercepted rainfall. This backward and forward motion could have induced a modification of the spatial configuration of cameras and calibration should have been performed for each picture. It showed also that for a given experimental setting (with constant conditions such as camera setting, distance between two cameras, camera distance from soil surface), several sets of calibration parameters can be used for the reconstruction of the DEM that looks correct. Mirzaei et al. (2008b) showed the importance of the calibration procedure and they provided different important advices for using this method in soil surface study.

In the remaining experiments the shaft of support was not moved and calibration conditions were was the same during all rainfall period.

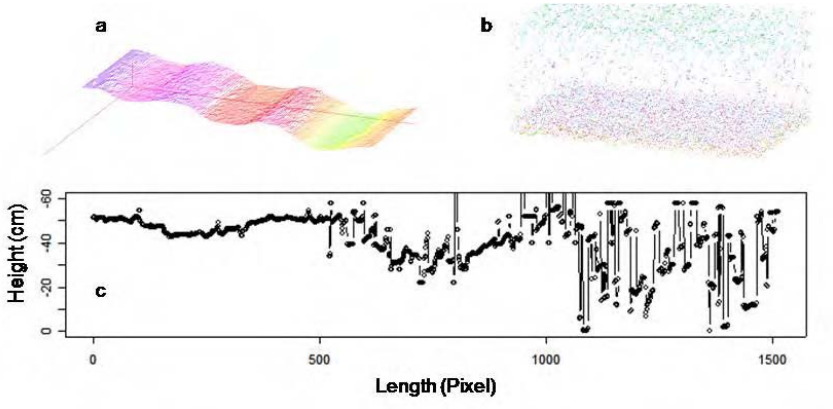

Figure 13: Using different calibration data a) before rainfall for the soil before rainfall b) before rainfall for the one of intermediate photos with water c) a profile from a DEM which had the best representation from 8 DEMs using 8 calibrations data in the same condition, water is present on the depressions (two depressions) witch the DEM reconstruction was failed.

Maquettes b:

For maquettes-b we obtained the DEMs which have the same problems as in maquette-a, as soon as the presence of water in the depressions, DEM reconstruction faced by the problem. We didn't present these results here.

On the field

Figure 14-a shows a DEM obtained before rainfall without excess water on the soil surface and Figure 14-b shows a DEM obtained for an intermediate image on the presence of surface puddles: PGM could not find corresponding points in the water regions. White and black points regarding to the legend show low and high altitude respectively. High differences between heights can be seen in water region which produce a profile such as the one for maquette-a (Figure 13-c). One of the reasons for mismatching in PGM can be explained by a relatively uniform and very smooth texture for the water region.

One of the important steps in the 3D reconstruction of an object using binocular-stereovision is the matching of homologous points (i.e. the projection of one object point into the two images) to obtain

disparity map. Matching process between two points is established by measuring the similarity of neighboring points. This similarity is calculated as the correlation between gray values of the pixels surrounding the two candidate points. Each pixel in the left-hand image is considered to be the centre of a fixed window with dimensions of M*N. A motion window of the same size moves in the right-hand image with the centre pixel over the same row number of the left-hand window. Here in all condition window size was 11*11. Then if the gray values of a region are very uniform the matching process meets difficulties. We tried to solve this problem by projecting an image with a different texture over the soil surface, but under field conditions the light of used projector was weak regarding to sunlight.

Despite the problems in the determination of the DEM with puddles, we calculated the amount of free water at the soil surface (hereafter referred to as DS for depression storage) and the proportion of horizontal surface occupied by puddles at three moments during rainfall. MDS was also calculated by a filling algorithm based on the DEMs obtained before and after rainfall. Borders were imposed in three sides of the DEMs, with an outlet on the right side of the plot which was in agreement with the experimental settings. Results are shown on Table 4.

MDS decreases slightly during rainfall as a result of raindrops impacts on the soil. The decrease is very low (0.94 to 0.84 mm) because of the structural stability of the soil and of the low kinetic energy of the rainfall. DS ranged from 1.4 mm (first time) to 1.1 mm (last time): it increases during rainfall, which is obviously in contradiction with our observation, and was always greater than the MDS, which is impossible. Therefore PGM is not able to monitor DS during rainfall on a qualitative or quantitative point of view. PGM must be used with another method.

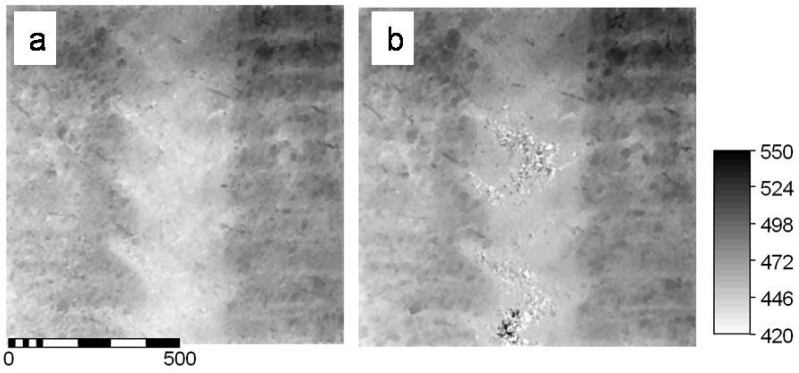

Figure 14: a) DEM visualization of the field plot before (a); and after rainfall (b), the scales are in mm, vertical scale represents surface elevation above an arbitrary horizontal plane. On fig. b, water puddles appears on the truck wheel trace but they induce wrong DEM reconstruction.

3.2.2 Using photogrammetry beside image processing

To obtain water contours, different methods were tested i) classification (train a classificator using a multi-channel image such as RGB image) ii) simple filtering iii) texture analysis. Classification method works automatically and needs only some train regions of soil surface and water region. However in this study normally it could not be able to make a well determination of water borders and its results are not presented here.

Before obtaining conours, usually a kind of filter is useful to determine the edge of an object. We

examined a large range of these filters known as edge-filters (like sobel, frie, laplace), smoothing-filters (median, mean, median-separate), texture-filter (*texture-laws*, *deviation-image*, *entropy-image*) or combination of them.

Table 4: calculated MDS and ponded area for each DEMs generated by only using PGM and PGM combination by image processing. Inter for intermediate image (during raifall),

	PGM		PGM+ Image processing		
	Ponded-area (%)	Detention (mm)	Ponded-area (%)	Average-Detention (mm)	Puddles number (-)
Before rainfall	32.52	0.94			
Inter-1	34.4	1.4	5.89	0.27	17
Inter-2	34.13	1.2	7.88	0.49	47
Inter-3	31.65	1.1	9.4	0.56	5
After rainfall	31.41	0.83			

Among all of these series, texture-analyzing before using the median-separate operator was easier and had good results for all experiments (we used it for maquette-a and field experiment because for maquettes-b a simple mean-image filter was enough).

In these studies with respect to methods presented below, all image processes were done over a gray scale image obtained from the original *rgb- image* with a colour-filter.

1) Maquette-a

11 intermediate images were selected at different time. As an example from this experiment, the extracting manner of water region was presented for maquette-a-10 some seconds after the end of rainfall on Figure 15, but results are identical for the other images.

In Maquette-a-10 some water was only present in the greatest depression near the outlet. The water boundaries are very blurred and even a human viewer has difficulties to recognize them. At a first glance it seems very difficult to find a segmentation criterion to separate water region from emerged soil surface. There is neither a clear edge nor a significant difference between the gray values of both areas. Thus it is not very promising to use an edge operator or a threshold operation. One solution of this problem is to use a texture analysis as the soil aggregates are more textured than the water puddles. To emphasize this difference, a texture transformation by Laws (MVTec, 2006a) was used. A range of different Laws' filter available in HALCON software was examined. Finally '*ee*', "*ss*" or combination of these filters (i.e. "*es*") gave the most satisfactory response.

The computed result after application of a Laws filter (Figure 15, b-1) could not be used directly to recognize water regions, because it is too speckled near the border of the depression. The corresponding histogram (Figure 15, b-2) didn't show a clear threshold to separate different regions.

After application of a Laws' filter, a *median-separate* filter was applied to the texture image (Figure 15, c-1). The corresponding histogram was clearly bimodal and the puddle was identified after

application of the appropriate threshold.

We noticed that with this method very thin water height cannot be monitor.

After determination of the contours of water regions, water storage, area, DEM which represent detention storage (Det-DEM) were obtained for each depression using the algorithm presented on Figure 4. We had to decide which DEM should be used, the one obtained before or the one obtained after rainfall. As it is mentioned soil surface has changed due to rainfall. However we decided to cross water contours with final DEM. Water storage was computed using LS-DEM and PGM-DEM for 11 intermediate images and it is plotted versus the ponded area on Figure 16. The agreement between both methods is very good: in that case, LS and PGM gave very similar DEM.

2) Maquettes b

1000 and 1500 ml water were added (corresponding to a water depth of 4 and 6 millimeter respectively) at the smooth maquette surface, and 1000 and 1750 milliliter (i.e. 4 and 7 millimeter respectively) at the rough maquette surface.

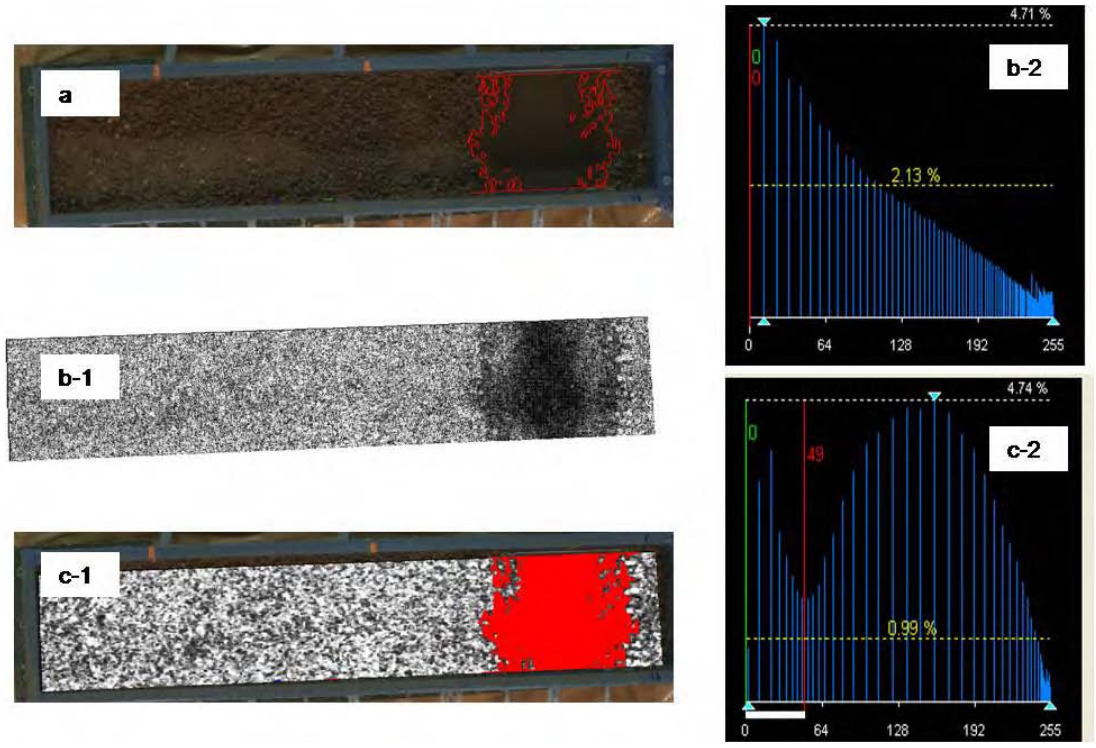

Figure 15: An example for determinig water contour in maquette-a, a) water contours for image number 10 obtained after image processing, b-1) image obtained after application of the "ee" Laws' mask, b-2) the corresponding histogram , c-1) identification of the puddle after filtering of the texture image with a *median separate* and thresholding based on the corresponding histrogram (c-2).

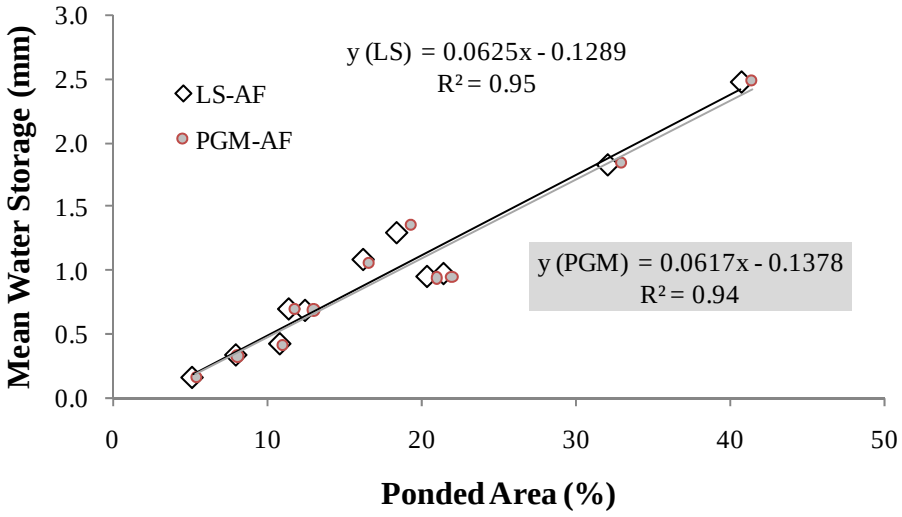

Figure 16: Mean water storage versus Ponded area in maquette-a using 11 photos intermediates.

Water contours were obtained using a mean filter over gray image followed by thresholding. The contours were very distinctive for the two maquettes as can be seen on Figure 17. In that case, the filtering process was simpler because of the high contrast between maquette surfaces (in white polyester) and water (darkened with suspended sediments).

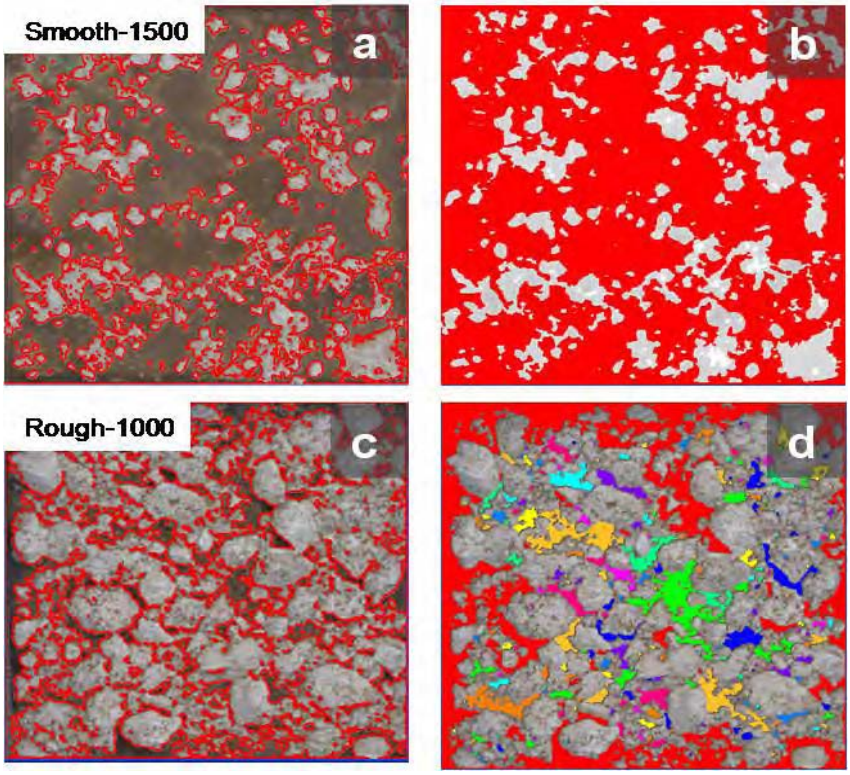

Figure 17: Determination of puddles boundaries (left column) and of individual puddles (right column,each closed puddles is identified by a specific color) performed on the smooth-maquette (upper row) and on the rough-maquette (lower row).

Comparison of the water storage maps showed a good correspondence between LS and PGM (Figure 18) despite some differences which could be caused by the coordinate system transformation. However, DS and corresponding area were very similar in both maquettes (Figure 19). For the smooth maquette DS values are very close to the added water amount: a volume of 1000 ml (respect. 1500 ml) corresponds to a mean water height of 4 mm (respect. 6 mm) and the calculated value is of 4.16 mm (respect. 5.58 mm).. For the rough-maquette, huge differences between calculated and theoretical water heights appear: calculated water height is 1.99 mm (respect. 2.85 mm) whereas the theoretical value is 4 mm (respect. 7 mm) for an added water volume of 1000 ml (respect. 1750 ml). This poor agreement for the rough maquette was expected because (i) in the rough plot a large part of water was stored in the border of the plot (see Figure 17d) that was eliminated during the process and also because (ii) this maquette was not completely impermeable as some cracks occurred in the polyester maquette.

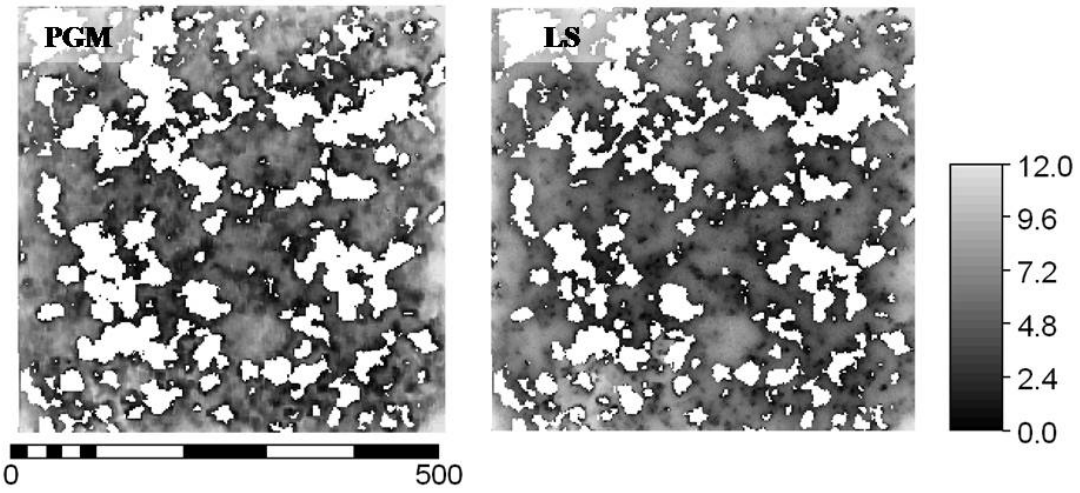

Figure 18: map of water storage heights obtained on the smooth-maquette by using the PGM-DEM (left side) and the LS-DEM (right side) after addition of 1500 ml of water. The vertical gray scale represents the water height (mm).

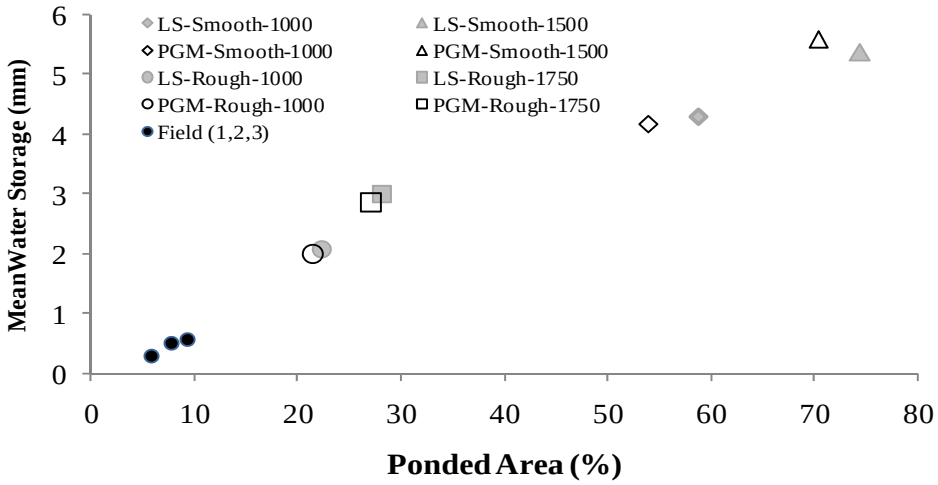

Figure 19: Mean water storage correspond its ponded area on two maquettes rough, smooth and on the field experiment, for field mehtods only PGM data are availible.

3) On the field

For the soil without water (Figure 20-a1), application of a Laws' mask followed by a *median_separate* filter (Fig. 20-a2) did not produced a histogram (e.g. bimodal histogram) (Fig.20-a3) of gray values with some criterion to separate different regions. The same procedure applied during rainfall when puddles appeared (Fig. 20-b1) resulted in a highly contrasted image (Fig. 20-b2) and a clearly bimodal histogram of gray values (Fig. 20b3).However, this process was detected not only puddles boundaries but also some other regions, such as the shadow of the frame. Other information is thus necessary to obtain water boundaries alone. In our experimental conditions, filtering of these bias was simply obtained with the application of the *max-gray* value feature on the obtained regions in precedent step gray image of the interested region that gave a histogram with distinctive parts (3 peaks) (Figure 20-c-2). By choosing the first two peaks, ponded areas (depicted in dark blue) could be isolated from other region (Figure 20-c-1). However other filters could be chosen according to the experimental conditions.

In the case of the field experiment, no quantitative validation may be conducted on the calculation of the volume of puddles, but on a qualitative and visual approach, the process looked very promising: with a semi-automatic image processing method, it is possible to monitor the evolution of puddles at the soil surface during and after the end of rainfall events. Therefore, we applied directly this process on three intermediate images taken during rainfall simulation to study the evolution of excess rainfall at the soil surface.

The ponded area as well as the DS increased during rainfall (Table 4, Figure 19) as soil depressions were filled with excess water. During first stage, the number of individual puddles increased (from 0 to 17 and then to 47): this corresponds to the filling of small, non connected depressions because of the heterogeneity of soil infiltrability at a very local scale. As water depth increases, some puddles get connected and the number of individual puddles decrease (from 47 to 5). This was in agreement with our visual observations during the experiments.

This method is thus able to calculate DS values and to give micro-scale information about depth of the water on the soil surface, as can be seen in Figure 21. Water of some depressions (at the upper part of figure 21) disappeared 38 seconds after rainfall simulation in which water was infiltrated.

4. Conclusion

Photogrammetry data showed good agreement with laser method as a reference method. These agreements are very similar for the ponded area and mean water depressions. Photogrammetry method alone may not be able to monitor the water depression storage. It must be used with image processing. About 2 hours are needed for an expert to obtain water storage map. All calculations (DEM reconstruction and image processing) could be performed with the Halcon software which considerably decreased calculation times. However others image processing software and GIS packages could be used as well. In our case, DEM reconstruction and image processing were performed with the Halcon software, and calculations on DS (ponded area, mean water height, ….) were performed with the GIS software ILWIS.. In all our cas studies, texture analyzing using Laws' masks followed by a *median_separate* operator could give a well basis for finding water puddles region. Beside these processes, the other features such as *fuzzy_entropy*, *min_max_gray* of the obtained regions could efficiently help to separate water puddles from other regions when ambiguities are still

present after texture analysis (areas in the shadow for instance). The advantages of this method are as follows:

i) using PGM which may be easier to use relative to LS under field conditions and even in the laboratory,

ii) very fast data acquisition: a couple of photos can be taken under rainfall within a few seconds,

iii) monitoring of data at the micro-scale (1 m^2 with a resolution of a few mm^2) concerning DS, puddles and their connectivity (topology) : these data could be very useful for the validation of distributed surface runoff models e.g. Esteves et al., (2000) and for the characterization of the influence of soil surface characteristics on runoff genesis,

iv) the program is partly automated and user intervention is very limited.

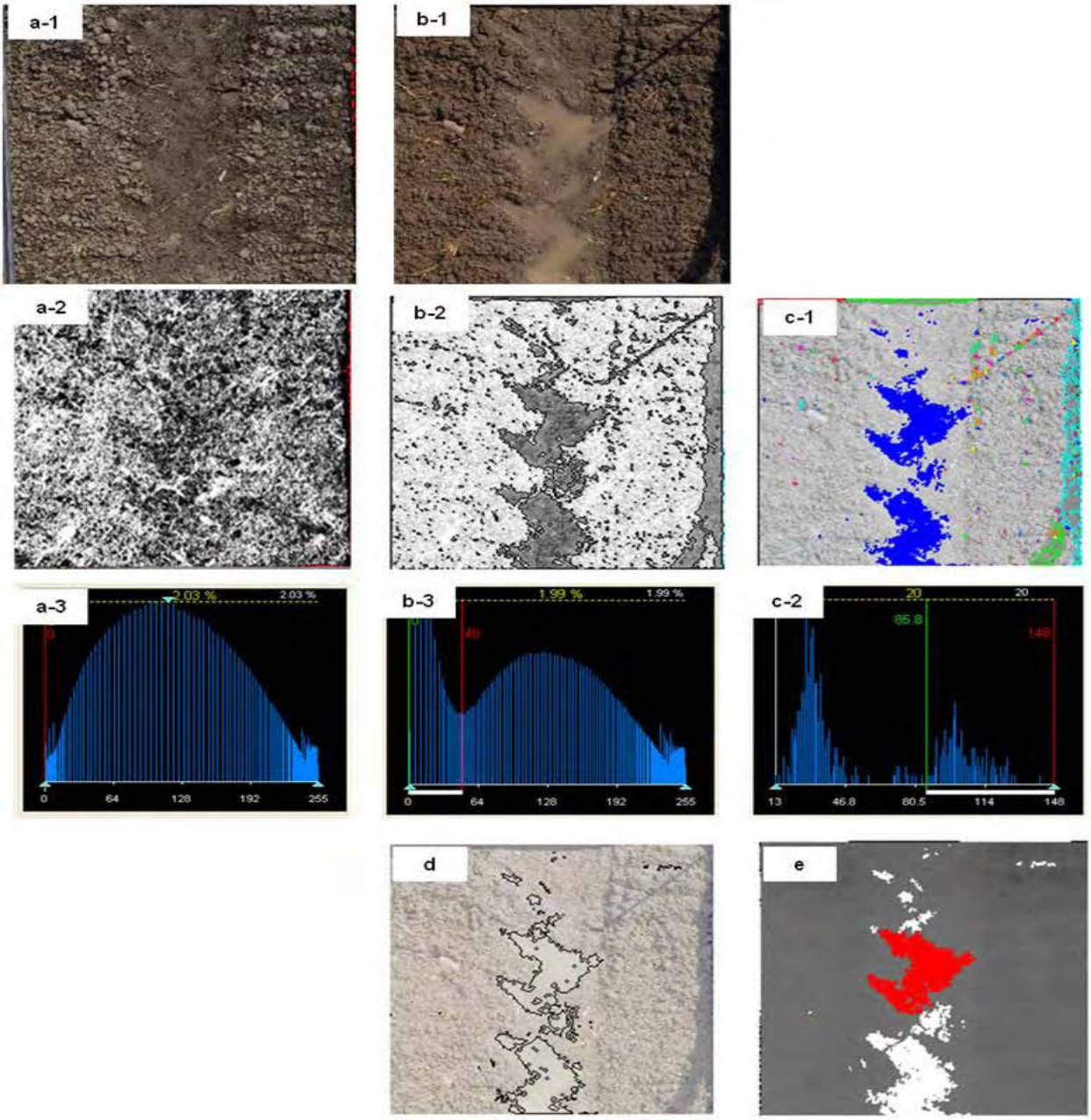

Figure 20: A complete example to show water contour extraction on the field condition: original photos before rainfall (a-1) and during rainfall simulation (b-1). Photos obtained after application of "ss" Laws' mask followed by a median-separate operator (a-2 and b-2) and their corresponding histograms of gray values (a-3 and b-3). Use of the Gray_Max histogram (c-2) to separate water region (colored in dark blue in c-1) from other regions, obtained water contours (d), and crossing of water region with DEM directly in the Halcon software.

It remained yet a problem: which DEM before or after rainfall must be used to analysis data, as soil surface evolves during rainfall as a function of the soil aggregates stabilities and rainfall energy kinetic. However this problem is not resolved anywhere.

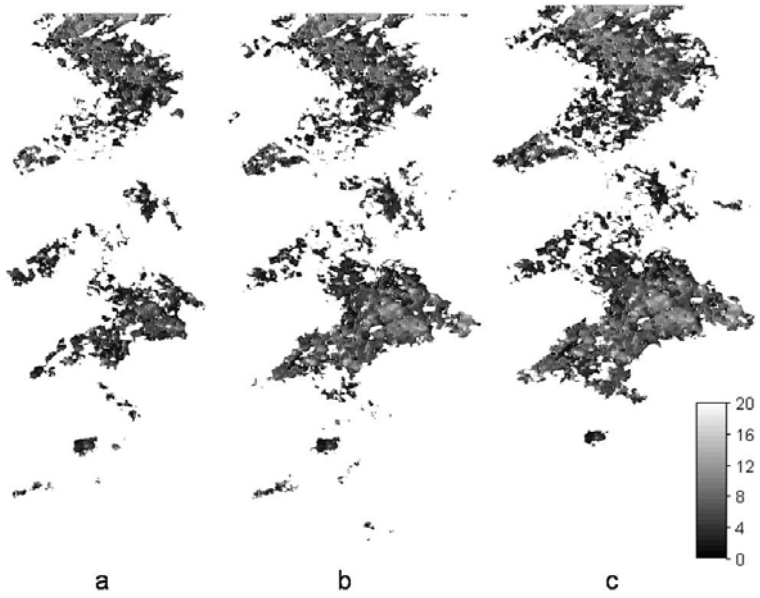

Figure 21: depression water monitoring on the field using image processing. a, b, c shows progressive filling of the depressions respectively after 34 , 50 minute during rainfall and 38 seconds after rainfall simulation. (Total rainfall was 1:03:00)

Reference

Abedini, M.J., Dickinson, W.T. and Rudra, R.P., 2006. On depressional storages: The effect of DEM spatial resolution. Journal of Hydrology, 318(1-4): 138-150.

Bogner, C., Wolf, B., Schlather, M. and Huwe, B., 2008. Analysing flow patterns from dye tracer experiments in a forest soil using extreme value statistics. European Journal of Soil Science, 59: 103-113.

Courault, D., P., B. and M.C., G., 1993. Monitoring surface changes of bare soils due to slaking using spectral measurements. Soil Sci. Soc. Am., 57: 1595–1601.

Darboux, F., 1999. Modélisations numéique et expérimentale du ruissellement. Effets de la rugosite sur les distances de transfert, 170 pp.

Darboux, F., Davy, P., Gascuel-Odoux, C. and Huang, C., 2001. Evolution of soil surface roughness and flowpath connectivity in overland flow experiments. Catena, 46(2-3): 125-139.

Darboux, F. and Huang, C., 2003. An instantaneous-profile laser scanner to measure soil surface microtopography. Soil Science Society of America Journal, 67(1): 92-99.

De Jong van Lier, Q., Sparovek, G., Flanagan, D.C., Bloem, E.M. and Schnug, E., 2005. Runoff mapping using WEPP erosion model and GIS tools. Computers & Geosciences, 31(10): 1270-1276.

Eltz, F.L.F. and Norton, L.D., 1997. Surface roughness changes as affected by rainfall erosivity, tillage, and canopy cover. Soil Science Society of America Journal, 61(6): 1746-1755.

Esteves, M., Faucher, X., Galle, S. and Vauclin, M., 2000. Overland flow and infiltration modelling for small plots during unsteady rain: numerical results versus observed values. Journal of Hydrology, 228(3-4): 265-282.

Fox, D.M., Le Bissonnais, Y. and Bruand, A., 1998a. The effect of ponding depth on infiltration in a crusted surface depression. CATENA, 32(2): 87-100.

Fox, D.M., Le Bissonnais, Y. and Quétin, P., 1998b. The implications of spatial variability in surface seal hydraulic resistance for infiltration in a mound and depression microtopography. CATENA, 32(2): 101-114.

Garcia-Sanchez L., 1997. Modélisation de la dynamique ruissellement-infiltration en fonction des états de surface, Université des Sciences et Techniques de Languedoc, France, 125 pp.

Gayle, G.A. and Skaggs, R.W., 1978. Surface storage on bedded cultivated lands. . Transactions of the ASAE, 21(1): 101–104, 109.

Hansen, B., Schjonning, P. and Sibbesen, E., 1999. Roughness indices for estimation of depression storage capacity of tilled soil surfaces. Soil and Tillage Research, 52(1-2): 103-111.

Helming, K., Romkens, M.J.M. and Prasad, S.N., 1998. Surface roughness related processes of runoff and soil loss: A flume study. Soil Science Society of America Journal, 62(1): 243-250.

Huang, C. and Bradford, J.M.B., 1990. Depressional storage for Markov-Gaussian surfaces. Water Resour. Res., 26 2235–2242.

Jenson, S.K. and Domingue, J.O., 1988. Extracting Topographic Structure from Digital Elevation Data for Geographic Information System Analysis. PHOTOGRAMMETRIC ENGINEERING & REMOTE SENSING, 54(11): 1593-1600.

Jester, W. and Klik, A., 2005. Soil surface roughness measurement--methods, applicability, and surface representation. CATENA, 64(2-3): 174-192.

Jetten, V., 2002. LISEM user manual, version 2.x. Draft version January 2002. Utrecht Centre for Environment and Landscape Dynamics, Utrecht University, The Netherlands: 48.

Jetten, V., Boiffin, J. and DeRoo, A., 1996. Defining monitoring strategies for runoff and erosion studies in agricultural catchments: A simulation approach. European Journal of Soil Science, 47(4): 579-592.

Kamphorst, E.C., 2000. Mesures et méthodes d'estimation de la capacité de stockage d'eau dans le micro-relief créé par les opérations de travail du sol, 'Institut National Agronomique Paris-Grignon, 158 pp.

Kamphorst, E.C., Chadoeuf, J., Jetten, V. and Guerif, J., 2005. Generating 3D soil surfaces from 2D height measurements to determine depression storage. CATENA, 62(2-3): 189-205.

Kamphorst, E.C. and Duval, Y., 2001. Validation of a numerical method to quantify depression storage by direct measurements on moulded surfaces. CATENA, 43(1): 1-14.

Kamphorst, E.C. et al., 2000. Predicting depressional storage from soil surface roughness. Soil Science Society of America Journal, 64(5): 1749-1758.

Langford, K.J. and Turner, A.K., 1972. Effects of rain and depression storage on overland flow. Transactions of the Institution of Engineers, Australia, 14(2): 137–141.

Le Bissonnais Y. et al., Le dispositif "simulation de pluie" et son utilisation dans le cadre des recherches sur l'érosion des sols (INRA Orléans). RIDES, is acciable http://www-rides.u-strasbg.fr/equipements/simulorleans.html.

Linsley, R.K.J., Kohler, M.A. and Paulhus, J.L.H., 1947. Applied Hydrology, Applied Hydrology, New-York, USA, pp. 269

Mirzaei, M.R. and Ruy, S., 2008. Effect of rainfall on soil microtopography evaluated using photogrammetry. Submitted in Soil Sci Soc Am J.

Mirzaei, M.R., Ruy, S., Darboux, F., Gaudu, J.C. and Renaux, B., 2008a. Assessing the influence of the variability of soil surface characteristics on infiltration and runoff: an experimental approach in the lab, EGU General Assembly, Vienne.

Mirzaei, M.R., Ruy, S., Ghazavi, G. and Boaner, C., in press. Soil microtopography studies using Stereophography and Laser-Scaning methods., Journal of Science and Technology of Agriculture and Natural Resources.

Mirzaei, M.R., Ruy, S., Ziarati, T., Rist, A. and Khaledian, M.R., 2008b. monitoring roughness changes caused by rainfall using photogrammetry. Submitted in CATENA.

Mirzaei, M.R., Ziarati, T., Gaudu, J.C. and Ruy, S., 2008c. Evaluation of the precision of close-range photogrammetry to assess DEM of the soil surface., EGU General Assembly, Vienne.

Mitchell, J.K. and Jones, B.A.J., 1976. Micro-relief depression storage: analysis of models the depth-storage function Water Resources Association, 12(6): 1205-1221.

Monteith, N.H., 1974. The role of surface roughness in runoff. Soil conservation journal 42-45.

Moore, I.D. and Larson, C.L., 1979. Estimating microrelief surface storage from point data. Trans. ASAE, 22: 1073–1077.

MVTec, S.G. (Editor), 2006a. HALCON application note "Machine Vision in World Coordinates" version 7.1. Mûnchen, Germany, 144 pp.

MVTec, S.G. (Editor), 2006b. Refrenc HDevelop, version 7.1. Mûnchen, Germany, 144 pp.

Mwendera, E.J. and Feyen, J., 1992. Estimation of depression storage and Manning's resistance coefficient from random roughness measurements. Geoderma, 52(3-4): 235-250.

Onstad, C.A., 1984. Depresional storage on tilled soil surfaces. Transactions of the ASAE, 27: 729-732.

Onstad, C.A., Wolfe, M.L., Larson, C.L. and Slack, D.C., 1984. Tilled soil subsidence during repeated wetting. Trans. ASAE 27: 733–736.

Planchon, O. and Darboux, F., 2001. A fast, simple and versatile algorithm to fill the depressions of digital elevation models. CATENA, 46(2-3): 159-176.

Rieke-Zapp, D.H. and Nearing, M.A., 2005. Digital close range photogrammetry for measurement of soil erosion. Photogrammetric Record, 20(109): 69-87.

Sneddon, J. and Chapman, T.G., 1989. Measurement and analysis of depression storage on a hillslope. Hydrol. Processes 3: 1–13.

Stone, J.J., Lane, L.J., Shirley, E.D. and Hernandez, M., 1995. Hill slop surface hydrology, USDA - Water erosion prediction projects, Hillslope profile and watershed model documentation. National Soil Erosion Research Laboratory, Indiana 47907, USA.

Taconet, O. and Ciarletti, V., 2007. Estimating soil roughness indices on a ridge-and-furrow surface using stereo photogrammetry. Soil and Tillage Research, 93(1): 64-76.

Ullah, W. and Dickinson, W.T., 1979. Quantitative description of depression storage using a digital surface model, I. Determination of depression storage. Journal of Hydrology, 42: 63-75.

Ziarati, T., Ruy, S. and Mirzaei, M.R., Juin 2007. Caractériser les possibilités de la stéréophotographie pour le suivi de différents indices de rugosité sous l'action des pluies, INRA, Avignon.

Annexe 8 calcul de la conductivité hydraulique à saturation par la méthode du perméamètre à charge variable

Le dispositif, ainsi que les notations, sont décrits sur la Figure **Erreur ! Il n'y a pas de texte répondant à ce style dans ce document.**-22.

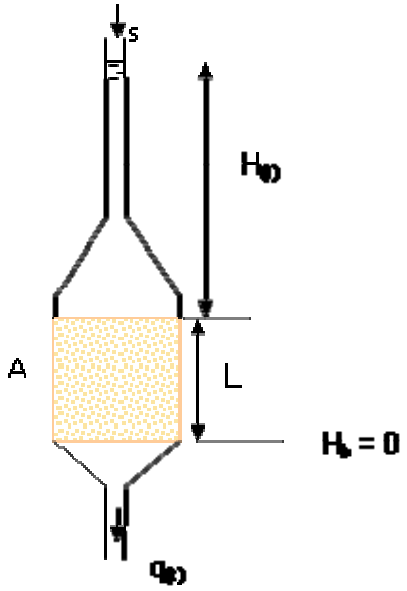

Figure Erreur ! Il n'y a pas de texte répondant à ce style dans ce document.**-22 : schéma de principe du perméamètre à charge variable.**

Le milieu poreux à caractériser présente une section A et une hauteur L. La conservation de la masse couplée à la loi de Darcy permet de relier le flux *q(t)* traversant l'échantillon sous une charge H en fonction de l'évolution temporelle de la charge *H(t)* présente dans un tube de section *s* :

$$\begin{aligned} q(t)\cdot A &= s\cdot\frac{dH}{dt} \\ q(t) &= -K_s\cdot\frac{H(t)}{L} \end{aligned} \Rightarrow \frac{dH}{dt} = -k_s\frac{A}{sL}H(t) \Rightarrow H(t) = H_0.e^{-\frac{K_S}{L}.\frac{A}{s}.(t-t_0)},$$

où H_0 est la charge initiale à l'instant t_0. La mesure de l'évolution *H(t)* nous permet alors de déduire la valeur *Ks* de l'échantillon, ou encore la valeur *L/Ks* qui est la résistance hydraulique totale R_T de l'échantillon.

Dans notre dispositif, l'échantillon est composite et est constitué d'une part de la toile nylon, positionnée pour retenir le sable, et d'autre part de l'échantillon de sable proprement dit. La résistance hydraulique totale de l'échantillon composite est la somme des résistances de chacune des composants, à savoir la résistance de la toile R_{toile} mesurée par ailleurs (4^e-4 h), et la résistance du sable $R_s=L/K_s$. On peut donc en déduire le K_s du sable par la relation :

$$K_s = \frac{L}{R_s} = \frac{L}{R_T - R_{toile}}$$

Pour l'échantillon 232 (sable S31, voir Figure **Erreur ! Il n'y a pas de texte répondant à ce style dans ce document.**-23), on trouve une valeur K_s de 4.31 mm h^{-1}.

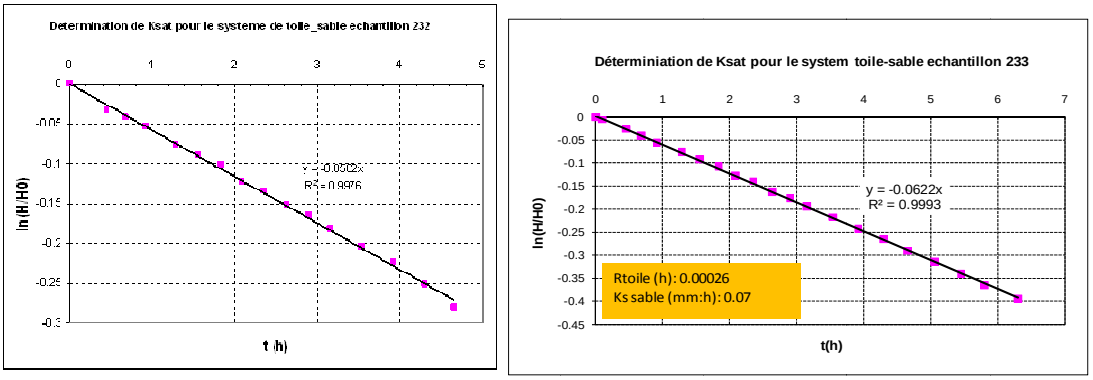

Figure Erreur ! Il n'y a pas de texte répondant à ce style dans ce document.**-23: La résistance hydraulique dans deux échantillons**

Annexe 9: Adimensionnalisation de l’équation de Richards

On écrit l'équation sous la forme :

$$C(u)\cdot\frac{\partial u}{\partial t}=\vec{\nabla}\cdot\left(K(u)\cdot\vec{\nabla}(u)\right)$$

Soit :

- L_0 une échelle de longueur (m) :
  - Ex. : L_0= 1 m = le côté du cube, on prend la même échelle de longueur dans les trois directions de l'espace,
- K_0 une perméabilité caractéristique (m s^{-1}) :
  - Ex. : $K_0 = K_s$ conductivité hydraulique à saturation
- C_0 une capacité capillaire caractéristique (m^{-1}) :
  - Ex. : on prend par exemple le maximum de la capacité capillaire, ou bien l'équivalent de la capacité capillaire à saturation (coefficient d'emmagasinement),
- τ_0 un temps caractéristique (s) :
  - τ_0 est définit à partir des variables L_0, K_0 et C_0 (voir ci dessous).

L'équation de Richards devient :

$$C_0\cdot\frac{C(u)}{C_0}\cdot\frac{L_0}{\tau_0}\frac{\partial\left(u/L_0\right)}{\partial\left(t/\tau_0\right)}=\frac{K_0\cdot L_0}{{L_0}^2}\vec{\nabla}'\cdot\left(\frac{K(u)}{K_0}\cdot\vec{\nabla}'\left(u/L_0\right)\right)$$

On note avec le symbole « ' » les grandeurs adimensionnelles :

$$\frac{C_0\cdot{L_0}^2}{K_0\cdot\tau_0}\cdot C'(u'-z')\cdot\frac{\partial u'}{\partial t'}=\vec{\nabla}'\cdot\left(K'(u'-z')\cdot\vec{\nabla}'(u')\right)$$

Finalement, les formes dimensionnelles et adimensionnelles de l'équation de Richards sont formellement identiques si on écrit :

$$\begin{cases} u'=\dfrac{u}{L_0}\quad z'=\dfrac{z}{L_0}\quad t'=\dfrac{t}{\tau_0} \\ C'(\ )=\dfrac{C(\ )}{C_0}\quad K'(\ )=\dfrac{K(\ )}{K_0} \\ \dfrac{C_0\cdot{L_0}^2}{K_0\cdot\tau_0}=1\Leftrightarrow\tau_0=\dfrac{C_0\cdot{L_0}^2}{K_0} \\ C'(u'-z')\cdot\dfrac{\partial u'}{\partial t'}=\vec{\nabla}'\cdot\left(K'(u'-z')\cdot\vec{\nabla}'(u')\right) \end{cases}$$

Les propriétés hydrodynamiques s'écrivent alors :

- courbe de rétention :

$$\frac{\theta-\theta_r}{\theta_s-\theta_r}=\left(1+\left(\alpha|h|\right)^n\right)^{-m} \Rightarrow \frac{\theta'-\theta'_r}{\theta'_s-\theta'_r}=\left(1+\left(\alpha'|h'|\right)^{n'}\right)^{-m'},$$

avec $\theta'=\theta, \quad n'=n, \quad m'=m, \quad h'=\frac{h}{L_0}, \quad \alpha'=\alpha\cdot L_0$;

- courbe de conductivité hydraulique :

$$K=K_s\cdot S_e^{\tau}\cdot\left(1-\left(1-S_e^{1/m}\right)^m\right)^2 \Rightarrow K'=\frac{K}{K_0}=\left(\frac{K_s}{K_0}\right)\cdot S_e'^{\tau}\cdot\left(1-\left(1-S_e'^{1/m'}\right)^{m'}\right)^2,$$

avec $S'_e=S_e, \quad m'=m$;

- courbe de capacité capillaire :

$$\begin{cases} h\le 0 & : \quad C(h)=\dfrac{d\theta}{dh}=(\theta_s-\theta_r)\cdot n\cdot m\cdot\alpha\cdot\left(\alpha\cdot|h|\right)^{n-1}\cdot\left(1+\left(\alpha\cdot|h|\right)^n\right)^{-m-1}+\beta\cdot(\theta-\theta_r) \\ h\ge 0 & : \quad C(h)=\beta\cdot(\theta_s-\theta_r) \end{cases}$$

$$\Downarrow$$

$$\begin{cases} h\le 0 & : \quad C'(h')=\dfrac{C(h)}{C_0}=\dfrac{1}{\beta'}\cdot n'\cdot m'\cdot\alpha'\cdot\left(\alpha'\cdot|h'|\right)^{n'-1}\cdot\left(1+\left(\alpha'\cdot|h'|\right)^{n'}\right)^{-m'-1}+S'_e \\ h\ge 0 & : \quad C'(h')=1 \end{cases}$$

avec $S'_e=S_e, \quad n'=n, \quad m'=m, \quad h'=\frac{h}{L_0}, \quad \alpha'=\alpha\cdot L_0, \quad \beta'=\beta\cdot L_0$

Les conditions limites deviennent :

	Dimensionnel	Adimensionnel
Dirichlet[1]	$u = u_0$	$u' = u'_0$
Neumann[2]	$\phi = \phi_0 = -K(u-z)\cdot\vec{\nabla}(u)\cdot$	$\phi' = \phi'_0 = K'(u'-z')\cdot\vec{\nabla}'(u')$
Mixte[3]	$\phi = \phi_0 - \lambda\cdot(u-z)$	$\phi' = \phi'_0 - \lambda'\cdot(u'-z')$

[1] : $u = u_0 \Leftrightarrow \frac{u}{L_0} = \frac{u_0}{L_0} \Leftrightarrow u' = u'_0$

[2] : $\vec{\phi} = \vec{\phi}_0 = -K(u-z)\cdot\vec{\nabla}(u) = -K_0\cdot\frac{K(u-z)}{K_0}\cdot\frac{1}{L_0}\cdot\vec{\nabla}'\left(L_0\cdot\frac{u}{L_0}\right) \Leftrightarrow \vec{\phi}' = \vec{\phi}'_0 = K'(u'-z')\cdot\vec{\nabla}'(u')$

[3] : $\phi = \phi_0 - \lambda\cdot(u-z) = K_0\cdot\phi'_0 - \lambda\cdot L_0\cdot(u'-z') \Leftrightarrow \phi' = \frac{\phi}{K_0} = \phi'_0 - \lambda'\cdot(u'-z')$,

avec $\lambda' = \lambda\cdot\frac{L_0}{K_0}$, $\phi'_0 = \frac{\phi_0}{K_0}$

Résumé

La répartition des pluies entre infiltration, détention superficielle et ruissellement sous contrôle dynamique des états de surface doivent être mieux compris et intégrés dans les modèles de ruissellement. D'un point de vue expérimental, il manque une mesure effective de la détention superficielle qui nécessite une mesure fiable du microrelief du sol. D'un point de vue théorique, les lois utilisées dans les modèles en considérant un milieu homogène peuvent être inadéquates car le sol est un milieu complexe et hétérogène. L'objectif de ce travail concernait ces deux aspects.

Dans un premier temps nous avons développé un capteur photogrammétrique (matériel et logiciel) d'une part pour obtenir des modèles numériques de terrain à petite échelle (surface de 1 m²), précis et avec une résolution spatiale fine (1 mm dans les deux directions horizontales), et d'autre part pour suivre l'évolution de la détention superficielle d'eau au cours de la pluie. Ce capteur a été validé par comparaison avec un capteur de référence (rugosimètre laser).

Dans un deuxième temps, nous avons caractérisé l'effet de l'hétérogénéité du sol et du microrelief de sa surface dans le partage infiltration-ruissellement. Pour mieux comprendre le rôle des hétérogénéités du sol dans le partage infiltration–ruissellement, nous avons travaillé sous simulation de pluie sur une parcelle naturelle de 1 m², horizontale, sans rugosité marquée ni variabilité apparente des états de surface. Les résultats ont montré qu'il existe une forte variabilité locale des propriétés hydrodynamiques (courbes de rétention et de conductivité hydraulique). L'influence de ces hétérogénéités sur le ruissellement a été déterminée par l'utilisation du modèle PASTIS. Des expérimentations en conditions contrôlées sur une maquette physique de sol ont permis de mettre en relation l'infiltration distribuée dans le sol et la genèse du ruissellement à la surface. Un code a finalement été développé et validé pour gérer la redistribution latérale des excès d'eau à la surface du sol. Ce code peut être couplé à un modèle mécaniste d'infiltration distribuée 3D.

Mot-clés : microrelief, rugosité, détention superficielle, ruissellement, simulation de pluie, analyse d'image, modèle numérique de terrain, stéréophotogrammétrie, rugosimètre laser

¤¤¤

Abstract

Soil surface properties can affect and control the dynamics of the rainfall distribution between infiltration-detention-runoff. These affects must be better understood and integrated into models of runoff. From an experimental point of view, it lacks an effective measure of detention surface that requires a reliable measure of the soil surface microrelief. From a theoretical point of view, the laws used in the infiltration-runoff models, considering a homogeneous environment, may be inadequate because the soil is a complex and heterogeneous milieu. The objective of this work involved therefore these two aspects.

As a first step we have developed a sensor photogrammetric (hardware and software) on the one hand to obtain digital elevation models in a small-scale (area of 1 m^2), precise and with a fine resolution (1 mm in both directions horizontal), and on the other hand to monitor the water detention on the soil surface during rainfall. This sensor has been validated by comparison with a reference sensor (laser scanner).

In a second step, we characterized the effect of the heterogeneity of soil and microrelief of its surface in the infiltration-runoff modeling. To better understand the role of the heterogeneity of the ground in water partition using infiltration–runoff models, we worked under simulated rainfall on a parcel of 1 m^2, horizontal, without any marked roughness or apparent variability of surface. The results showed that there is a high variability of local hydrodynamic properties (retention and hydraulic conductivity curves). The influence of these heterogeneities on the runoff was determined by using the model PASTIS. Experiments in controlled conditions on a soil maquette have helped to connect the distributed infiltration and the genesis of the surface runoff. A code was finally developed and validated to manage the distribution side of excess water on the surface. This code can be coupled to a 3D mechanistic-distributed infiltration model infiltration distributed.

Keywords: microrelief, roughness, depressionnal storage, runoff, rainfall simulation, image processing, digital elevation model, stereophotogrammetry, laser scanner